Design of a Short to Medium Range

Hybrid Transport Aircraft

A Project Presented to
The Faculty of the Department of Aerospace Engineering
San José State University

In Partial Fulfillment of the Requirements for the Degree
Master of Science in Aerospace Engineering

by

Sarah M. Ortega

approved by
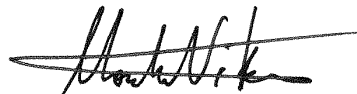
Dr. Nikos J. Mourtos
Faculty Advisor

Nomenclature

A	=	aspect ratio
A/C	=	aircraft
AEP	=	airplane estimated price
A_h	=	horizontal tail aspect ratio
A_{inl}	=	capture area per inlet in square feet
A_v	=	vertical tail aspect ratio
ac	=	aerodynamic center
AH_j	=	number of flight hours per year for crew member j
ASP	=	avionics systems price
b	=	wingspan
B.L.	=	wing buttock lines
C_L	=	lift coefficient
C_D	=	drag coefficient
Cr	=	cruise
c	=	chord
c_r	=	root chord
c_t	=	tip chord
CGR	=	climb gradient
cg	=	center of gravity
$C_{n_{\delta_r}}$	=	control power derivative
$C_{lab/ap}$	=	labor cost of airframe and system maintenance
$C_{lab/eng}$	=	labor cost of engine maintenance
$C_{mat/ap}$	=	cost of maintenance materials for the airframe and systems
$C_{mat/eng}$	=	cost of maintenance materials for the engines
C_{amb}	=	applied maintenance burden
C_{dap}	=	cost of airplane depreciation
C_{deng}	=	cost of engine depreciation
C_{dav}	=	cost of avionics system depreciation
C_{dapsp}	=	cost of airplane spare parts depreciation
C_{dengsp}	=	cost of engine spare parts depreciation
C_{lf}	=	direct operating cost due to landing fees
C_{aplf}	=	airplane landing fee per landing
C_{nf}	=	navigation fee
C_{apnf}	=	navigation fee charged per airplane per flight
C_{rt}	=	direct cost of registry taxes
DOC	=	direct operating cost
DOC_{lnr}	=	direct operating cost of landing fees
DOC_{fin}	=	direct operating cost of financing the airplane
DP_{ap}	=	airplane depreciation period
DP_{av}	=	airplane avionics system depreciation period
DP_{engsp}	=	depreciation period for engine spare parts
e	=	battery specific energy, Oswald constant
E_{bat}	=	energy of batteries
E_τ	=	propulsive energy required

EP   = engine price
ESPPF   = engine spare parts price factor
F_{dap} = airframe depreciation factor
F_{dav} = airplane avionics system depreciation factor
f = equivalent parasite area
F.S.   = fuselage stations
FAA   = Federal Aviation Administration
FAR   = Federal Aviation Regulations
FT   = Fischer-Tropsch
F_{engsp} = engine spare parts factor
f_{rt} = factor depending on airplane size
g   = gravitational acceleration
h = height
h_{fus} = height of fuselage in feet
HTA   = Hybrid Transport Aircraft
i_w = incidence angle
j   = crew member type
K   = drag due to lift polar coefficient
K_g = gust alleviation factor
k_j = factor accounting for crew vacation pay, cost of training crew insurance, etc.
LE   = leading edge
LG   = landing gear
Ltr   = loiter
l_{fus} = length of fuselage in feet
l_h = distance from wing root quarter cord to horizontal tail quarter cord in ft
l_n = nacelle length
n   = load factor
n_{c_j} = number of crew members of type j
N_D = drag induced yawing moment
N_e = number of engines
$n_{lim_{pos}}$ = positive limit naneuvering load factor
$n_{lim_{neg}}$ = negative limit naneuvering load factor
N_{inl} = number of inlets
N_{pax} = number of passengers
N_{pil} = number of pilots
mgc   = mean geometric chord
M_H = maximum Mach number at sea level
M_{ff} = mission fuel fraction
M_{res} = reserve fuel fraction
M_{tfo} = trapped fuel fraction
MEA   = More Electric Aircraft
p = battery specific power
P_r = power required (propulsive)
P_2 = maximum static pressure at engine compressor face in psi
q   = dynamic pressure in psf
$\bar{q}$ = design dive dynamic pressure in psf

RC   = rate of climb
Re_r = Reynold's number at root chord
Re_t = Reynold's number at chord tip
R_{bl} = block distance
R_{cl} = climb distance
R_{de} = descent distance
R_{man} = maneuvering distance
S   = wing reference surface area
S_h = horizontal tail area
S_v = vertical tail area
S   = gross wing area
SAL_j = yearly salary per crew member
S_{TOFL} = takeoff field length
T   = time of flight
T_{phase} = time of flight for a certain phase
TBW   = Truss Braced Wing
t/c   = thickness ratio
T_{cl} = time to climb
T/W   = thrust loading (or thrust to weight ratio)
t_{r_h} = horizontal tail maximum root thickness
t_{r_v} = vertical tail maximum root thickness
TEF_j = travel expense factor per crew member j
W/S   = Wing loading
W_{ai} = air induction system weight
W_{api} = weight of air-conditioning, pressurization, anti-icing and de-icing system
W_{apu} = weight of auxiliary power unit (APU)
W_{bat} = weight of batteries
W_{bc} = weight of baggage and cargo handling equipment
W_e = empty weight
W_{els} = weight of electrical system
W_{eng} = weight of engine
W_f = fuel weight
W_{fc} = weight of flight control system
W_{fur} = weight of furnishings
W_{hs} = weight of hydraulic and pneumatic system
W_i = weight of instruments
W_{iae} = weight of the instrumentation, avionics, and electronics
W_{oe} = operating empty weight
W_{ops} = weight of operational items
W_{ox} = weight of oxygen system
W_{pl} = payload weight
W_{pt} = weight of paint
W_{tfo} = trapped fuel weight
W_{to} = take off weight
W_L = landing weight
W_{fs} = fuel system weight

W_{fus} = weight of fuselage in lbs
w_{fus} = width of fuselage
W_p = propulsion system
W_{pwr} = powerplant weight
W_{struct} = weight of structure
$U_{ann_{bl}}$ = annual utilization in block hours
V = velocity
V_B = design speed for maximum gust intensity
V_A = approach speed
V_C = design cruise speed
V_{cr} = cruise velocity
V_D = design diving speed
V_M = design maneuvering speed
V_{pax} = passenger cabin volume
V_S = +1g stall speed or minimum speed at which airplane is controllable
x_v, x_h, x_c = distance from center of gravity to aerodynamic center of the surface
y_t = lateral thrust moment arm of most critical engine
z_h = distance from vertical tail to root, where horizontal tail is mounted on vertical tail
η_p = propeller efficiency
ρ = air density
Λ = quarter chord sweep angle
λ = taper ratio
ε_w = twist angle
Γ_w = dihedral angle

Table of Contents

List of Figures

List of Tables

1.

The

The

The

While

As

1.1.

1.1.1.

With

Conventional propulsion systems thermally decompose oil in piston engines or gas

turbines. This in turn produces mechanical power which runs either a turbofan or turbo-

propeller. Gearboxes can increase efficiency

when they decouple the fan from the turbine or

turbofan engine. Despite the ability to increase

efficiency, these propulsion systems emit

exhaust
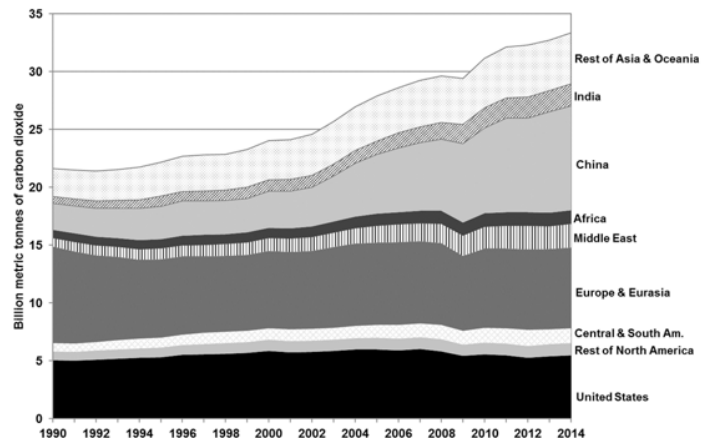
Figure 1. World Carbon Dioxide Emissions

Both

70%

Error! Reference source not found., illustrates the billions of metric tons of CO_2 that

Direct CO_2 Emissions From 1 Gallon of Fuel (measured in pounds per gallon)
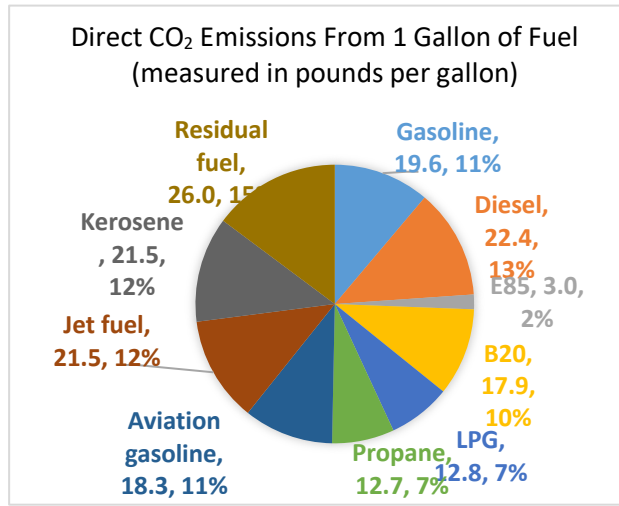
are emitted annually by each country world-wide. CO_2 has a lifetime of up to 200 years and has a global warming potential direct effect of 100 years, so its annual contribution effects are present for decades to come. Transportation produces approximately 31.8% of these emissions, contributing to green house gases. (Davis, Williams, & Boundy,

2016) **Error! Reference source not found.** summarizes the types

Figure 2. Direct CO_2 emissions from 1 gallon of fuel (lbs/gal)

of fuel emissions in pounds per gallon that contribute to direct CO_2 emissions. Aviation

gasoline, or Av-gas, contributes 11% and jet fuel contributes 12%. (Davis, Williams, & Boundy,

2016) With an increase in the number of general aviation aircraft in use, these emissions will not

decrease without changes to aircraft or fuel. General aviation consist of aircraft following

general operating and flight rules, aircraft with a minimum seating capacity of 20 or maximum

payload of 6,000 lbs that are not for hire, agricultural aircraft, rotorcraft external load operators,

and commuter or on-demand aircraft not covered under FAR regulations part 121. From 1970-

2014, the number of general aviation aircraft increased by around 1% per year, as summarized in

Error! Reference source not found.. As a result in the number of increased aircraft, the energy

used has increased by about 2% per year and 2.3% from 2004-2014. (Davis, Williams, &

Boundy, 2016)

Number of General Aviation Aircraft

Figure 3. Number of General Aviation Aircraft from 1970 to 2014

Besides producing a high volume of pollutants, aircraft also contribute to the use of fossil fuels. The United States imported 564,000,000 tons of oil in 2008 and has since increased oil importation. Transportation used a significant portion of

the

In

1.2

1.2.1.

Although

1.2.2.

Another consideration is the candidate for hydrocarbon feedstock. If some form of plants were used, there would need to be adequate farmland to sustain the fuel. This farmland would need to be acquired without deforestation techniques, where the smoke from fires would contribute to green house gases and increase pollution. Algae holds promise as a future option due to its oil production. A comparison of algae to other feedstocks is present in Figure 4 and

Figure 4. Alternative Biofuels
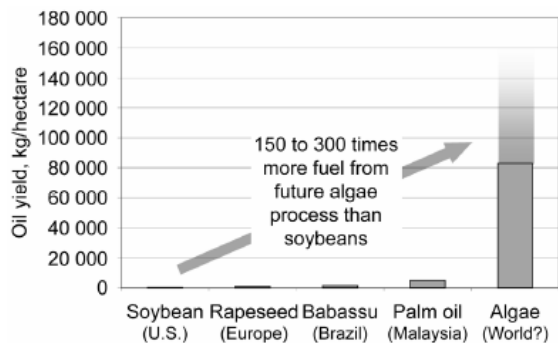
depicts the significantly higher oil production as compared to other biofuels. It is estimated to produce 10,000-20,000 gallons per acre per year of oil, a dramatic increase from the use of soybean oil.

Logistically,

1.2.3. Alternative Fuel Comparisons

Since

1.2.4. Lithium Ion Batteries

Other

Lithium ion batteries have been utilized in many applications, including electric vehicles

and electronics. These batteries are considered the most commercially available, power-dense

batteries. Graphite carbon composes the anode of the batteries; while lithiated metal oxides like

$LiMO_2$ and $LiCoO_2$ are used as cathodes. With charging, the cathode transforms into lithium

ions, which then move towards the anode through lithium salts combining with external

electrons. (Farhadi & Mohammed, 2016) Battery measurements consist of specific energy

densities, measured in Wh/kg, volumetric energy densities, measured in Wh/liter, and specific

power, measured in W/kg. Although Li-ion batteries are more costly, priced at $0.82 per Wh,
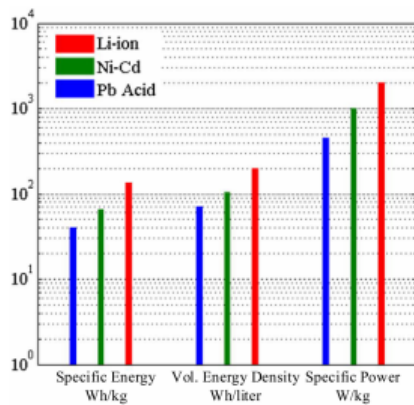
compared to Ni-Cd and Pb-acid, at $0.42 and $0.28, respectively, they have the highest energy density offered, which means they are the smallest in both volume and weight for the amount of energy stored. Figure 5 illustrates the capabilities of Li-ion batteries' specific energy, volumetric energy density, and specific power, and compares them against

Figure 5. Comparison of different types of

Ni-Cd and Pb-acid batteries. (Tariq, Maswood, Gajanayake, & Gupta, 2017). Studies have

stated that Li-ion battery energy densities are increasing 8-10% per year, with power doubling

every 10 years. The maximum specific energy density value potentially being 5200 Wh/kg

(Ullman). Figure 6 illustrates a summary of efficiency, discharge time, operating temperature, and lifespan of Li-ion batteries compared to other energy storage technologies.

Lithium ion batteries are 95-99% efficient. They have lifespans of 5-20 years with long discharge times and a wide range of temperatures in which they can operate. Seal level temperatures are usually around 15ºC and flight temperatures range from -44 ºC to -56 ºC at cruise altitude. Considerations could be made to protect the batteries in the cool atmosphere. The long discharge time makes these batteries ideal for transportation applications. High energy storage batteries with long discharge time lead to maximum system efficiency combined with minimal cost, weight, and volume. (Farhadi & Mohammed, 2016) With cost, weight, and volume being critical factors in aircraft design, lithium ion batteries demonstrate good promise statistically and have illustrated their capabilities through their use in small aircraft.
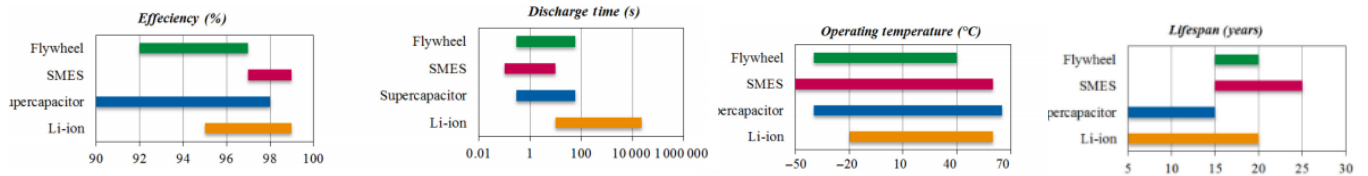
Figure 6. Performance Comparison of Li-ion Batteries

Batteries

A

With the increased level of technology for batteries, designing and building light and general aviation aircraft is becoming a reality. Although initially costly in production, these aircraft will not rely on fuel and will therefore have immense savings in the future. Prices will also dwindle with increasing availability of technology and scale economy effects. Table 1 lists electric aircraft that have flown as of 2016. (Riboldi & Gualdoni, 2016) These aircraft were referenced to perform an electric aircraft sizing for a light or general aviation aircraft.

Table 1. Preliminary database of Electric Aircraft

#	Model	W_{to}/g [kg]	W_e/g [kg]	W_{bat}/g [kg]	W_m/g [kg]	Pm [kW]	e [Wh/kg]	p [W/kg]
1	ElectroLight 2	315	188	34	7.0	19.4	163.2	795.6
2	LAK-17B FES	550	246	32	7.3	35.3	131.3	910.9
3	Lange Aviation Antares 20E	660	440	77	29.1	42.0	136.0	794.0
4	Lange Aviation Antares 23E	850	496	77	29.1	42.0	136.0	794.0
5	Pipistrel Taurus Electro G2	550	253	42	11.0	40.0	113.1	952.4
6	UAV Factory Penguin BE	21.5	9.83	4.41	0.650	2.7	145.0	807.1
7	Yuneec International E430	470	157	74	19.0	40.0	153.7	801.0
8	Silent 2	300	200	36	8.5	13.0	113.9	792.4

1.3.

To perform the sizing of the battery of a small airplane designed for cross country flying

or training, the weight was first considered. For an electric aircraft, the weight is a combination

of the weight of the payload, batteries, electric motor, and the empty weight of the vehicle itself,

a

s

$$W_{to} = W_e + W_{pl} + W_{bat} + W_m \qquad\qquad (1)$$

The mission profile consisted of the usual phases of take-off, climb, cruise, loiter, and

i

land. Typical flight sizing, relies on fuel fractions to define the fuel necessary for each portion

l

of the flight. (Roskam, Airplane Design Part 1: Preliminary Sizing of Airplanes, 2017) Since the

l

fuel would not change, and the weight would stay constant, this method of sizing would not be

u

appropriate. Instead, a relationship between the weights and the mission requirements was

s

examined. In electric aircraft, the most significant phases that affect the power are climbing,

t

cruising, and loitering. The power required for climb can be calculated through Eq. $Prclimb=$

r

$W_{to}RC + \frac{1}{2}\rho^{climb}V^{climb^3}SC_D^{climb}$ (2) relating air density during the

a

climb, constant airspeed, wing reference surface, the value of the drag coefficient, and the rate of

t

climb.

e

$$P_r^{climb} = W_{to}RC + \frac{1}{2}\rho^{climb}V^{climb^3}SC_D^{climb} \qquad\qquad (2)$$

d

Using

Error! Reference source not found.)

i

where

n

Error! Reference source not found.)

and the Oswald coefficient, *e*. With clean values of K and C_D, the lift coefficient can be

calculated using $CL=2Wto\rho V2S$ *(3).*

$$C_L = \frac{2W_{to}}{\rho V^2 S} \qquad (3)$$

The next factor for sizing is the energy required. This involves energy required to climb,

cruise, loiter, and land. To estimate the energy required to climb, the time to climb and the

power required for the climb are taken into consideration, where the time to climb is defined in

$TTC=hcruise\ RC$ (4)

$$TTC = \frac{h^{cruise}}{RC} \qquad (4)$$

and the energy required for climb is defined in the following equation. (Riboldi & Gualdoni,

2016)

$$E^{climb} = P_r^{climb} TTC \qquad (5)$$

The energy required for cruise and loiter can be assumed to be the same. Different values

will be calculated because the densities, velocities, and drag coefficients differ for the phases.

(Riboldi & Gualdoni, 2016)

$$P_r = \frac{1}{2}\rho V^3 S C_D \qquad (6)$$

From there, the energy required for each phase can be calculated using

$$E^{phase} = P_r^{phase} T^{phase} \qquad (7)$$

where the time of each phase relies on the range of the phase and the cruise speed at that phase.

(Riboldi & Gualdoni, 2016) Finally, the battery weight can be determined. With this

calculation, the propulsive efficiency is assumed to be less than 100%, providing the batteries

and motor with a higher requirement. The mission profile battery weight can be calculated using

the following equation. (Riboldi & Gualdoni, 2016)

$$W_{bat,MP} = \frac{g}{\eta_p} max \left\{ \frac{E^{climb}+E^{cruise}+E^{loiter}}{e} , \frac{max\{P_r^{climb}, P_r^{cruise}, P_r^{loiter}\}}{p} \right\} \qquad (8)$$

This sizing examination is limited in that it applies to current technology and small

aircraft.   Sizing aircraft in other weight categories could prove to be more challenging,

especially with relying on current battery technology. A solution to transferring this process to a

larger aircraft, and utilizing current technology, could be to size a hybrid aircraft that could rely

both on the reusable power of batteries and on fuel to compensate for the additional size and

weight strain.

Hybrid aircraft are defined as aircraft where the propulsion is powered by more than one

type of energy source (Thauvin, et al., 2016). Different fuel sources provide the ability to

improve the aircraft's performance, reduce fossil fuel reliance, reduce noise levels, and emit

fewer pollutants. Forms of Electrical Energy Storage (EES) would benefit hybrid vehicles in

their ability to store and use electric power, as needed.

Research was performed on an aircraft with twin-turbo propeller engines with 3500

thermal horsepower per engine, with the capabilities of traveling 400 nautical miles, at a ceiling

of 20,000 ft. The aircraft was also designed using technology for 2035, which would provide

batteries with higher energy densities (Thauvin, et al., 2016). This aircraft's mission overview

can be viewed in Table 2. Its mission profile with the comparison of down-sized gas powered

turbine and standard conditions can be viewed in

Figure 7. *Mission Profile Comparison of Sample Aircraft*. The mission profile illustrates

the capabilities of added power provided by an energy storage unit combined with a reduced

engine. Also visible in the mission profile is added power sent to the storage unit during descent.

Energy recovering through the use of EES can be achieved through a few different

mechanisms. The research on this specific aircraft and the energy recovery examined the energy

gained through braking and through gravitational potential energy. The amount of energy

recovered and stored through braking is fairly minimal. For the research aircraft, the equivalent

amount of fuel saved is 2 kg, which is less than the amoung of fuel needed to taxi. These results

stemmed from assuming a gas turbine efficiency of 40%, and the braking system consisting of

disc brakes, thrust reversers, and airbrakes. (Thauvin, et al., 2016) Producing the equivalent of 2

kg of fuel or 0.19% of total energy used during this mission seems insubstantial.

Table 2. Mission Overview of Sample Aircraft

Phase	Time (min)	Distance (nm)	Fuel (kg)	% Block Fuel
Taxi out	3.0	0.0	9	2.0%
Take-off	1.3	0.0	21	4.8%
Climb	16.1	54.6	177	40.0%
Cruise	22.0	101.0	186	42.1%
Descent	9.9	44.4	32	7.2%
Approach & Landing	2.0	0.0	14	3.2%
Taxi in	1.0	0.0	3	0.7%
Total	55.3	200.0	442	100.0%
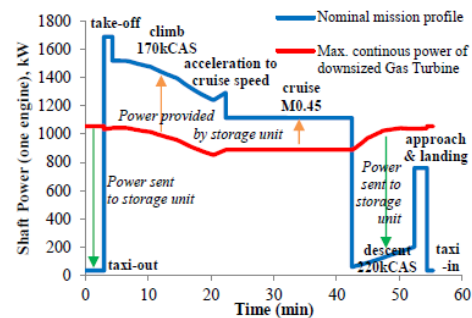
Figure 7. Mission Profile Comparison of Sample Aircraft

Utilizing gravitational potential energy during descent by windmilling propellers

produces energy that can be stored in the EES. On the experimental aircraft, four different

propeller modes were tested: folded, feathered, transparency, and wind turbine. Folded propeller

blades ideally produce zero drag during descent. Feathered blades rotate parallel to the direction

of the airflow. These add to the drag of the aircraft. Transparency blades result in rotating

propellers that don't generate thrust or drag. Wind turbine blades add drag and energy to the

EES. Results from these trade studies demonstrated that propellers should be folded during

descent, and with a hybrid power generation system, transparency mode is most beneficial

during normal operations. *(Thauvin, et al., 2016)*

Other results regarding power efficiency provided additional improvements in operation. The propeller efficiency could be increased by 49% if a hybrid electric system is utilized during taxi, removing the minimum speed constraint. Energy during taxi could be decreased by 90% if the taxi and descent phase could operate on purely electric power. Another consideration coud be to use a single larger engine that has two times the power. This improves efficiency by 10.5%, but removes redundancies in the event of engine failure. Finally, the engine could be sized to perform the climbing phase, with that phase being the most energy demanding. (Thauvin, et al., 2016) Each of these considerations could be used to analyze and design future aircraft of various sizes and explore the balance of the two power sources.

Other considerations for different types of batteries that could prove more energy dense in future years have also been studied. Lithium ion batteries currently have a mass specific energy content of Wh/kg, with a potential of 250 Wh/kg. Other variations of lithium batteries could produce higher specific energies. Research is being conducted on Lithium-Sulfur (Li-S) and Lithium-Oxygen (Li-O) batteries. Additionally, Zinc-Air (Zn-air) also have higher theoretical specific densities. Their specific densities are summarized in Table 3, and an illustration of their performance is present in

Figure 8. (Hepperle) These batteries could potentially provide an AV-gas fuel equivalent of 3800 Wh/kg, and power an electric aircraft. However, current technology is still limited. Hence,

the hybrid aircraft could provide an alternative aircraft which combines current battery

technology with reduced fuel and emissions.

Table 3. Summary of Theoretical Specific Energy

System	theoretical specific energy	expected in 2025
Li-Ion (2012)	390 Wh/kg	250 Wh/kg
Zn-air	1090 Wh/kg	400-500 Wh/kg
Li-S	2570 Wh/kg	500-1250 Wh/kg
Li-O$_2$	3500 Wh/kg	800-1750 Wh/kg
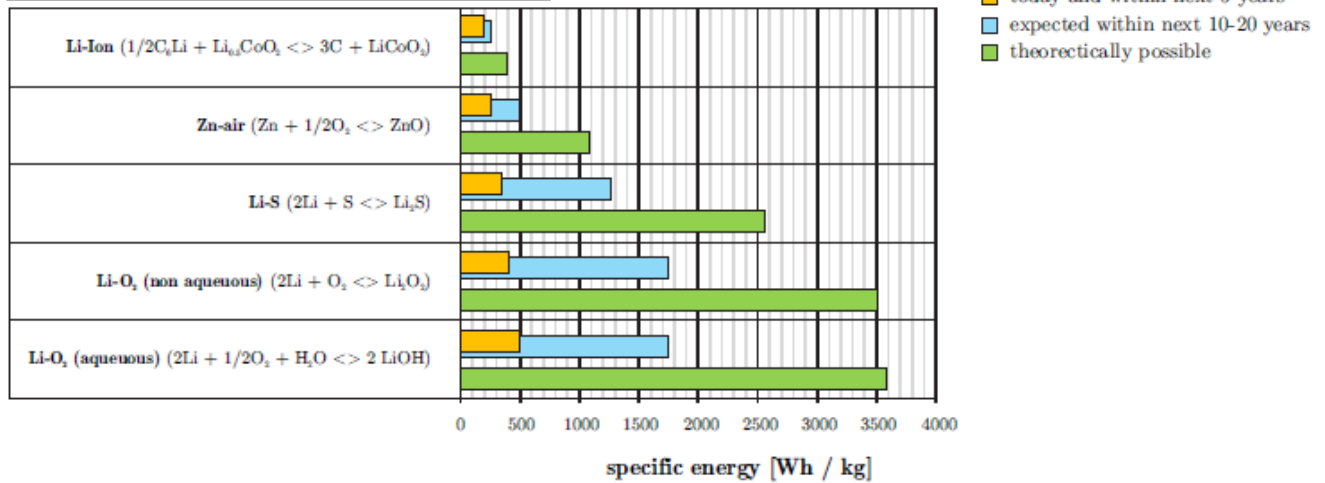
Figure 8. Current and expected battery technology

1.4.   Project Objective

The purpose and objective of this project is to design a hybrid powered aircraft with the

following mission specifications. The payload will consist of a FAA maximum of 124

passengers and 2 crew members along with their luggage. The aircraft will have a maximum

range of 1720 nautical miles at maximum payload and a cruise speed of 500 kts. The required

takeoff field length will be 5,500 ft, and the required landing distance is 3,960 ft. The maximum

cruise altitude will be 40,000 ft. With the use of alternative power, provided by both Lithium ion

batteries and fuel, the project will focus on design trade-offs to power the short-range, narrow-

body aircraft that will reduce fuel usage, and provide a cheaper, cleaner, more energy-efficient

hybrid commercial vehicle.

1.5. Mission Specifications

1.5.1. Mission Specifications

The following consist of mission requirements for the HTA:

- Payload capacity: All Economy with 96 at 6 abreast; FAA limit: 124

- Number of crew members required: 2 pilots, 2 cabin attendants

- Range: 1720 nm

- Cruise speed and Mach number: 500 kts (M=0.75)

- Cruise altitutde: 40,000 ft

- Take-off field length: 5,500 ft

- Landing field length: 3,960 ft

- Approach speed: 128 knots

- Noise requirements: ≤97.5 EPNdb

1.5.2. Mission Profile
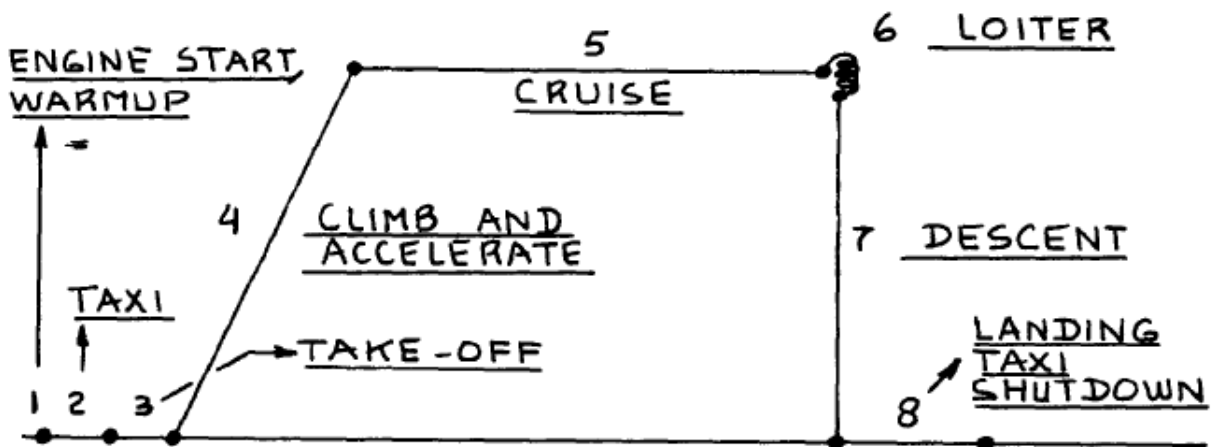
Figure 9. Mission Profile

1.6. Methodology

This hybrid aircraft will be designed and sized through a combination of techniques that will account for both the fuel and batteries. Initially, Roskam's approach using an estimated take-off weight and fuel fractions will be used to address the changing fuel weight during the various phases of the flight. The battery weight will be constant and will be sized using the work of Riboldi and Gualdoni. Trade studies will be performed to assess the best usage of fuel and batteries during each flight phase.

Once the weight has been sized, performance sizing and verification will be performed, using the smallest size engine with the lowest weight. Then the design of the fuselage will take place. This will be based on the 737-100 series aircraft, but modifications may be made to suit the payload and change in power supply. From there, the wing will be sized. Again, this will be based on the 737-100 aircraft, but changes may be made if parametric studies support changes in sweep angle, wing thickness, or taper ratio. High lift systems will be applied if they are beneficial. Analysis on the empinage design will be similar to the analysis of the wing. The last feature of the aircraft to design will be the landing gear that promotes stability and control and maintains the appropriate weight.

Drag analysis will additionally be performed to estimate the drag of the entire aircraft and calculate a L:D ratio. If the aircraft, after all additions and design changes, is within 0.5% of its initial weight, small changes will be made to reduce or resize. However, if the weight is not within 0.5%, the aircraft sizing will need to be iterated until it is within 0.5% of the initial weight.

1.7. Comparative Study of Airplanes with Similar Mission Performance

1.7.1. Comparison of Weights, Performance, and Geometries of Similar Airplanes

Table 4. Comparison of Aircraft Weights

	Boeing 737-100	Boeing 737-200	Airbus A320NEO	Embraer ERJ-170-100	ARJ21-700STD	Bombardier CRJ200- ER	SUGAR Volt 765-096-RevA
Max Design Takeoff Weight (lbs)	97,000	100,000	174,165	79,344	89,287	51,000	150,000
Max Design Landing Weight (lbs)	89,700	95,000	146,165	72,311	83,037	47,000	143,300
Max Design Zero Fuel Weight (lbs)	81,700	85,000	138,450	66,447	77,062	44,000	135,300
Operating Empty Weight (lbs)	58,600	59,900	92,814	48,733	55,016	30,500	88,800
Max Structural Payload (lbs)	23,100	25,100	44,974	19,918	19,698	13,500	30,800
Seating Capacity	96 (FAA: 124) (2 class)	124 (FAA:136) (2 class)	150 (FAA: 180) (2 class)	70 (single class)	90	50	154
Usable Fuel (gallons)	3,540	3,460	6,268	3,071	3,417	2,052	2,196
Max Fuel Capacity (gallons)	4,720	4,780	6289.6	3,093	3,196	2,135	5,416
Source(s)	(Boeing Commercial Airplanes, 2013)	(Boeing Commercial Airplanes, 2013)	(Airbus Commerial Aircraft, n.d.)	(Jane's All the World's Aircraft, 2013)	(Jane's All the World's Aircraft, 2013)	(Jane's All the World's Aircraft, 2013)	(Bradley & Droney, Subsonic Ultra Green Aircraft Research: Phase II-Volume II-Hybrid Electric Design Exploration, 2015)

*Table 5.*Comparison of Aircraft Performance (Assuming standard conditions at sea level)

	Boeing 737-100	Boeing 737-200	Airbus A320NEO	Embraer ERJ-170-100	ARJ21-700STD	CRJ200-ER	SUGAR Volt 765-096-RevA
Max Cruise Speed (Mach number)	0.82	0.82	0.82	0.82	0.82	0.85	0.7
Cruise Speed (mph)	580	580	598	529	518	534	537
Takeoff Field Length (MTOW) (ft)	5,499	5,499	6,857	4,866	5,578	5,800	8,180
Landing Field Length (ft)	3,960	3,960	5,020	4,029	5,086	4,850	--------
Service Ceiling (ft)	35,000	37,000	19,500	41,000	20,340	41,000	--------

Cruising Altitude (ft)	23,500	23,500	37,000	41,000	35,000	37,000	42,000
Range (nm)	1,720	2,645	3,078 (3,700 with sharklets)	1,800	1,200	1,893	3,500
Source(s)	(Boeing Commercial Airplanes, 2013)	(Boeing Commercial Airplanes, 2013)	(Airbus Commerial Aircraft, n.d.) (Jane's All the World's Aircraft, 2013)	(Jane's All the World's Aircraft, 2013)	(Jane's All the World's Aircraft, 2013)	(Jane's All the World's Aircraft, 2013)	(Bradley & Droney, Subsonic Ultra Green Aircraft Research: Phase II-Volume II-Hybrid Electric Design Exploration, 2015) (Bradley & Droney, Subsonic Ultra Green Aircraft Research: Phase I Final Report, 2011)

Table 6. Comparison of Aircraft Geometries

	Boeing 737-100	Boeing 737-200	Airbus A320NEO	Embraer ERJ-170-100	ARJ21-700STD	CRJ200-ER	SUGAR Volt 765-096-RevA
Overall length (ft)	94 ft	100 ft 2 in	123 ft 3.25 in	98 ft 1.25 in	109 ft 9.5 in	87 ft 10 in	139.7
Height (ft) (at max W_{oe})	37 ft 2 in	37 ft 3 in	38 ft 7 in	31 ft 11.25 in	27 ft 8.25 in	20 ft 5 in	35
Wing Area (ft^2)	1098	1098	1317.5	782.8	859.6	587.1	1477.11
Wing span	93 ft	93 ft	117 ft 5.5 (including sharkets)	85 ft 3.5 in	89 ft 6.5 in	69 ft 7 in	169.3
Cabin width	12 ft 4 in	12 ft 4in	12 ft 1.75 in	8 ft 11.75 in	10 ft 3.75 in	8 ft 5 in	----------
Fuselage width	12 ft 4 in	12 ft 4 in	12 ft 11.5 in	9 ft 11 in		8 ft 10 in	148.7
Fuselage length	90 ft 7 in	96 ft 11 in	123 ft 3 in	98 ft 1 in	99 ft 10 in	80 ft	124.8
Total Bulk Cargo (ft^3)	650	875	403	515	711.4	318	----------
Source(s)	(Boeing Commercial Airplanes, 2013)	(Boeing Commercial Airplanes, 2013)	(Airbus Commerial Aircraft, n.d.) (Jane's All the World's Aircraft, 2013)	(Jane's All the World's Aircraft, 2013)	(Jane's All the World's Aircraft, 2013)	(Jane's All the World's Aircraft, 2013)	(Bradley & Droney, Subsonic Ultra Green Aircraft Research: Phase II-Volume II-Hybrid Electric Design Exploration, 2015)

1.7.2. Configuration Comparison of Similar Airplanes

Figure 10. Boeing 737-100 aircraft configurations *(Boeing Commercial Airplanes, 2013)*
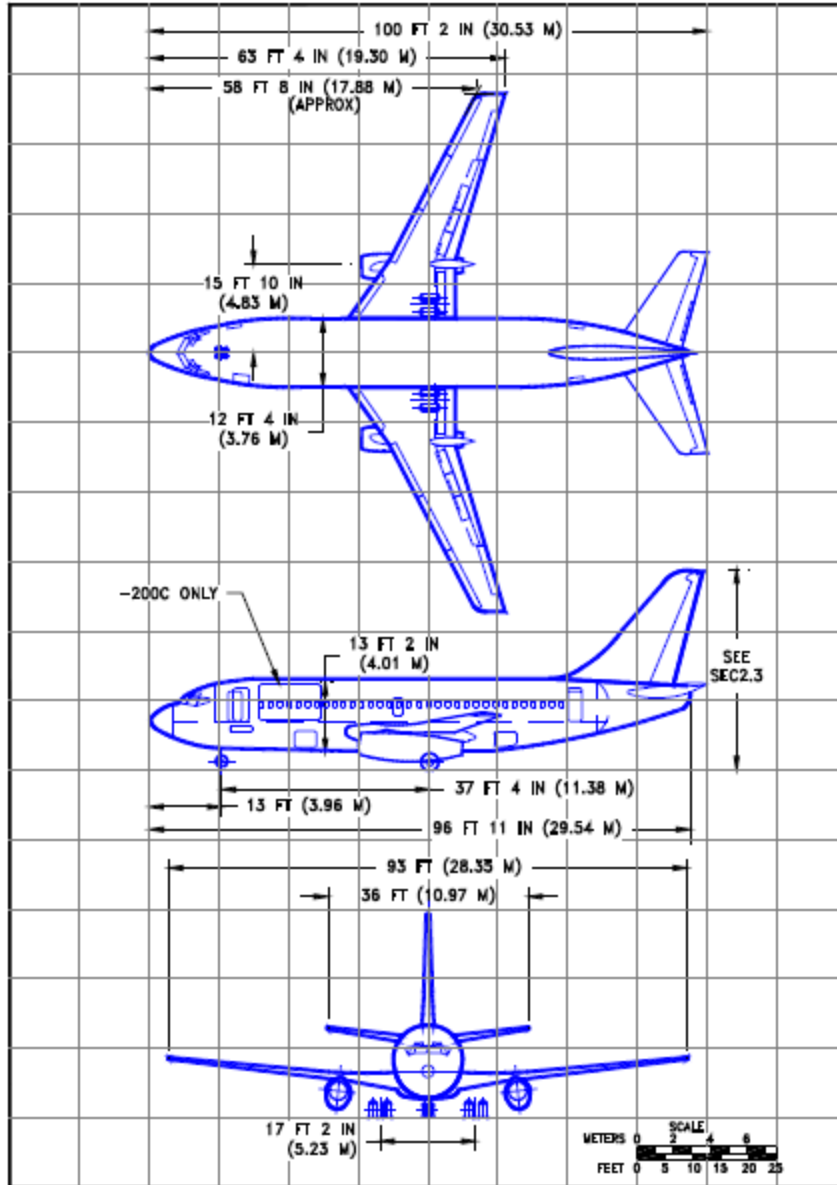
Figure 11. Boeing 737-200 aircraft configuration. *(Boeing Commercial Airplanes, 2013)*
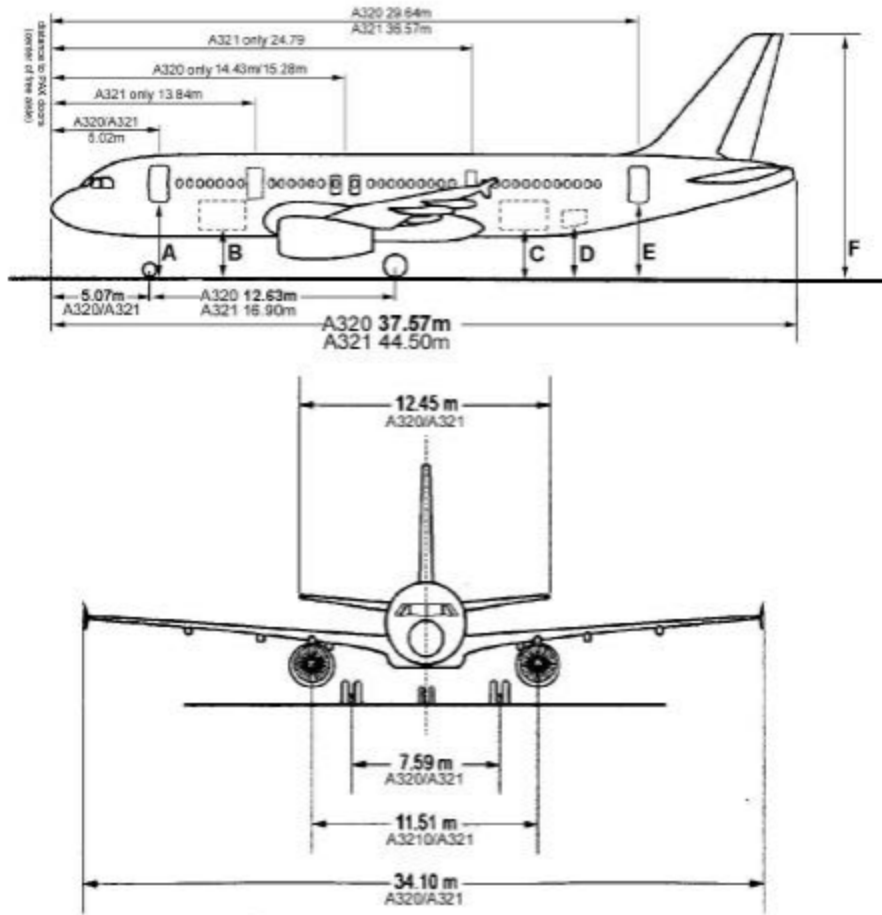
Figure 12. Airbus A320NEO aircraft configuration *(Airbus Commerial Aircraft, n.d.)*
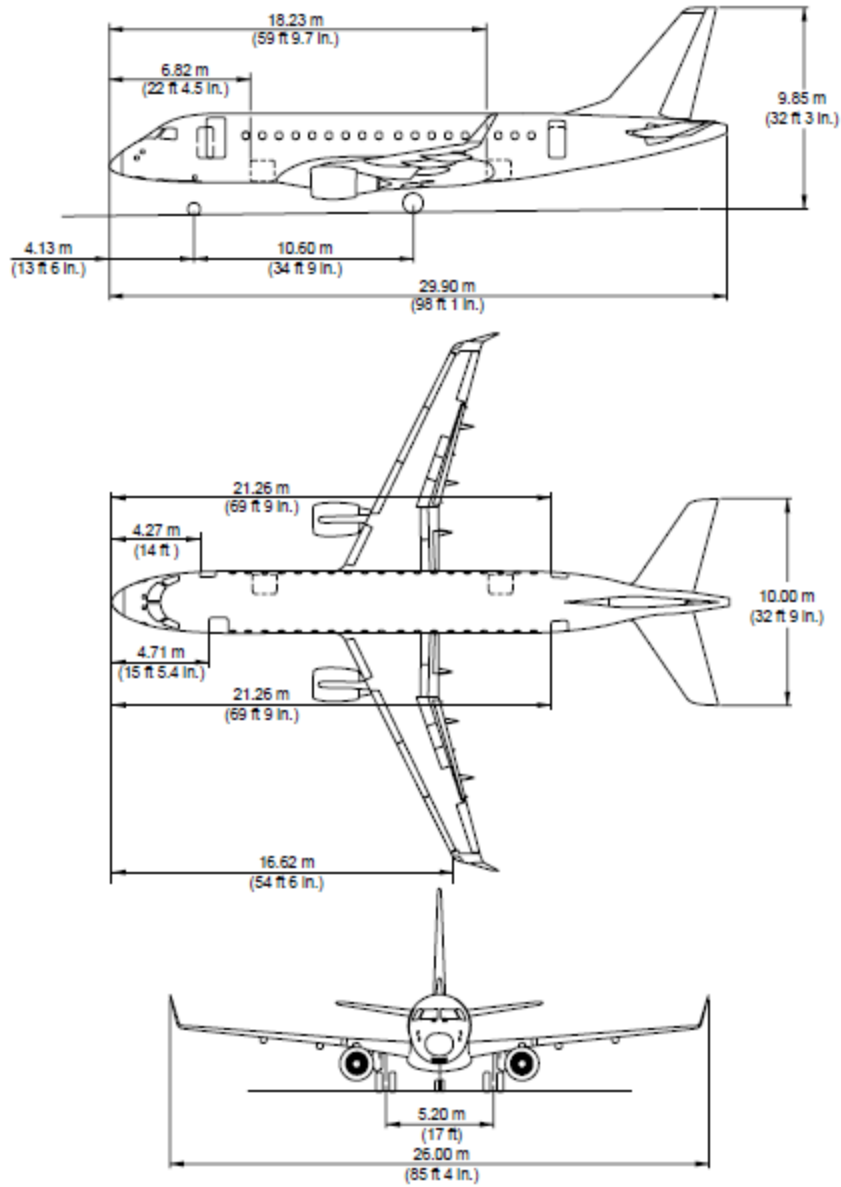
Figure 13. Embraer ERJ-170-100 aircraft configuration *(Jane's All the World's Aircraft, 2013)*
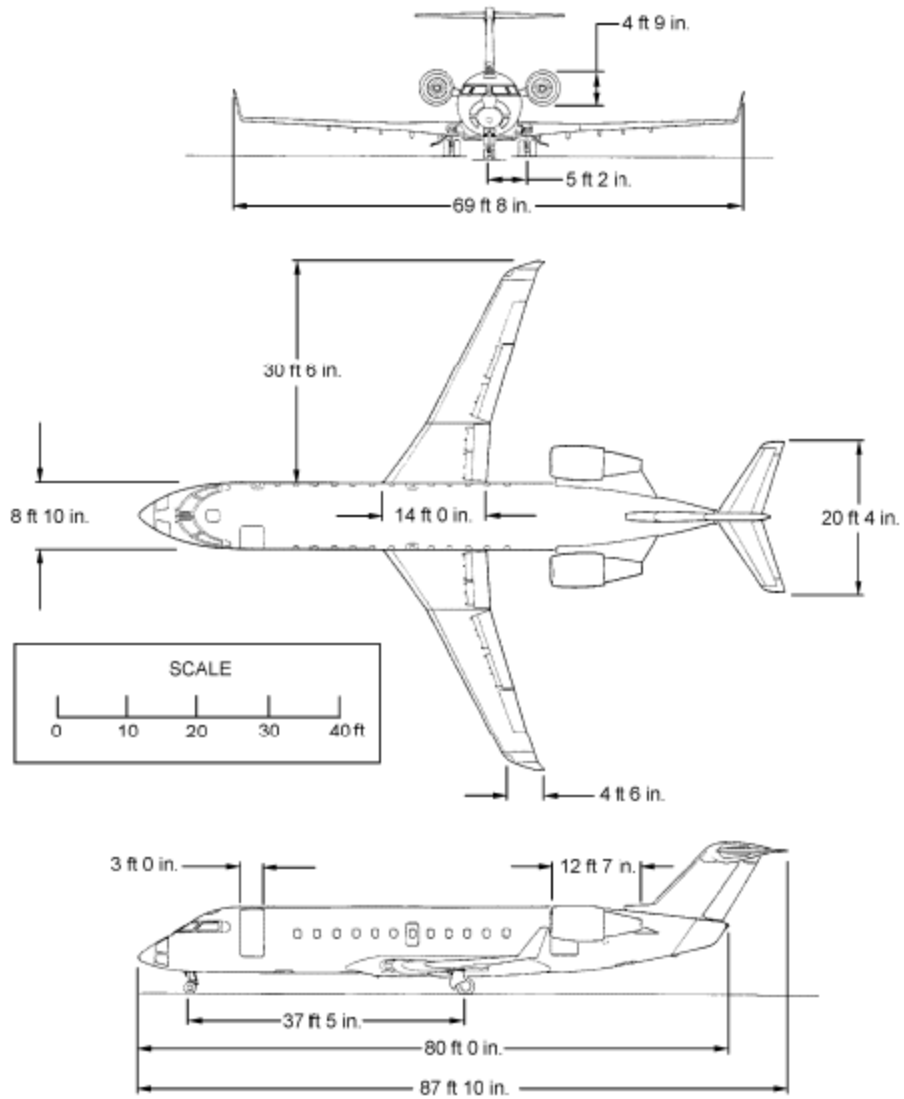
Figure 14. CRJ200-ER aircraft configuration *(Canadair Regional Jet, 2016)*
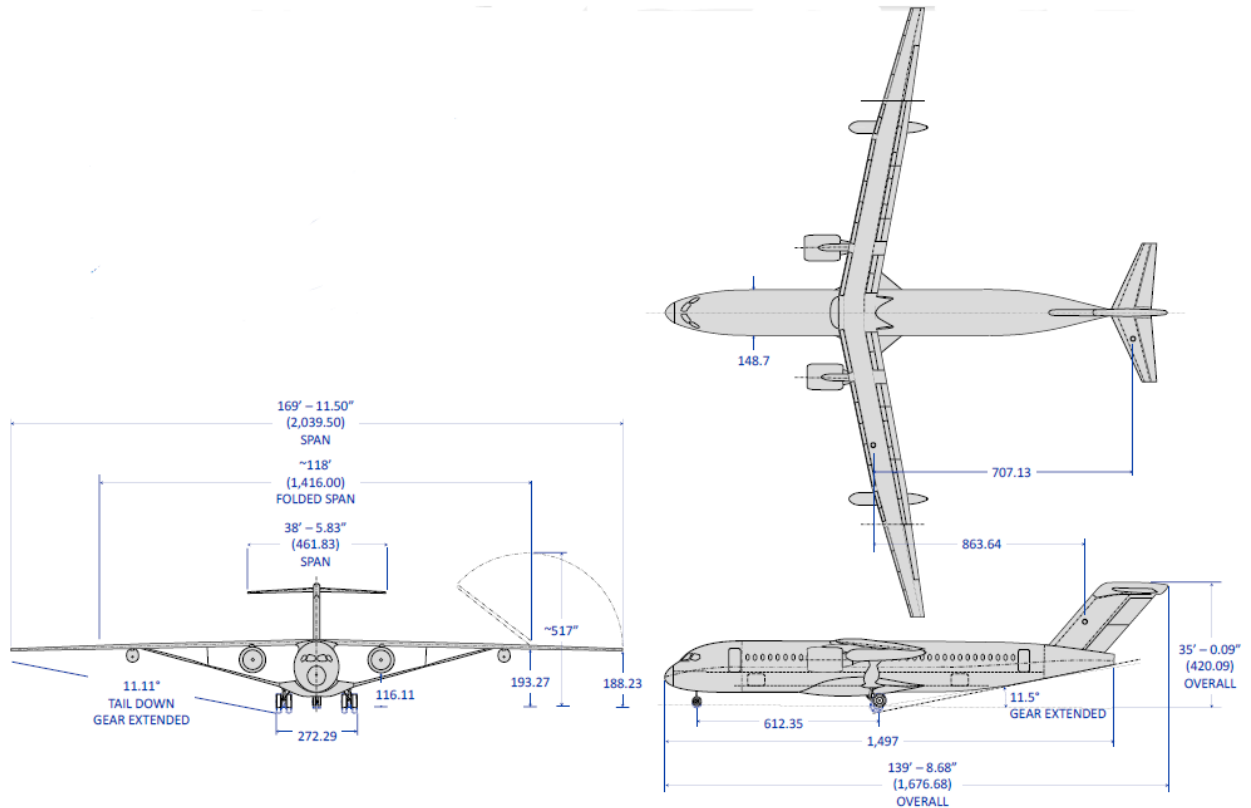
Figure 15. SUGAR Volt 765-096 RevA aircraft configuration (Bradley & Droney, Subsonic Ultra Green Aircraft Research: Phase II- Volume II- Hybrid Electric Design Exploration, 2015)

1.8. Discussion

The configuration designs of the 737-100, 737-200, A320NEO, ERJ-170-100, CRJ200-ER, and SUGAR Volt 765-096 RevA demonstrate common characteristics of transport aircraft, as observed by Figure 10. *Boeing 737-100 aircraft configurations* Figure *15.* SUGAR Volt 765-096 RevA aircraft configuration Aircraft configurations allow for many architectural options. Among these options are the wing sweep, wing style, wing position, propulsion system integration, and other added aerodynamic features. Each of these features contributes to the aircraft's ideal design for performance, design for handling qualities, and meeting FAA requirements on safety, ability, and noise.

The aircraft configurations display wings that have been aft swept. The sweep angle depends on the speed of the aircraft. Subsonic speeds allow for small sweep angles. Transonic speeds delay increase in drag, due to higher Mach numbers, by sweeping the wings 30 º -35º. Supersonic aircraft have sweep angles of 45º -70º. (Mason, 2006) The sampled aircraft have small sweep angles, with the Boeing 737-100 having a sweep angle of 25 º and the SUGAR Volt 765-096 RevA having sweep angle of 12.52º. (Bradley & Droney, Subsonic Ultra Green Aircraft Research: Phase II- Volume II- Hybrid Electric Design Exploration, 2015)

Each of the aircraft also features a low wing, excluding the SUGAR Volt 765-096 RevA. This typically provides efficient use of the fuselage cargo space and easy retraction of landing gear. This characteristic also allows for better maneuverability and smooth landing. The SUGAR Volt aircraft had additional systems to integrate involving batteries, which changed the wing configuration. It features a high wing Truss Braced Wing (TBW), which is predicted to save fuel consumption by 5-10% compared with conventional low wings. (NASA, 2014)

For the propulsion integration, the 737-100, 737-200, A320NEO, and ERJ-170-100 have two pod mounted engines suspended below the wings. This meets civil aircraft requirements of having more than one engine in the event that one becomes inoperable. The airplane must be able to complete take-off in the event of one engine failure or only 50% power with 2 engines. (Obert, 2009) The CRJ200-ER has two pod mounted engines fitted to the rear of the fuselage. These two locations, below the wings and on the aft of the fuselage, are common configurations for jet transport engines. Boeing has demonstrated that suspended engines don't incur a drag penalty. (Obert, 2009) This structural design of placing engines in nacelles suspended below the wings has several advantages. Among these are load relief, with the engines opposing the lift force; easy engine access for maintenance and repairs; and safety since the engines are further

from the passengers. (Obert, 2009) The SUGAR Volt 765-096 RevA has two engines suspended below the wings along with two battery pods suspended below the wings. This configuration allows for easy charge or exchange of batteries for quick transitions between flights. Additionally, it balances the load of the battery pod weight. (Bradley & Droney, Subsonic Ultra Green Aircraft Research: Phase II- Volume II- Hybrid Electric Design Exploration, 2015)

The tail and fin configurations also differ for the CRJ200-ER and SUGAR Volt 765-096 RevA aircraft compared to the 737-100, 737-200, A230NEO, and ERJ-170-100. The CRJ200-ER and SUGAR Volt 765-096 RevA feature a T-tail; while the other aircraft feature fuselage mounted conventional tails. Along with the fuselage mounted tails, the aircraft also have tail plane mounted fins. These different configurations provide different aircraft control. A T-tail, which is an empennage configuration where the tailplane is attached to the top of the fin, typically accompanies fuselage mounted engines. With a T-tail arrangement, there is a risk for the horizontal tail becoming engrossed by the wake of the wing at high angles of attack. (Mason, 2006) This is likely why the more common configuration is the conventional fuselage mounted tail.

The Airbus A320NEO also has added sharklets to their wings. The Sharklet wingtip devices are 7.9 feet wingtips that are standard on all NEO aircraft. They reduce fuel burn by approximately 4%, and reduce annual CO_2 emissions by approximately 9,000 tons per aircraft. (Airbus Commerial Aircraft, n.d.) This added feature could be added to other A320 aircraft as well as other aircraft models.

In summary, choosing various configurations can improve safety, increase performance, and, with added features, reduce fuel consumption. The four common aircraft configurations illustrate that the low swept wing, with two pod mounted engines suspended from the wing and

tail plane mounted fins meets the requirements of short to mid-range flights by providing greater

structural efficiency, less weight, and satisfactory stall characteristics. New advances in design

also demonstrate the benefits of the high wing TBW, as well as integration of batteries for hybrid

and electric vehicles.

2. Configuration Selection

2.1. Overall Configuration

The HTA will have a conventional configuration due to the expansive database of

conventional aircraft and design modeled after the Boeing 737 aircraft. From here, the

configurations of the fuselage, engine, wing, empennage, and landing gear will be presented with

short discussions on the rationale for selections.

2.1.1. Fuselage Configuration

The conventional fuselage will be designed to hold two cockpit crew members, 96

passengers at 6 abreast, and 2 flight attendants. Since it is designed for a short to medium range

flight, an approximate value of 175 lbs per person and 30 lbs of luggage per person will be

chosen for both the crew and the passengers. This totals 20,500 lbs, with 3,000 lbs being

designated for cargo. This cargo will be stored below the cabin floor in cargo containers that

have a capacity of 80 ft^3. According to Roskam, typical luggage density is 12.5 lb/ft^3 (Roskam,

Airplane Design Part 1: Preliminary Sizing of Airplanes, 2017). Therefore, 240 ft^3 of baggage

volume will be required for bagge storage in 3 containers.

With 6 abreast seating, there will be 16 rows, which maintains a shorter fuselage.

Although 5 abreast seating may be more comfortable for passengers, this would add an

additional 4 rows of seating, which increases the fuselage length and the aircraft weight.   The

seat pitch for tourist/economy/coach passengers ranges from 34-36 inches, and could be 30-32

inches for high density seating arrangements. (Roskam, Airplane Design Part 1: Preliminary Sizing of Airplanes, 2017) The hybrid aircraft will have a 34 in. seat pitch, and 18 in. aisles to provide a comfortable mode of transportation. Further design layouts of the fuselage will be presented in the fuselage design section.

2.1.2. Engine Configuration

The hybrid aircraft will have two engines suspended below the wings. Two engines provides for redundancy in the event of a single engine failure or 50% failure of both engines. The engines will be stored in nacelles, and two battery pods will also be stored in nacelles attached under the wing. Having the batteries outside of the aircraft allows for easier access when charging and easier exchange of the batteries for quick transitions between flights. 737-100 model airplanes used JT8D turbofan engines. For the hybrid airplane, the design could include two hFan engines with 1,380 hp and thrust equivalent to 21,000 lbf of Boeing thrust.

Although buried engines produce less drag, having the engines stored in pods outside the fuselage also provides the ability to easily repair or exchange as technology improves. This configuration also provides optimal engine operation, in-flight wing bending relief, and engine stability. Mounting the engines above the wings also has advantages, including less debris ingestion and lower noise levels. However, this is not beneficial aerodynamically, and will not be considered.

2.1.3. Wing Configuration

For the wing configuration, the airplane will have a low Cantilever wing. Low wings are ideal for transport vehicles due to the increased safety of the aircraft, increased cargo volume, and ease of maneuverability. High wings are generally best for short take-offs and landings, but offer very little cargo space. Mid wings provide the least drag during flight due to their design,

with the wings being continuous with the fuselage. This design would not be ideal for the hybrid

transport due to the fact that the fuselage volume is reduced to accommodate the wings.

The wings will be swept aft with the characteristics of the wings, including sweep angle,

aspect ratio, thickness ratio, and other features, being discussed and explored in detail later.

2.1.4. Empennage Configuration

The empennage consists of the stabilizing tail and added features on the aircraft. The

configuration for the hybrid transport aircraft will be a single verticle tail mounted to the

fuselage. Mounting to the fuselage provides adequate support. Since the tails are designed to

help recover from stalling and spinning, the vertical configuration is more reliable than the T-tail

configuration, which may be affected by the air flow, potentially causing deep stall.

2.1.5. Landing Gear Configuration

Since the hybrid vehicle is a narrow-body vehicle, the bicycle landing gear can easily be

used. This does limit the takeoff and landing locations to level ground since the landing gear

will not be able to rotate. With retractable landing gear mounted on the fuselage, the drag during

flight will not be increased, and the gears are well-supported. Having the landing gear mounted

to the nose of the fuselage provides more stability than aft wheel mounted landing gear.

However, this position increases the weight. Since weight is such a large factor in the design,

due to the already heavy batteries, mounting the retractable landing gear to the aft of the wheel

would be beneficial.

The remaining aspects of the configuration, including number of main fear struts, number

of tires, and the retraction kinematics will be discussed in detail when the landing gear is sized.

In summary the overall configuration of the aircraft will be a conventional fuselage

designed to comfortably hold 96 passengers and their luggage, The aircraft will be supported by

conventional low wings with 2 engines mounted below the wings and 2 batteries mounted below

the wings. The vertical tail will provide the stability during flight, and the tricycle aft wheel

retractable landing gear will provide adequate support with minimal weight for landing.

3.   Weight Sizing and Weight Sensitivities

Using data for takeoff weights and empty weights of similar aircraft, a plot of gross

takeoff weight vs. empty weight will be analyzed. The axes will be scaled logarithmically to

create a log-log plot of the weight data.. The regression coefficients will be calculated to

determine the weight required for takeoff and for the overall mission. A sensitivity study will be

performed using the AAA Program.

3.1 Data Base for Takeoff Weights and Empty Weights of Similar Airplanes

The following data in Table 7 provide takeoff weights and empty weights for comparison

to the HTA. Roskam additionally provides transport jet weights for comparison. The takeoff

weights and empty weights can be related linearly when graphing the log of the takeoff weight

and the log of the empty weight. The plot of this relationship is illustrated in Figure 16.

Table 7. Aircraft Takeoff and Empty Weights

Aircraft	Takeoff Weight (lbs)	Empty Weight (lbs)	Source
765-093 FREE	182,600	94,400	(Bradley & Droney, Subsonic Ultra Green Aircraft Research: Phase II- Volume II- Hybrid Electric Design Exploration, 2015)
765-095 SUGAR High	138,300	81,700	(Bradley & Droney, Subsonic Ultra Green Aircraft Research: Phase II- Volume II- Hybrid Electric Design Exploration, 2015)
Balanced 765-095 (1,380 Hp)	140,700	84,300	(Bradley & Droney, Subsonic Ultra Green Aircraft Research: Phase II- Volume II- Hybrid Electric Design Exploration, 2015)
Balanced 765-095 (1,750 Hp)	139,700	83,800	(Bradley & Droney, Subsonic Ultra Green Aircraft Research: Phase II- Volume II- Hybrid Electric Design Exploration, 2015)
Core Shutdown 765-095 (7,150 Hp)	190,000	102,600	(Bradley & Droney, Subsonic Ultra Green Aircraft Research: Phase II- Volume II- Hybrid Electric Design Exploration, 2015)
Boeing 737-100	97,000	58,600	(Boeing Commercial Airplanes, 2013)
Boeing 737-200	100,000	59,900	(Boeing Commercial Airplanes, 2013)
Airbus A320NEO	174,165	92,814	(Jane's All the World's Aircraft, 2013)
Embraer ERJ-170-100	79,344	48,733	(Jane's All the World's Aircraft, 2013)
ARJ21-700STD	89,287	55,016	(Jane's All the World's Aircraft, 2013)
CRJ200- ER	51,000	30,500	(Jane's All the World's Aircraft, 2013)

SUGAR Volt 765-096 RevA	150,000	88,800	(Bradley & Droney, Subsonic Ultra Green Aircraft Research: Phase II- Volume II- Hybrid Electric Design Exploration, 2015)
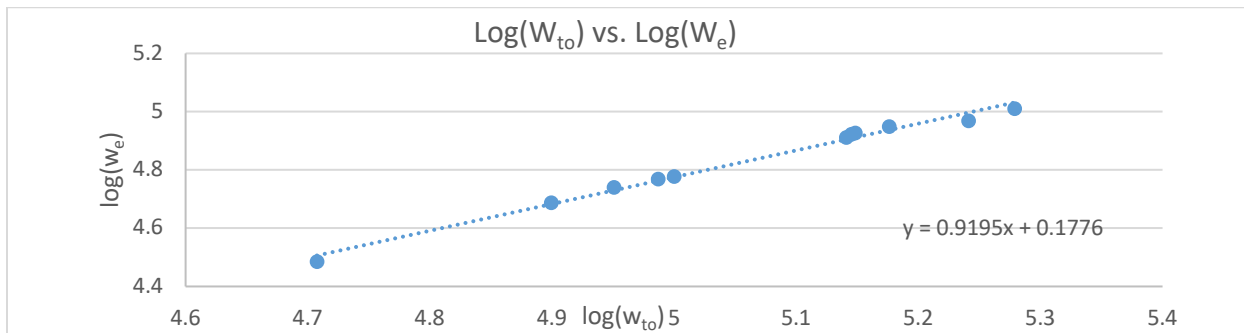
Figure 16. Log-Log Plot of Takeoff Weight vs. Empty Weight with included trendline and linear regression equation

From the plot, the regression line constants A and B can be determined, since the log of

the weights has the following relationship:

$$log(W_{to}) = A + B*log(W_e) \tag{9}$$

Thus, A=0.1776 and B= 0.9195, as demonstrated by the regression equation in the plot. In Part 1

of Roskam's Airplane Design Volumes, Roskam lists the regression line constants for various

airplane types. These are included in Figure 17. The B values obtained in this analysis are

similar, with B having an 11.44% margin of error. However, the A values are very different.

This could be due to the type of aircraft in the database. 5 of the 12 aircraft included are hybrid

vehicles. The remaining 7 are conventional fuel-powered aircraft. The A value for this database

differs by -113.2%, with the transport jet A coefficient calculated as 0.0833 and the B value as

1.0383.

The other factor that could impact the weights could be the materials used for the primary

and secondary structures, which would affect the takeoff weight and empty weight. Roskam's

database consists of Boeing 727, 737, 747, 757 and 767 aircraft, McDonnell Douglas DC 8, 9,

and 10 aircraft, Airbus A300 and A310 aircraft, and several others. The Boeing aircraft were

constructed from aluminum alloy, aluminum, and graphite composites. (Jane's All the World's

Aircraft, 2013) The Airbus aircraft were constructed from aluminum alloy, steel, and titanium.

The SUGAR aircraft have incorporated metal-matrix composites, ceramics, high temperature

polymer composites, thermoplastic composites, carbon, and nanocomposites. These will lighten

the weight of the structure, landing gear, and engine nacelles. (Bradley, Droney, & Allen, 2015)

```
        Table 2.15 Regression Line Constants A and B of Equation (2.16)
        ================================================================

  Airplane Type              A        B       Airplane Type          A        B

  1. Homebuilts                                8. Military Trainers
     Pers. fun and                                Jets             0.6632   0.8640
     transportation        0.3411   0.9519        Turboprops      -1.4041   1.4660
                                                  Turboprops
     Scaled Fighters       0.5542   0.8654        without No.2     0.1677   0.9978
     Composites            0.8222   0.8050        Piston/Props     0.5627   0.8761

  2. Single Engine                             9. Fighters
     Propeller Driven     -0.1440   1.1162        Jets(+ ext.load)0.5091   0.9505
                                                  Jets(clean)      0.1362   1.0116
  3. Twin Engine                                  Turboprops(+     0.2705   0.9830
     Propeller Driven      0.0966   1.0298         ext.load)
     Composites            0.1130   1.0403
                                            10. Mil. Patrol, Bomb and Transport
  4. Agricultural         -0.4398   1.1946        Jets            -0.2009   1.1037
                                                  Turboprops      -0.4179   1.1446
  5. Business Jets         0.2678   0.9979    11. Flying Boats,
                                                  Amphibious and
  6. Regional TBP          0.3774   0.9647        Float Airplanes 0.1703   1.0083
                                            12. Supersonic
  7. Transport Jets        0.0833   1.0383        Cruise           0.4221   0.9876
```

Figure 17. Regression Line Constants for Aircraft

For future calculations, both Roskam's constants and the calculated constants will

initially be used and comparisons in results will be made before determining the constant that

will be used in the end.

3.2. Determination of Mission Weights

The following mission weights will be estimated: $W_{pl}, W_{to}, W_f, W_e,$ and W_{bat} using

comparisons to similar aircraft, calculations from Roskam and Riboldi, and iterating through the

AAA program to verify and refine estimations.

Takeoff weight, $W_{to,}$ consists of the sum of the operating empty weight of the aircraft,

$W_{oe,}$ with the weight of the fuel, $W_{f,}$ weight of the payload, W_{pl} and the added weight of the

b

a

t

$Wto=Woe+Wf+Wpl+Wbat$ (10).

$$W_{to} = W_{oe} + W_f + W_{pl} + W_{bat} \qquad (10)$$

Note that the operating empty weight consists of the sum of the empty weight, weight of the

trapped fuel and oil, and the weight of the crew, as summarized in $Woe= W_e + W_{tfo} +$

W_{crew} (11)

$$W_{oe} = W_e + W_{tfo} + W_{crew} \qquad (11)$$

For $Wto= W_{oe} + W_f + W_{pl} + W_{bat}$ (10), the weights of

each of the parts will need to be calculated. Although the payload weight is known, the

remaining values will need to be calculated. The process for this will be conducted as follows.

Initially, a takeoff weight will be estimated using data from similar aircraft. From there, the

weights of the fuel, and batteries will be calculated. Roskam's fuel fraction method will be used

to calculate the mission fuel weight; while Riboldi's battery sizing method will be employed to

estimate mission battery weight. Then, the operating empty weight will be calculated to find an

allowable value of the empty weight. AAA will be used to iterate and find an empty weight

within 0.5% of the tentative empty weight.

3.3. Manual Calculation of Mission Weights

3.3.1. Payload Weight

The payload weight consists of the passengers and their luggage. Based on the desired

configuration of the cabin, 96 passengers will be assumed to weigh 175 lbs each and carry 30 lbs

of luggage. Thus the total payload weight is 19,680 lbs.

3.3.2. Estimated Takeoff Weight Method 1

To estimate the takeoff weight, there are two methods. The first consists of examining a

database of aircraft and comparing W_{to} to $W_{pl.}$ The database, displayed in Table 8, consists of

turbojet transport aircraft and conceptual hybrid aircraft. Using the data, an average ratio of W_{pl}

to W_{to} was calculated as 0.237. Since the payload weight is a known value, the takeoff weight

can be estimated using the ratio. Using a 96 passenger payload yields a takeoff weight value of

83,006.38 lbs. If the payload is increased to hold 100 passengers, the takeoff weight increases to

86,464.98 lbs. Finally, if the payload is increased to 108 passengers, the takeoff weight estimate

is 93,382.18 lbs.

Table 8. Data for W_{to} Comparison

	737-100	737-200	A320NEO	ERJ-170-100	ARJ21-700STD	CRJ200 - ER	SUGAR Volt 765-096-RevA	737-300	McDD DC9-80	A320
W_{to}	97,000	100,000	174,165	79,344	89,287	51,000	150,000	135,000	140,000	145,000
W_{pl}	23,100	25,100	44,974	19,918	19,698	13,500	30,800	35,000	38,000	42,000

The second method to calculate takeoff weight involves knowledge of more values.

Therefore, it will be discussed later. With an estimation of takeoff weight from the database,

calculating the fuel weight will be the next step.

3.3.3. Determination of Mission Fuel Weight

To determine the mission fuel weight, W_f, the weight of the fuel used during the mission

and the weight of the reserve fuel will need to be known. To calculate the weight of the fuel for

the mission, Roskam's fuel fraction method will be employed. This consists of breaking down

the mission into phases and estimating the fuel for each phase. The phases for the mission are:

Phase 1: Engine start and warm-up, Phase 2: Taxi, Phase 3: Takeoff, Phase 4: Climb, Phase 5

Cruise, Phase 6: Loiter, Phase 7: Descent, and Phase 8: Land, taxi, and shut-down.   This process

will be presented for the 96 passenger payload and considered for a fuel powered flight. From

there, fuel can be reduced by using batteries to power various phases of flight and eliminating

parts of the fuell fraction process. AAA will then be used to calculate weights for the aircraft if it

had used all fuel, to compare, as well as using fuel for stages 1-4 vs. fuel for stages 1-3, and 5.

To calculate the mission fuel weight, the sum of the fuel used and the fuel in reserves will need to be known.

$$W_f = W_{f_{used}} + W_{f_{res}} \qquad (12)$$

$W_{f_{used}}$ is the fuel used during the mission; while $W_{f_{res}}$ is the fuel reserves required for the mission. These reserves are specified by FAR regulations.   For a fully fuel-powered aircraft, the reserves will be 25% of the fuel used. The reserve quanitities will change depending on the fuel used during different mission phases. The fuel used will be calculated using the fuel fraction method. Each phase will have an estimated or calculated fuel fraction, which is the ratio of the ending weight of the phase to the beginning weight of the phase.

Table 9. Suggested Fuel-Fractions for Mission Phases

Mission Phase No. (See Fig.2.1) Airplane Type:	Engine Start, Warm-up 1	Taxi 2	Take-off 3	Climb 4	Descent 7	Landing Taxi, Shutdown 8
1. Homebuilt	0.998	0.998	0.998	0.995	0.995	0.995
2. Single Engine	0.995	0.997	0.998	0.992	0.993	0.993
3. Twin Engine	0.992	0.996	0.996	0.990	0.992	0.992
4. Agricultural	0.996	0.995	0.996	0.998	0.999	0.998
5. Business Jets	0.990	0.995	0.995	0.980	0.990	0.992
6. Regional TBP's	0.990	0.995	0.995	0.985	0.985	0.995
7. Transport Jets	0.990	0.990	0.995	0.980	0.990	0.992
8. Military Trainers	0.990	0.990	0.990	0.980	0.990	0.995
9. Fighters	0.990	0.990	0.990	0.96-0.90	0.990	0.995
10. Mil.Patrol, Bomb, Transport	0.990	0.990	0.995	0.980	0.990	0.992
11. Flying Boats, Amphibious, Float Airplanes	0.992	0.990	0.996	0.985	0.990	0.990
12. Supersonic Cruise	0.990	0.995	0.995	0.92-0.87	0.985	0.992

As seen in Table 9, the fuel fractions for phases 1, 2, 3, 4, 7, and 8, have been estimated and published by Roskam. (Roskam, Airplane Design Part 1: Preliminary Sizing of Airplanes, 2017) These values for transport jets will be used in the calculation of the fuel-powered aircraft. The phase 1 fuel fraction of 0.990 is the ratio of W_1/W_{to}. The phase 2 fuel fraction of 0.990 is the ratio of

W_2/W_1. 0.995 is the ratio of W_3/W_2, which is the phase 3 fuel fraction. 0.980 is the ratio of

W_4/W_3; 0.990 is the ratio of W_7/W_8, and 0.992 is the ratio of W_8/W_9. The fuel fractions,

W_5/W_4 and W_6/W_5, for phases 5 and 6, respectively, will be calculated.

F

o

r

$$R_{cr} = \left(\frac{V}{c_j}\right)_{cr} \left(\frac{L}{D}\right)_{cr} \ln\left(\frac{W_4}{W_5}\right) \tag{13}$$

The velocity for cruise is known, along with the range. The lift to drag ratio and specific fuel

a

consumption values can be found in Roskam's part 1. For transport jets in cruise, L/D ranges

from 15-24s and c_j ranges from 0.5-0.9. The following values will be used to estimate W_5/W_4:

j

$V = 500\ kts, c_j = 0.5, \frac{L}{D} = 22, and\ R_{cr} = 1656\ nm$. This yields $W_5/W_4 = 0.928$.

e

t   For the loiter phase, Breguet's endurance equation, equation $Eltr = \left(\frac{1}{c_{j_{ltr}}}\right)\left(\frac{L}{D}\right)_{ltr} \ln\left(\frac{W_5}{W_6}\right)$

(14) below, for jet airplanes can be used (Roskam, Airplane Design Part 1: Preliminary Sizing of

a
Airplanes, 2017).

i

$$E_{ltr} = \left(\frac{1}{c_{j_{ltr}}}\right)\left(\frac{L}{D}\right)_{ltr} \ln\left(\frac{W_5}{W_6}\right) \tag{14}$$

r

E_{ltr} is the loiter time in hours. According to Roskam, $c_{j_{ltr}}$ ranges from 0.4-0.6, and L/D for the
p

loiter phase ranges from 14-18. Using $E_{ltr} = 0.75\ hours, c_{j_{lrt}} = 0.4, and\ \frac{L}{D} = 18$,
l

a
$W_5/W_6 = 0.981$.

n   Now that the fuel fractions for each phase are known, the mission fuel fraction, M_{ff}, can

be calculated using $Mff = \left(\frac{W_1}{W_{to}}\right)\prod_{i=1}^{7} \frac{W_{i+1}}{W_i}$ (15) (Roskam,

Airplane Design Part 1: Preliminary Sizing of Airplanes, 2017).

B

r

$$M_{ff} = \left(\frac{W_1}{W_{to}}\right)\prod_{i=1}^{7}\frac{W_{i+1}}{W_i} \tag{15}$$

Therefore, $M_{ff} = 0.99 \cdot 0.99 \cdot 0.995 \cdot 0.98 \cdot 0.928 \cdot 0.981 \cdot 0.99 \cdot 0.992 = 0.854$. Using the

m

i

s

$$W_{f_{used}} = (1 - M_{ff})W_{to} \tag{16}$$

F

f

o

3.3.4.

m   A

f

q

u

$$log_{10}\,W_{to} = A + B \cdot log_{10}(C \cdot W_{to} - D) \tag{17}$$

h   Roskam's A and B values will be used since the calculated B value will not yield a real

d solution for the equation and hence not provide an estimated takeoff weight. D is the sum of the

p crew and passenger weight along with their cargo. Assuming 96 passengers and 4 cabin and

a n

e

f

$$C = \{1 - (1 + M_{res})(1 - M_{ff}) - M_{tfo}\} \tag{18}$$

M_{res} is the reserve fuel fraction; M_{ff} is the mission fuel fraction; and M_{tfo} is the trapped fuel and

oil fraction. M_{tfo} is assumed to be 0.005, and M_{res} is assumed to be 0.25. (Roskam, Airplane

Design Part 1: Preliminary Sizing of Airplanes, 2017) M_{ff} varies based on the amount of fuel

e
,

m

k

required. This calculation will be reviewed in the following section. For 100% fuel use,

M_{ff} =0.854. With fuel use during stages 1-4, M_{ff} =0.956. With fuel use during stages 1-3 and

5, M_{ff} =0.905.   Three different values of C were calculated based on the three different fuel

options. $C_{all\ fuel}$=0.813, C_{1-4}=0.9396, and $C_{1-3,5}$=0.876. These three different values provided

t

h

r

e

e

d

i   **3.3.5. Determining Allowable Value for Empty Weight**

f   To determine an allowable value for empty weight, for a fuel-powered aircraft, first a

tentative value for the operating empty weight is calculated, using the following equation:

e
$$W_{oe_{tent}} = W_{to_{guess}} - W_f - W_{pl} \qquad (19)$$

Since the $W_{to_{guess}}$, W_f, and W_{pl} are known, where $W_{to_{guess}}$ = 83,006.38 lbs, W_f =

15,111.6 lbs, and W_{pl} = 19,680 lbs, then $W_{oe_{tent}}$ = 48,214.8 lbs. Then, a tentative value for

the empty weight is calculated, using the following equation

t
$$W_{e_{tent}} = W_{oe_{tent}} - W_{tfo} - W_{crew} \qquad (20)$$

Since this is a tentative estimate, W_{tfo} will not be subtracted at this time. It can add as much as

0.5% of the takeoff weight, but can initially be neglected. (Roskam, Airplane Design Part 1:

Preliminary Sizing of Airplanes, 2017) With the weight of the crew and the tentative operating

empty weight, $W_{e_{tent}}$ = 48,214.8 − 820 = 47,394.8 lbs. This tentative weight is then

e

o

f

compared to a calculated weight. If these values are not within 0.5%, adjustments are made to

the takeoff weight guess and the process is iterated.

Figure 18 illustrates the trend of takeoff weights and empty weights for transport jets.

The regression line for the data has the following equation:

$$W_e = invlog_{10}((log_{10} W_{to} - A)/B)) \tag{21}$$

Since A and B are known, along with the guessed takeoff weight, W_e is calculated as 47,394.8

lbs. Since these two weights are close, but not within 0.5% of each other, adjustments will be

made to the takeoff weight guess and the empty weight will be recalculated. This process will be

completed using AAA.
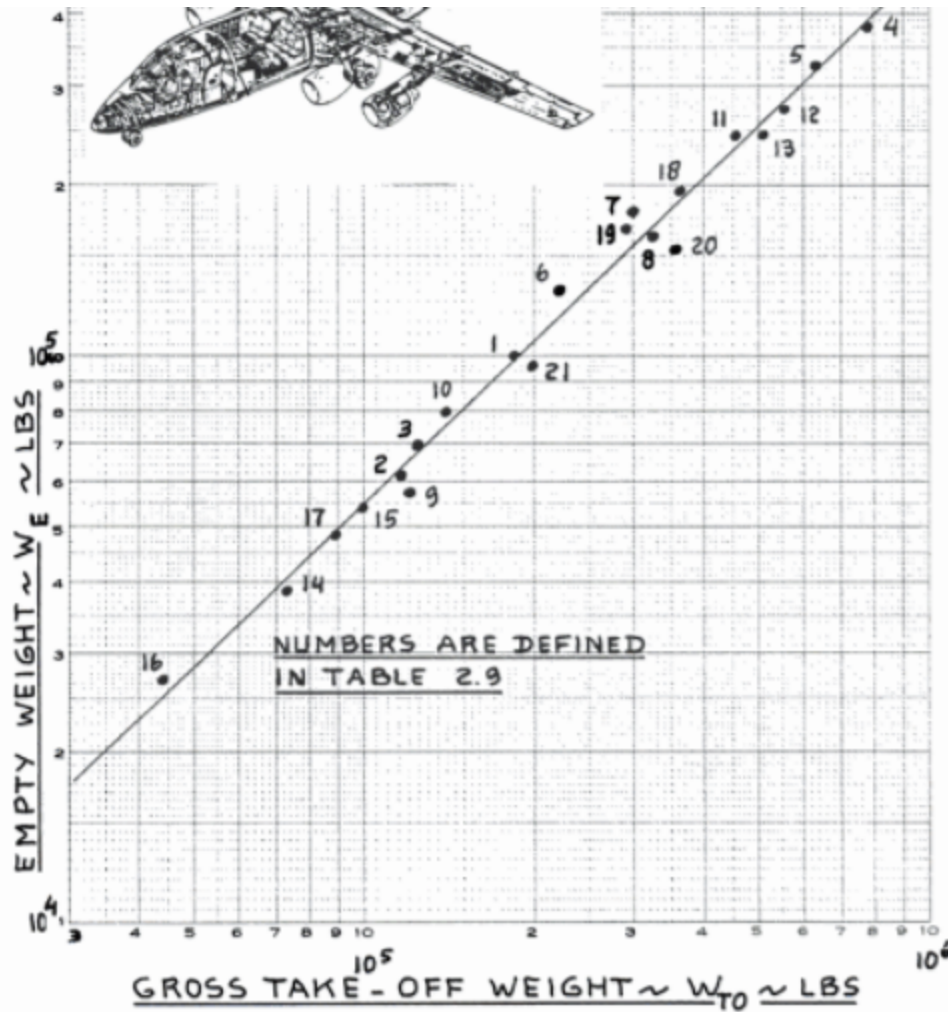
Figure 18. Weight Trends for Transport Jets

3.3.6.

To determine mission battery weight, the method of Riboldi and Gualdoni will be used.

C

I

T

A

T

I

O

N

specific power and specific energy values are values for lithium ion batteries by the year 2025,

and will likely increase further with advancements in batteries. (Hepperle)

        Since the climb, cruise, and loiter phases are the longest phases of the flight, the power

and energy required for these phases will be taken into account. To calculate the power and

e

n

e

r   From there, the power for each phase can be calculated, using S=1,341 ft^2 and the

g velocity at cruise to be 575 mph. The power at loiter is 405.34 watts, and the power at cruise is

y 736.42 watts.   The energy required for loiter is 1,094,411.5 joules, and the energy required for

cruise is 8,779,440.79 joules.

f   U

o

r

n

5.4. AAA Calculation of Mission Weights

h   The following figures summarize the output parameters generated by AAA given the

input parameters of the mission. The summary of data in the first two figures is for a twin

turbojet engine fuel-powered aircraft. The manual calculations and AAA calculations proved to

be very similar for the fuel-powered aircraft, with the AAA output weights being lower. AAA

calculated the design point takeoff weight to be 71,947.6 lbs and the empty weight to be 39,775.9

lbs. The manual calculation produced an estimate of 77,602.6 lbs for the takeoff weight and

45,439.32 lbs for the empty weight. For an all fuel-aircraft, AAA calculated 11,554 lbs of fuel,

o

n

e

including 25% reserves; while manual calculations found 15,111.6 lbs of fuel necessary, including the 25% reserve fuel.

Input Parameters

A	0.0833	$W_{passenger}$ 175 lb	W_{pilot} 175 lb	$N_{crew_{other}}$ 2	$M_{F_{res}}$ 25.000 %
B	1.0383	N_{pax} 96	N_{pilots} 2	W_{cargo} 0 lb	$W_{TO_{min}}$ 100.0 lb
$W_{TO_{est}}$ 97000.0 lb		W_{bag} 30 lb	$W_{crew_{other}}$ 205.0 lb	M_{tfo} 0.500 %	$W_{TO_{max}}$ 300000.0 lb

Output Parameters

M_{ff} 0.8715	$W_{F_{max}}$ 11554.0 lb	W_{crew} 760.0 lb	W_{useful} 31994.0 lb
$W_{F_{used}}$ 9243.2 lb	$W_{F_{res}}$ 2310.8 lb	N_{crew} 4	W_E 39593.8 lb
W_F 11554.0 lb	W_{tfo} 359.7 lb	W_{PL} 19680.0 lb	W_{TO} 71947.6 lb

Mission Profile Table: Output

	Mission Profile	W_{begin} lb	$\Delta W_{F_{used}}$ lb	$W_{F_{begin}}$ lb
1	Warmup	71947.6	719.5	11554.0
2	Taxi	71228.1	712.3	10834.6
3	Take-off	70515.8	352.6	10122.3
4	Climb	70163.3	166.2	9769.7
5	Cruise	69997.0	5075.5	9603.5
6	Loiter	64921.6	1073.1	4528.0
7	Descent	63848.5	638.5	3455.0
8	Land/Taxi	63210.0	505.7	2816.5

Figure 19. AAA output with all fuel aircraft with 2 turbojet engines
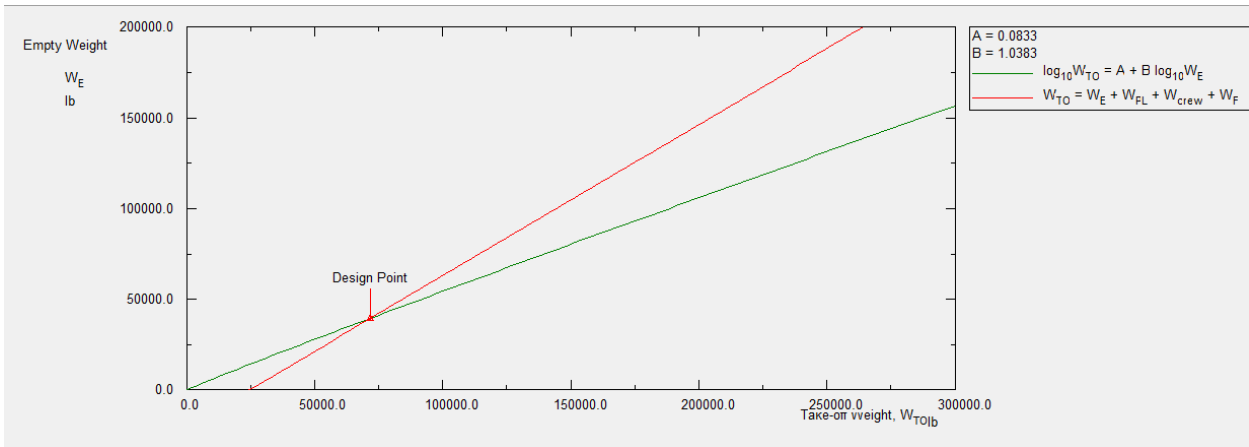
Figure 20. W_e vs. W_{to} of 2 turbojet engine fuel-powered aircraft with ideal design point of W_{to}=71,635.9 lbs and W_e=39,775.9 lbs

3.5.Takeoff Weight Sensitivities

3.5.1. Manual Calculations of Takeoff Weight Sensitivities

Aircraft takeoff weight depends on many factors. These include the payload weight, empty weight, range, endurance, lift to drag ratio, and specific fuel consumption. (Roskam, Airplane Design Part 1: Preliminary Sizing of Airplanes, 2017) Sensitivity studies will be performed on these to determine which parameters impact the design. Using Roskam's correlation coefficients of A=0.083 and B=1.038, the calculated C values, the combined crew and passenger payload weight, D=20,500 lbs, and the force, F=250,337.6 lbs, sensitivities for the takeoff weight to: payload, empty weight, range, endurance, cruise speed, L/D, and specific fuel consumption will be calculated for the HTA. Additionally, the airplane growth factor due to payload will be calculated. To illustrate the concept, calculations will be completed for the fuel-powered aircraft, initially, with sensitivities also being calculated for various amounts of fuel use. This includes using fuel in stages 1-4, 1-3 and 5, and sensitivities for an electric aircraft.

In order to calculate the sensitivities, the takeoff weight needs to be established. For the purposes of these sensitivities, the takeoff weight used will be the manually calculated takeoff weight of 77,602.6 lbs. Using equation log(Wto)= A+B*log(We)
(9) and taking the partial derivative of the takeoff weight with respect to the empty weight produces:

$$\frac{\partial W_{to}}{\partial W_e} = BW_{to}\left[invlog\left(\frac{log(W_{to})-A}{B}\right)\right]^{-1} \tag{22}$$

Substituting the values gives: $\frac{\partial W_{to}}{\partial W_e} = (1.038)(77{,}602.6)\left[invlog\left(\frac{log(77{,}602.6)-0.083}{1.038}\right)\right]^{-1}$ =1.89. As a result, for a fuel-powered aircraft, the takeoff weight must be increased by 1.89 lbs for each pound of increase in the empty weight. 1.89 is the growth factor due to empty weight for the fuel-powered aircraft. If the aircraft used fuel during phases 1-4, the growth factor would be

1.866, and it would remain the same for fuel use in phases 1-3 and 5. If the aircraft were all

electric, the growth factor would be 2.22.

To compute the sensitivities of the takeoff weight to the payload weight, the partial

d

e

r

$$\frac{\partial W_{to}}{\partial W_{pl}} = B(W_{to}) \ \{D - C(1 - B)W_{to}\}^{-1} \tag{23}$$

i

Substituting the remaining values produces $\frac{\partial W_{to}}{\partial W_{pl}} = 1.038(77,602.6)\{20,500 - 0.813(1 -$

v

$1.038)77,602.6\}^{-1} = 3.5$. Therefore, if the payload increases by 1 lb, the takeoff weight increases

by 3.5 lbs for the fuel powered aircraft. When fuel is used in stages 1-4, the airplane growth

factor due to payload is 2.5; with fuel use in stages 1-3, and 5, it's 3.5; and for an electric

airplane, the airplane growth factor due to payload is 2.2.

e   In order to calculate the sensitivity of takeoff weight to range, endurance, speed, specific

fuel consumption, and lift to drag ratio, a generic case will be considered. The variable y will

represent any parameter, excluding payload. Thus, the following equation represents the takeoff

weight sensitivity to a parameter y:

$$\frac{\partial W_{to}}{\partial y} = \{CW_{to}(1 - B) - D)^{-1}BW_{to}^2 \left(\frac{\partial C}{\partial y}\right) \tag{24}$$

Using Breguet's equations and

q $$F = -BW_{to}^2\{CW_{to}(1 - B) - D\}^{-1}(1 + M_{res})M_{ff} \tag{25}$$

Breguet's partials can be derived. They are available in Table 10, below. Using the manually

calculated values, F=250,337.6 lbs.

t

i

Table 10. Breguet Partials for Propeller and Jet Airplanes

n

		Propeller Driven	Jet
Range Case	$y = R$	$\partial \bar{R}/\partial y = c_p (375 \eta_p L/D)^{-1}$	$\partial \bar{R}/\partial y = c_j (VL/D)^{-1}$
Endurance Case	$y = E$	$\partial \bar{E}/\partial y = V c_p (375 \eta_p L/D)^{-1}$	$\partial \bar{E}/\partial y = c_j (L/D)^{-1}$
Range Case	$y = c_p$	$\partial \bar{R}/\partial y = R(375 \eta_p L/D)^{-1}$	$y = c_j$ $\partial \bar{R}/\partial y = R(VL/D)^{-1}$
Endurance Case	$y = c_p$	$\partial \bar{E}/\partial y = EV(375 \eta_p L/D)^{-1}$	$y = c_j$ $\partial \bar{E}/\partial y = E(L/D)^{-1}$
Range Case	$y = \eta_p$	$\partial \bar{R}/\partial y = -Rc_p (375 \eta_p^2 L/D)^{-1}$	Not Applicable
Endurance Case	$y = \eta_p$	$\partial \bar{E}/\partial y = -EV c_p (375 \eta_p^2 L/D)^{-1}$	Not Applicable
Range Case	$y = V$	Not Applicable	$\partial \bar{R}/\partial y = -Rc_j (V^2 L/D)^{-1}$
Endurance Case	$y = V$	$\partial \bar{E}/\partial y = Ec_p (375 \eta_p L/D)^{-1}$	Not Applicable
Range Case	$y = L/D$	$\partial \bar{R}/\partial y = -Rc_p (375 \eta_p (L/D)^2)^{-1}$	$\partial \bar{R}/\partial y = -Rc_j (V(L/D)^2)^{-1}$
Endurance Case	$y = L/D$	$\partial \bar{E}/\partial y = -EV c_p (375 \eta_p (L/D)^2)^{-1}$	$\partial \bar{E}/\partial y = -Ec_j (L/D)^{-2}$

Note: R in sm
V in mph

Note: R in nm or sm
V in kts or mph

Substituting in range and endurance for y, respectively, yields

$$\frac{\partial W_{to}}{\partial R} = F c_j \left(V \left(\frac{L}{D} \right) \right)^{-1} = 16.7 \text{ lbs/nm and } \frac{\partial W_{to}}{\partial E} = F c_j \left(\frac{L}{D} \right)^{-1} = 7{,}699.7 \text{ lbs/hr.}$$ In summary, if the

range of the fuel aircraft is decreased by 1 nm, the takeoff weight decreases by 16.7 lbs. If the

endurance is increased by 1 hour, the takeoff weight is increased by 5,563 lbs.

Continuing to use Breguet's partials in Table 10, the sensitivities of takeoff weight to

cruise speed will be calculated. Assuming a cruise speed of 500 kts or M=0.75, L/D=22, cruise

range of 1656 nm, and specific fuel consumption of 0.5, $\frac{\partial W_{to}}{\partial V} = -37.7$ lbs/kt. Therefore, if the

cruise speed could be increased without changing any parameters, the gross takeoff weight

would decrease. Despite these results, this sensitivity result is not practical. An increase in

cruise speed results in a decrease in the lift coefficient and thus a decrease in the lift to drag ratio.

The specific fuel consumption will also change. (Roskam, Airplane Design Part 1: Preliminary

Sizing of Airplanes, 2017) All of these factors change the sensitivity of takeoff weight to cruise speed.

Finally, sensitivities of takeoff weight to L/D and to specific fuel consumption will be calculated during cruise and loiter. For the cruise phase, a cruise speed of 500 kts will be assumed, along with L/D ratio of 22, c_j=0.5, and a force of 250,337.6 lbs. For the loiter phase, the lift to drag ratio will be 18, c_j=0.4, and F=250,337.6 lbs. Using Breguet's partials, the sensitivity of takeoff weight to L/D for range is -856.3; the sensitivity of takeoff weight to L/D for endurance is -154.5; the sensitivity of takeoff weight to c_j for range is 37,679.3; and the sensitivity of takeoff weight to c_j for endurance is 6,953.8. If L/D were increased, for both cruise and loiter, the takeoff weight would decrease. For cruise, if L/D were increased by 1, the takeoff weight would decrease by 856.3 lbs. Similarly. For loiter, if L/D were increased by 1, the takeoff weight would decrease by 154.5 lbs. For the specific fuel consumption, if c_j increases, the takeoff weight increases. For example, for the cruise phase, if c_j was incorrectly assumed to be 0.5 instead of 0.9, the takeoff weight would increase by 0.4*37,679.3 or 15,071.7 lbs. Similarly, if if c_j was incorrectly assumed to be 0.4 instead of 0.6, during loiter, the takeoff weight would increase by 0.2*6,953.8 or 1,390.8 lbs.

3.5.2. AAA Calculation of Takeoff Weight Sensitivities

The following data, displayed in Figure 21, summarizes AAA's calculations of takeoff weight sensitivities for a fuel-powered aircraft with a takeoff weight of 71,947.6 lbs. According to AAA, if the payload were to increase by 1 lb, the takeoff weight would increase by 3.29 lbs. If the crew weight were to increase by 1 lbs, the takeoff weight would increase by 3.29 lbs. Finally, if the empty weight were to increase by 1 lb, the takeoff weight would increase by 2.04 lbs. For an electric aircraft, the takeoff weight increases by 2.17 lbs per pound increase of

payload. The takeoff weight increases by 2.17 lbs for every 1 pound increase in crew, and the if

the empty weight increases by 1 pound, the takeoff weight increases by 1.86 lbs.

The sensitivities for the hybrid aircraft with fuel use in phases 1-4 or 1-3 and 5 have

similar values with their values being between the fuel-powered aircraft and the electric aircraft.

This holds true for both the manual calculations and the AAA calculations.
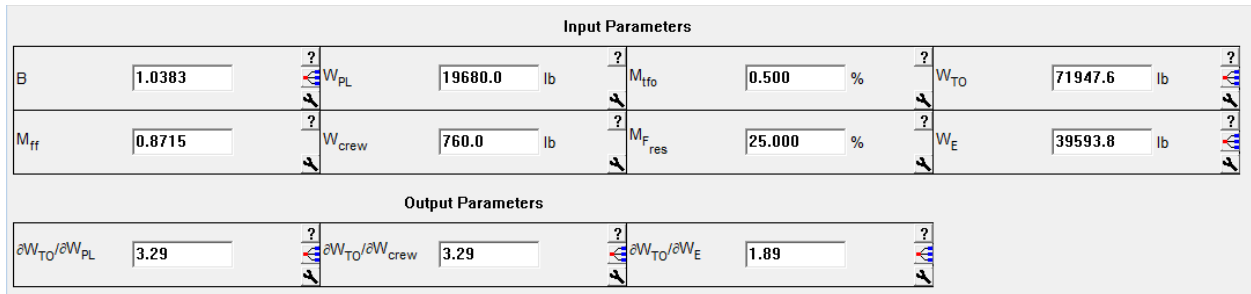
Figure 21. Takeoff weight sensitivities calculated by AAA for fuel-powered aircraft
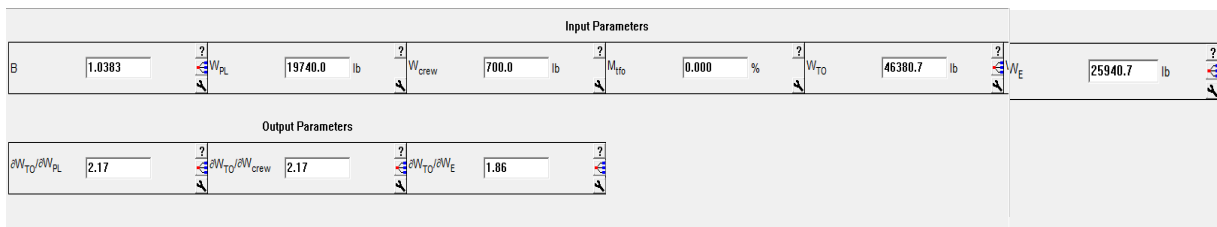
Figure 22. Takeoff weight sensitivities calculated by AAA for electric aircraft

3.6. Trade Studies

Trade studies of takeoff weight versus L/D, payload, range, and specific fuel

consumption will be performed. These trade studies are being performed on the HTA which will

use fuel in stages 1-4. Additionally, a trade study of range vs. payload will be performed by

AAA for the fuel-powered aircraft to compare.

3.7. Takeoff Weight vs. Critical Mission Parameters

3.7.1. Takeoff Weight vs. L/D
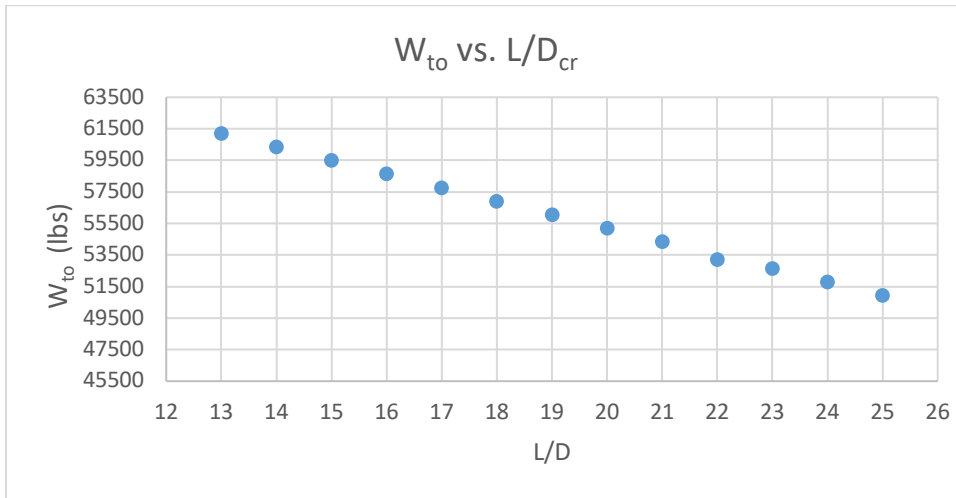
Figure 23. Takeoff Weight vs. L/D for Cruise
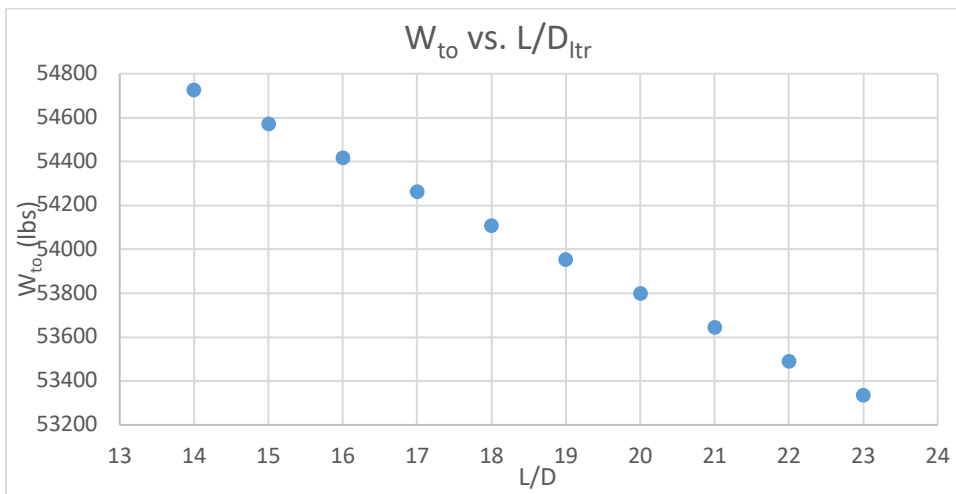
Figure 24. Takeoff Weight vs. L/D for Loiter

3.7.2. Takeoff Weight vs. Payload
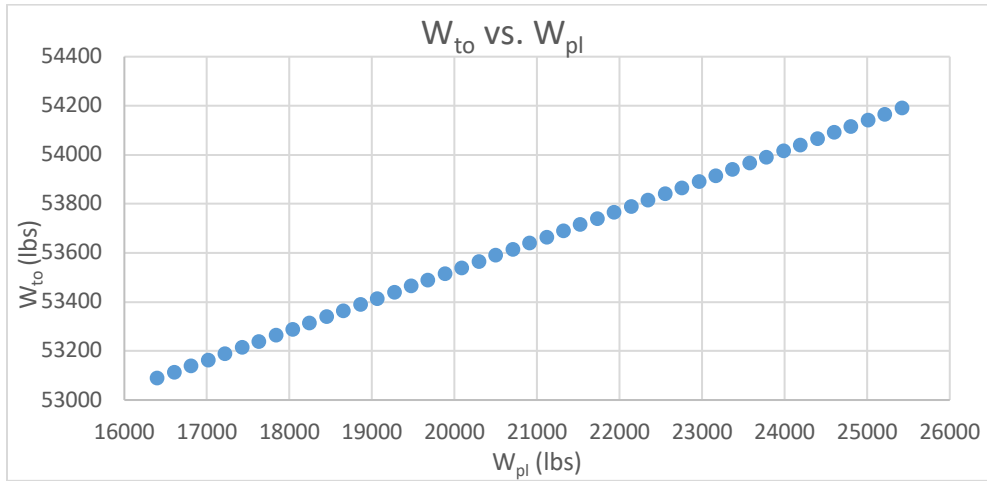
Figure 25. Takeoff Weight vs. Payload Weight (ranges from 80 passengers to 124 passengers)

3.7.3. Takeoff Weight vs. Range
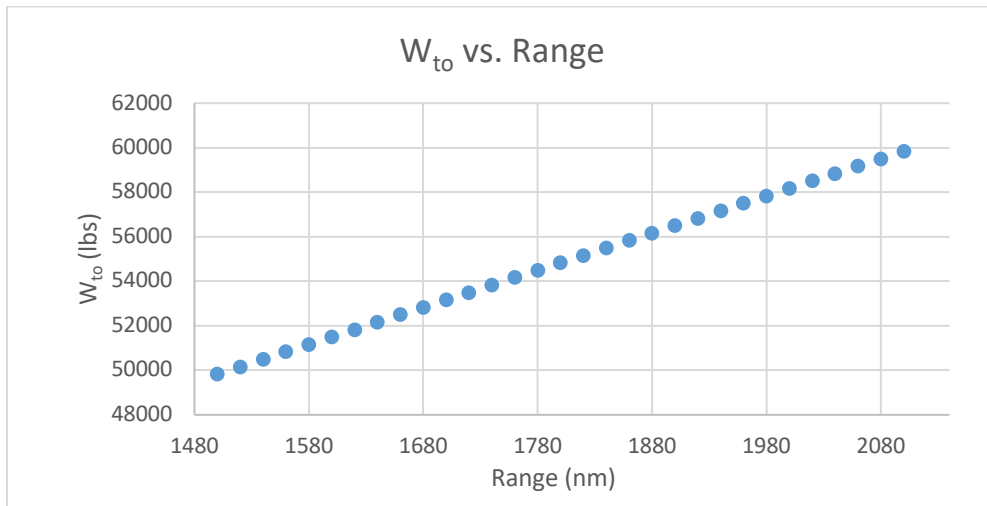
Figure 26. Takeoff Weight vs. Range

3.7.4. Takeoff Weight vs. Specific Fuel Consumption
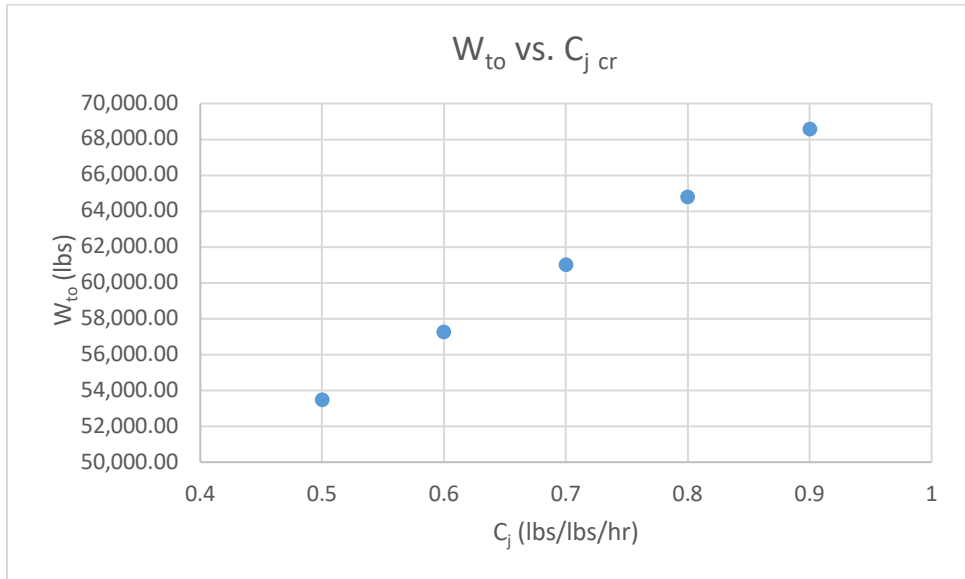
Figure 27. Takeoff Weight vs. Specific Fuel Consumption during Cruise
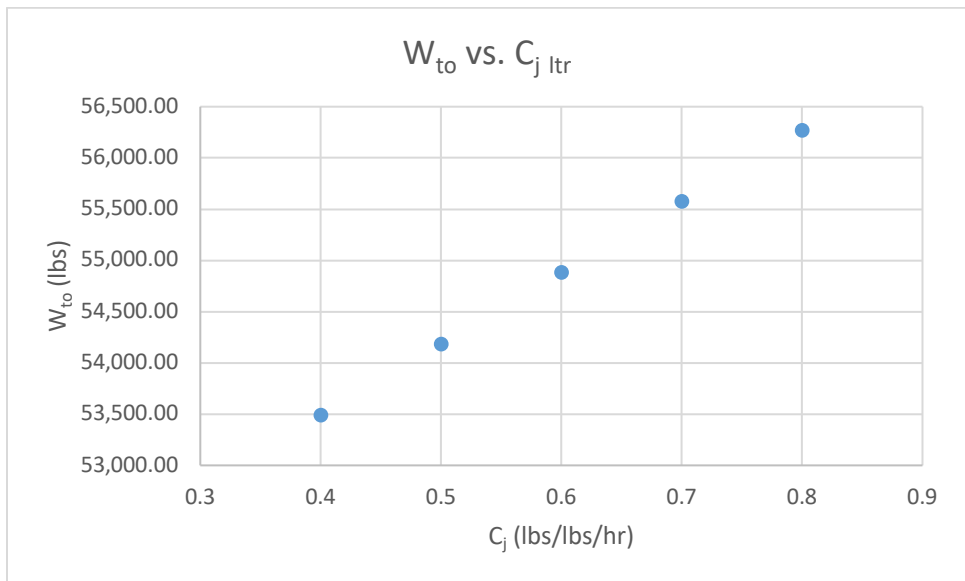
Figure 28. Takeoff Weight vs. Specific Fuel Consumption during Loiter
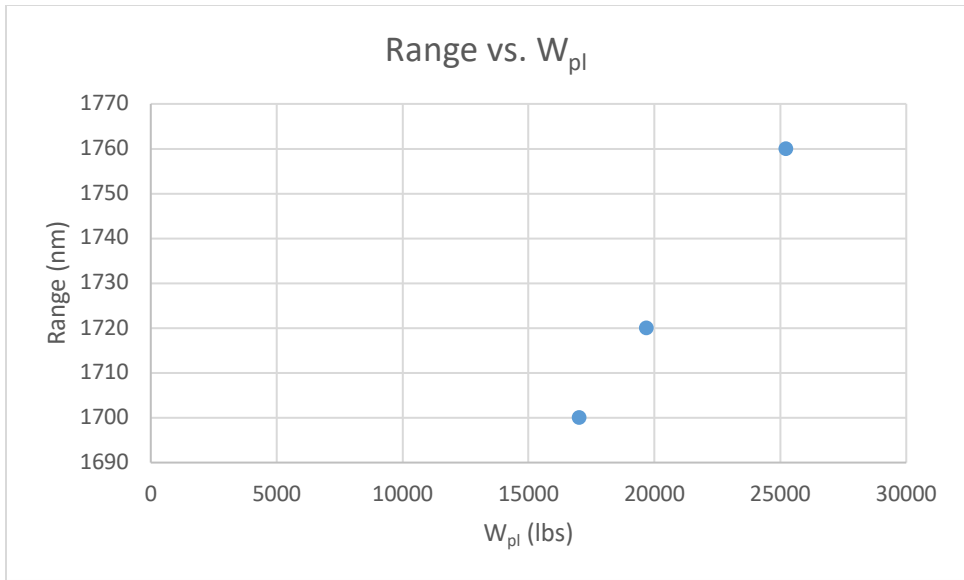
Figure 29. Range vs. Payload

3.8. AAA Calculation of Range vs. Payload
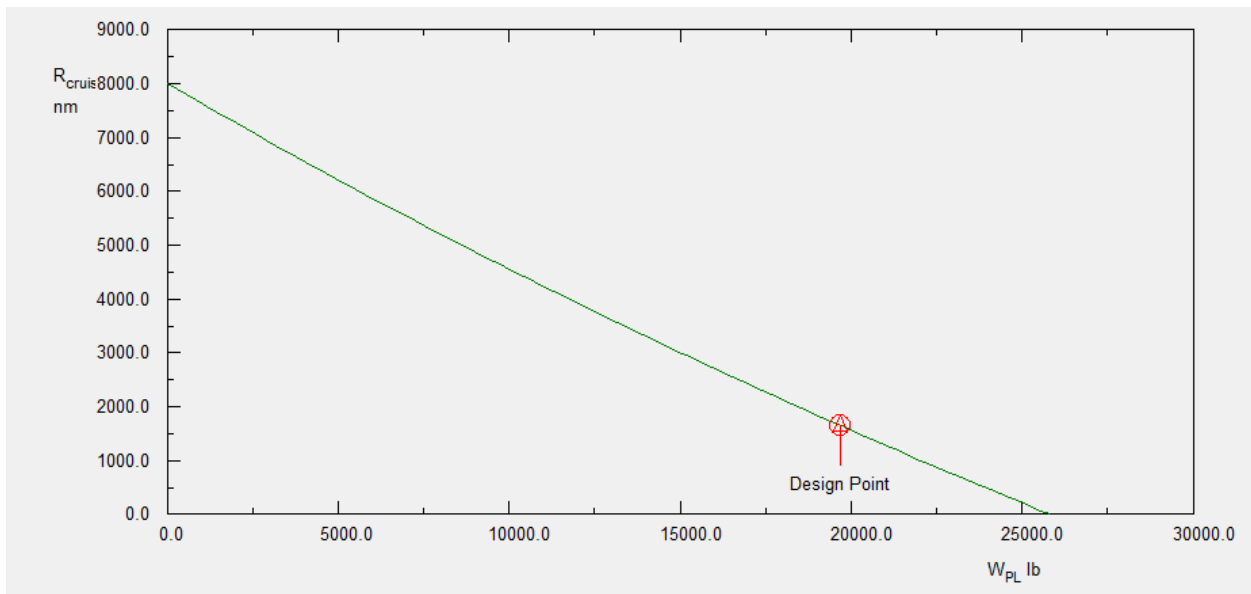
Figure 30. Range vs. Payload with design point W_{pl}=19,630.6 lb and R_{cr}=1,638.7 nm for fuel-powered aircraft

3.9. Trade Study Conclusions

The estimated takeoff weight of 53,778.38 lbs, which is the sum of the manually

calculated takeoff weight for the HTA and the batteries, assuming fuel is used during phases 1-4

of flight and lithium ion batteries supply the power for phases 5-8. This weight is represented in

the trade study graphs and lies between the design points for the electric aircraft the the fuel-

powered model.

The sensitivity studies demonstrated that the takeoff weight is strongly affected by the

empty weight, the payload, specific fuel consumption, and lift to drag ratio. The aircraft is able

to meet its mission specifications, based on the trade studies. From here constraint analyses will

be performed, and the remaining systems will be designed.

4. Determination of Performance Constraints

Using FAR 25 requirements, data presented in Roskam's Airplane Design volumes, and

the HTA mission requirements, the performance constraints to which the HTA will be sized will

be calculated and discussed. Calculations will be performed manually and with AAA. Then the

results will be compared and analyzed. The performance constraints of stall speed, takeoff field

length, landing field length, cruise speed, climb rate, time to climb to cruise, and maneuvering

have an impact on the performance of the aircraft. Aircraft wing area, takeoff thrust (or takeoff

power), maximum required lift coefficient for takeoff, and maximum required lift coefficient for

landing include stall speed compose the airplane design parameters that are affected by the stall

speed, takeoff field length, landing field length, cruise speed, climb rate, time to climb to cruise,

and maneuvering.

Together, the results will determine a range of values for wing loading, W/S, thrust

loading, T/W, and maximum lift coefficient, $C_L$max. These values will be the result of meeting

performance requirements, and specific values will be chose that allow for the lowest takeoff

weight and minimize cost.

4.1. Manual Calculation of Performance Constraints

4.1.1. Stall Speed Sizing

The HTA will be designed to meet stall speed requirements, which, in turn, will define an allowable W/S for a given maximum lift coefficient. $C_{L_{max}}$ is influenced by the wing and airfoil design, flap type and size, and the center of gravity location (Roskam, Airplane Design Part 1:

$$V_S = \left(\frac{2(W/S)}{\rho C_{L_{max}}}\right)^{1/2} \qquad (26)$$

stall speeds during takeoff, cruise, and landing at different M will be calculated. The 737-100 aircraft has a wing loading value of 433.33 kg/m². Assuming standard conditions on the ground and at altitude, $\rho = 1.225 \frac{kg}{m^3}$ and $\rho = 0.4135 \frac{kg}{m^3}$, respectively, $S = 102 m^2$ and varying $C_{L_{max}}$ values of 0.45, 03.5, and 0.3 at $M = 0.75, 0.74, and\ 0.78$, respectively, the stall speed during cruise with M=0.74, $C_{L_{max}} = 0.5$ at 40,000 ft is calculated as follows:

$$V_S = \left(\frac{2(433.33 kg/m^2)}{0.4135 kg/m^3 (0.5)}\right)^{1/2} = 125.8\ kts$$

The table below summarizes the stall speeds at various stages based on varying mach and lift coefficient values.

Table 11. Stall Speed Sizing

Parameter	Stage	Cruise	Cruise	Cruise	Cruise	Takeoff	Landing
C_L		0.45	0.5	0.3	0.58	1.75	2.73
V_s (kts)		116.9	162.5	125.9	132.7	39.1	53.9

4.1.2. Takeoff Distance Sizing

According to Roskam, takeoff weight, takeoff speed, thrust to weight ratio at takeoff, the aerodynamic drag coefficient, and pilot technique all play a role in takeoff distance sizing

(Roskam, Airplane Design Part 1: Preliminary Sizing of Airplanes, 2017). As a result, some

parameters will be assumed to be fixed; while others will be changed to determine the thrust

loading, T/W, for a given maximum lift coefficient and wing loading.

Since the field length required for takeoff, S_{TOFL}, is proportional to the wing loading,

thrust to weight ratio, and the maximum lift coefficient at takeoff, the following equation is true:

$$S_{TOFL} \propto \frac{(W/S)_{to}}{\sigma C_{L_{max}}(T/W)_{to}} = Top_{25} \qquad (27)$$

Note that Top_{25} is the takeoff parameterin lbs/ft^2, that meets FAR 25 requirements. Substituting

in values for the density ratio, varying $C_{L_{max}}$ values, and varying wing loading values, various

thrust loadings are calculated. As sample calculation with $\sigma = 0.861$ at 5000 ft elevation with

standard conditions and $C_{L_{max}} = 1.2$ and $(W/S)_{to} = 40 \ lbs/ft^2$ produces:

$$\frac{40 \ lbs/ft^2}{0.861(1.2)(217.3969 \ lbs/ft^2)} = 0.1533 \ lb/lbf = W/S_{to}$$

The following tables summarize varying lift coefficient values and wing loading values at

various altitudes of takeoff and at various field lengths.

Table 12. Takeoff Distance Sizing for S_{TOFL} =5000 ft at 0 ft altitude

$C_{L_{max to}}$	1.200	1.600	1.750	2.000	2.400
W/S$_{TO}$					
40.000	0.250	0.188	0.171	0.150	0.125
60.000	0.375	0.281	0.257	0.225	0.188
80.000	0.500	0.375	0.343	0.300	0.250
100.000	0.625	0.469	0.429	0.375	0.313
120.000	0.750	0.563	0.514	0.450	0.375
140.000	0.875	0.656	0.600	0.525	0.438
160.000	1.000	0.750	0.686	0.600	0.500

Table 13. Takeoff Distance Sizing for S_{TOFL} =6000 ft at 0 ft altitude

$C_{L_{max_{to}}}$ W/S$_{TO}$	1.200	1.600	1.750	2.000	2.400
40.000	0.208	0.156	0.143	0.125	0.104
60.000	0.313	0.234	0.214	0.188	0.156
80.000	0.417	0.313	0.286	0.250	0.208
100.000	0.521	0.391	0.357	0.313	0.260
120.000	0.625	0.469	0.429	0.375	0.313
140.000	0.729	0.547	0.500	0.438	0.365
160.000	0.833	0.625	0.571	0.500	0.417

Table 14. Takeoff Distance Sizing for S_{TOFL} =9468 ft at 5000 ft altitude

$C_{L_{max_{to}}}$ W/S$_{TO}$	1.200	1.600	1.750	2.000	2.400
40.000	0.153	0.115	0.105	0.092	0.077
60.000	0.230	0.172	0.158	0.138	0.115
80.000	0.307	0.230	0.210	0.184	0.153
100.000	0.383	0.287	0.263	0.230	0.192
120.000	0.460	0.345	0.315	0.276	0.230
140.000	0.537	0.402	0.368	0.322	0.268
160.000	0.613	0.460	0.421	0.368	0.307

Table 15. Takeoff Distance Sizing for S_{TOFL} =10800 ft at 8000 ft altitude

$C_{L_{max_{to}}}$ W/S$_{TO}$	1.200	1.600	1.750	2.000	2.400
40.000	0.147	0.110	0.101	0.088	0.074
60.000	0.221	0.166	0.151	0.133	0.110
80.000	0.295	0.221	0.202	0.177	0.147
100.000	0.368	0.276	0.252	0.221	0.184
120.000	0.442	0.331	0.303	0.265	0.221
140.000	0.515	0.387	0.353	0.309	0.258
160.000	0.589	0.442	0.404	0.353	0.295

4.1.3. Landing Distance Sizing

Parameters affecting the landing distance include the landing weight, approach speed, method to decelerate, the pilot's landing technique, and the quality of the aircraft (Roskam, Airplane Design Part 1: Preliminary Sizing of Airplanes, 2017). Considering that the aircraft is a hybrid, the landing weight will be heavier than conventional transport aircraft. Comparing the conceptual SUGAR aircraft weight ratio of maximum landing weight to takeoff weight, or W_L/W_{to}, provides a strong estimate for hybrid transport weight ratios. Although the fuel depreciates during the stages of the flight, the battery weight does not change, and therefore, the plane will be heavier at landing than an identical fuel-powered aircraft.

The following assumptions will be made for the landing distance sizing: standard conditions, applied brakes to stop the aircraft, and a takeoff weight of 77, 602 lbs. Various approach speeds, field lengths, weight ratios, and lift coefficients at landing will determine the possible wing loading values for the HTA.

Using the desired approach speed, the field length can be found.

$$S_{FL} = 0.3V_A^2 \tag{28}$$

From there, the stall speed at landing can be found using:

$$V_A = 1.3V_{S_L} \tag{29}$$

Then, the $(W/S)_L$ results from

$$(W/S)_L = \frac{V_{S_L}^2(0.002378)}{2} * C_{L_{max_L}} \tag{30}$$

Thus, for an approach speed of 128 kts, the field length is 4915 ft. The landing stall speed is 98.46 kts. Using a $C_{L_{max_L}}$ value of 1.7, the wing loading at landing is 55.8. Then the takeoff wing loading value can be calculated with $W/S_{to} = \frac{W/S_L}{0.96} = 58.2$.

The W_L/W_{to} values considered include 0.85, 0.9, 0.93, and 0.96. Together with the

varying maximum landing C$_L$ values of 1.7, 2, 2.3, 2.6, and 2.73, and the range of approach

speeds from 114 kts to 129 kts, the field length and the wing loading at takeoff were calculated.

The summary of the manual calculations is pesented in the tables below.

Table 16. W/S$_{to}$ with W$_L$/W$_{to}$=0.85

		$C_{L_{max_L}}$						
V$_A$ (kts)	S$_{FL}$ (ft)	1.700	2.000	2.300	2.600	2.730	3.000	3.400
128.000	4915.200	65.689	77.281	88.873	100.465	105.488	115.921	131.377
114.900	3960.603	52.931	62.272	71.613	80.953	85.001	93.408	105.862
115.470	4000.000	53.458	62.891	72.325	81.759	85.846	94.337	106.915
122.474	4500.000	60.140	70.753	81.365	91.978	96.577	106.129	120.279
129.099	5000.000	66.822	78.614	90.406	102.198	107.308	117.921	133.644

Table 17. W/S$_{to}$ with W$_L$/W$_{to}$=0.9

		$C_{L_{max_L}}$						
V$_A$ (kts)	S$_{FL}$ (ft)	1.700	2.000	2.300	2.600	2.730	3.000	3.400
128.000	4915.200	62.039	72.987	83.935	94.884	99.628	109.481	124.078
114.900	3960.603	49.990	58.812	67.634	76.456	80.279	88.218	99.981
115.470	4000.000	50.488	59.397	68.307	77.216	81.077	89.096	100.975
122.474	4500.000	56.799	66.822	76.845	86.868	91.212	100.233	113.597
129.099	5000.000	63.110	74.247	85.384	96.521	101.347	111.370	126.219

Table 18. W/S$_{to}$ with W$_L$/W$_{to}$=0.93

		$C_{L_{max_L}}$						
V$_A$ (kts)	S$_{FL}$ (ft)	1.700	2.000	2.300	2.600	2.730	3.000	3.400
128.000	4915.200	60.038	70.633	81.228	91.823	96.414	105.949	120.076
114.900	3960.603	48.378	56.915	65.452	73.990	77.689	85.373	96.756
115.470	4000.000	48.859	57.481	66.103	74.726	78.462	86.222	97.718
122.474	4500.000	54.966	64.666	74.366	84.066	88.270	97.000	109.933
129.099	5000.000	61.074	71.851	82.629	93.407	98.077	107.777	122.148

Table 19. W/S$_{to}$ with W$_L$/W$_{to}$=0.96

V$_A$ (kts)	S$_{FL}$ (ft)	$C_{L_{max_L}}$ 1.700	2.000	2.300	2.600	2.730	3.000	3.400
128.000	4915.200	58.162	68.426	78.689	88.953	93.401	102.638	116.324
114.900	3960.603	46.866	55.136	63.407	71.677	75.261	82.705	93.732
115.470	4000.000	47.332	55.685	64.038	72.390	76.010	83.527	94.664
122.474	4500.000	53.249	62.646	72.042	81.439	85.511	93.968	106.497
129.099	5000.000	59.165	69.606	80.047	90.488	95.012	104.409	118.330

4.1.4. Climb Requirement Sizing

In order to size to the climb requirement, the drag polar is necessary to find. The drag coefficient can be summarized as:

$$C_D = C_{D_0} + \frac{C_L^2}{\pi A e} \qquad (31)$$

$$C_{D_0} = f/S \qquad (32)$$

Since the HTA is modeled after the Boeing 737-100 aircraft, Roskam's correlation coefficients for parasite area vs. wetted area will be used along with the regression line coefficients for takeoff weight vs. wetted area. These regression coefficients are a= -2.5229, b=1, c=0.0199, and d=0.7531. These coefficients are used in the following equations:

$$log_{10}(f) = a + b * log_{10}(S_{wet}) \qquad (33)$$

$$log_{10}(S_{wet}) = c + d * log_{10}(W_{to}) \qquad (34)$$

Using A=8.83, from the Boeing 737-100 model and the e values from Roskam, the drag polars

c

a

n

Table 20. Configuration Parameters and Drag Polars

Configuration	C_{D_0}	A	e		C_{D_i}	$C_{L_{max}}$	C_D
Clean	0.013772	8.83	0.85		0.205265	2.2	0.219037
Takeoff flaps	0.0334	8.83	0.8		0.137999	1.75	0.171399

c

a

landing flaps	0.0784	8.83	0.75	0.358223	2.73	0.436623
gear down	0.015	8.83	------	-------	------	------

These values can be used to calculate the thrust loading at takeoff that meets FAR 25 specifications. The following FAR specifications are for a takeoff climb.   For FAR 25.111 (OEI), the configuration consists of gears up, takeoff flaps, ground effects, CGR>0.012 and $1.2V_{S_{to}}$. For FAR 25.121 (OEI), the configuration consists of gears down, takeoff flaps, ground effects, CGR>0, and the speed ranging between V_{LOF} and $1.2V_{S_{to}}$. For FAR 25.121 (OEI), the configuration consists of gear up, takeoff flaps, no ground effects, and speed at $1.2V_{S_{to}}$. For FAR 121 (OEI), the configuration consists of gears up, flaps up, maximum continuous thrust on remaining engines, CGR>0.012, and speed at $1.25V_S$ (Roskam, Airplane Design Part 1: Preliminary Sizing of Airplanes, 2017).

In the event of a necessary landing climb from a balked landing, there are two FAR specifications to meet. FAR 25.119 (AEO) requires CGR>0.032, and a configuration of gears down, landing flaps, takeoff thrust on all engines, maximum design landing weight, and $1.3V_{S_L}$. FAR 25.121 (OEI) requires CGR>0.021, and a configuration of gears down, approach flaps, takeoff thrust on remaining engines, and $1.5V_{S_A}$. (Roskam, Airplane Design Part 1: Preliminary Sizing of Airplanes, 2017) A summary of these results is presented in the tables below.

Table 21. FAR 25.111 (gears down, TO flaps, with additional T/W calculated for *50°C* increase)

C_L modified	1.215278
C_D	0.09995
L/D	17.50869
T/W_{to}	0.138229
T/W_{to} (Modified for +50°C)	0.172786

Table 22. FAR 25.121 (gears down, TO flaps, with additional T/W calculated for *50°C* increase)

$C_{L_{LOF}}$ (V=$1.1V_{S_{TO}}$)	1.446281

C_D	0.127655
L/D	11.3296
T/W$_{to}$	0.176529
C_L (for $V_2 = 1.2V_{S_{TO}}$)	1.215278
C_D	0.11495
L/D	10.57219
T/W$_{to}$	0.189175
*Since V_2 is the more critical value, we will calculate T/W_to modified temperature	
T/W$_{to}$ (Modified for +50ºC)	0.220661

Table 23. FAR 25.111 (gears down, TO flaps, with additional T/W calculated for *50ºC* increase)

C_L modified	1.215278
C_D	0.09995
L/D	12.15881
T/W$_{to}$	0.21249
T/W$_{to}$ (Modified for +50ºC)	0.265612

Table 24. FAR 25.121 (gears up, flaps up, with additional T/W calculated for *50ºC* increase and maximum thrust at 0.94)

C_L modified	1.408
C_D	0.102477
L/D	13.7397
T/W$_{to}$	0.145437
T/W$_{to}$ (Modified for +50ºC and 94% thrust)	0.1934

Table 25. FAR 25.119 (AEO) (balked landing, gears down, flaps down)

C_L modified	1.615385
C_D	0.218824
L/D	7.382124
T/W$_{to}$	0.167462
W_L	72946.44
T/W$_{to}$ (Modified for +50ºC)	0.222689

Table 26. FAR 25.121 (OEI) (balked landing, gears down, flaps down)

C_L modified	1.035556
C_D	0.122444

L/D	8.457407
T/W$_{to}$	0.278479
W_L	72946.44
T/W$_{to}$ (Modified for +50ºC)	0.327213

From the data presented in the tables, the rate of climb at altitude and sea level, along

with the altitude, absolute ceiling, and other parameters can be found. This information is

summarized in Table 27.

Table 27. Sizing to Time to Climb Requirements

Sizing to Time to Climb Requirements		
rate of climb at altitude h (ft/min)	RC_h	366.2041
rate of climb at sea level (ft/min)	RC_0	3295.837
Height (ft)	h	40000
absolute ceiling (ft)	h_{abs}	45000
time to climb (min)	t_{Cl}	30
rate of climb (ft/min)	RC	3158.786
	V	957.3788
	T/W (english)	3.377
	L/D	12.88834
	W/S	291.184
	density	0.000738

4.1.5. Maneuvering Requirement Sizing

Maneuvering requirements are generally listed in mission specifications for military

aircraft, agrigultural aircraft, or acrobatic aircraft. Since the HTA's mission specifications do not

include maneuvering capabilities, the aircraft will not be sized to meet these capabilities.

4.1.6. Cruise Speed Requirement Sizing

In order to size to cruise speed requirements, the following equations will be used

(Roskam, Airplane Design Part 1: Preliminary Sizing of Airplanes, 2017).

$$T_{reqd} = C_D \bar{q} S = C_{D_0} \bar{q} S + \frac{C_L^2 \bar{q} S}{\pi A e} \qquad (36)$$

$$W = C_L \bar{q} S \tag{37}$$

Combining the two equations by dividing by the weight yields:

$$\frac{T}{W_{reqd}} = \frac{C_{D_0} \bar{q} S}{W} + \frac{C_L^2 \bar{q} S}{W \pi A e} \tag{38}$$

4.2. AAA Calculation of Performance Constraints

4.2.1. Stall Speed Sizing
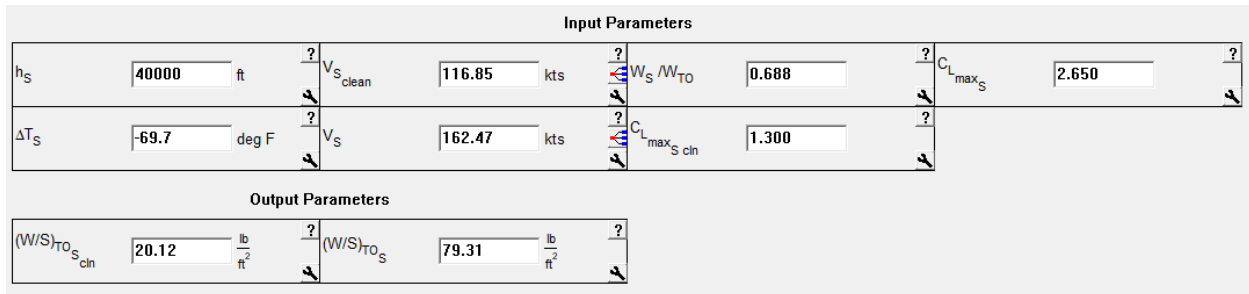
Figure 31. AAA results of stall speed sizing

4.2.2. Takeoff Distance Sizing
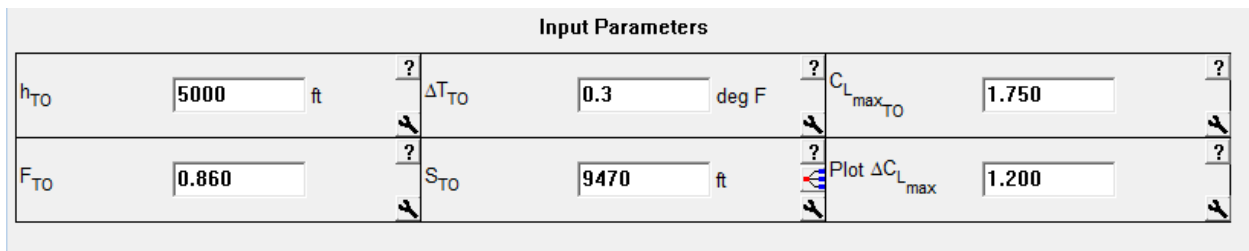
Figure 32. AAA results of takeoff distance sizing

4.2.3. Landing Distance Sizing
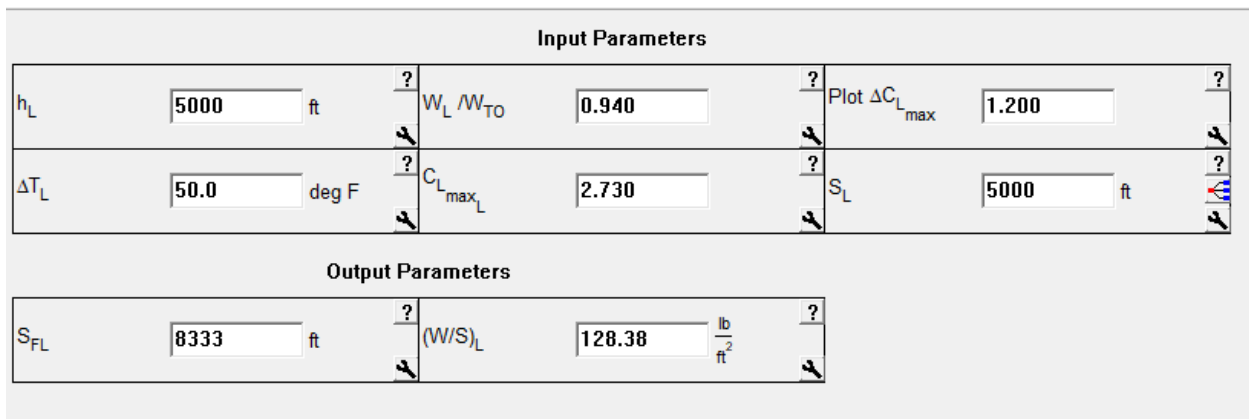
Figure 33. AAA results of landing distance sizing

4.2.4. Climb Requirement Sizing

Figure 34. AAA results of climb requirement sizing

4.2.5. Cruise Speed Requirement Sizing

Figure 35. AAA results of cruise speed requirement sizing

4.2.6. Matching Plot
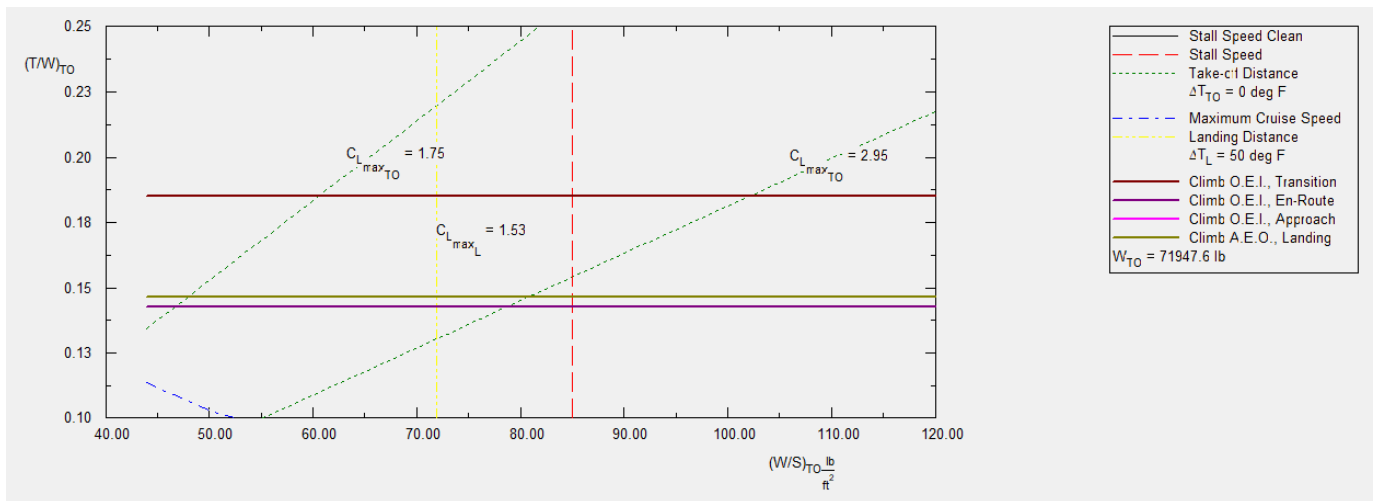
Figure 36. AAA results of the performance sizing plot

From the performance sizing plot, a design point with a wing loading of 128.34 lb/ft² and a thrust

to weight ratio of 0.31 has been chosen. This yelds a $C_{L_{max_L}}$=2.73 , $C_{L_{max_{TO}}}$=2.25, $S_w =$

560.61 ft^2, and a thrust of 21,766 lbs.

5. Fuselage and Cockpit Design

The cockpit and fuselage design will be modeled after the Boeing 737-100 model aircraft.

Utilizing Roskam's *Airplane Design Part* 3, each of these sections will be designed with using

typical arrangements that take into account human factors.

5.1. Cockpit Design

The cockpit will be designed for two pilots with standard heights and weight. The

cockpit will be initially sized to hold two male crew members, as female crew members are

typically smaller. The pilots will be assumed to weigh 175 lbs, based on body component

weights and the fact that they will not be wearing a helmet. For dimensions, the body width

consists of the shoulder width, which will be estimated at 21 in. across, the width at the elbows,

estimated at 22 in. across, and the hip width at 18 in. across. The weights and dimensions include

flight clothing. The remaining dimension assumptions are illustrated in Figure 37, below.
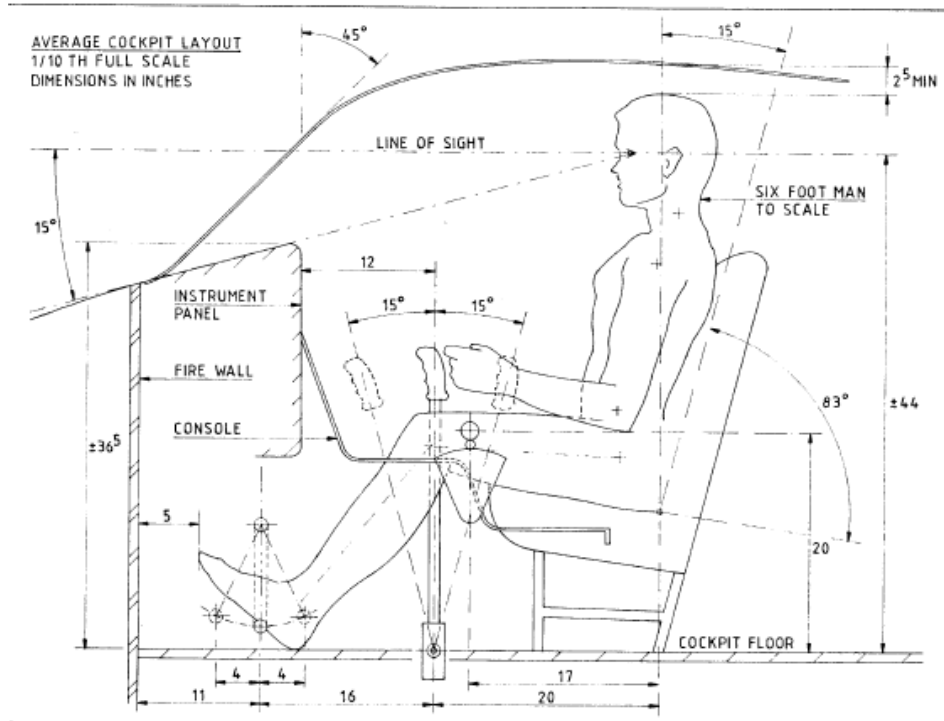
Figure 37. Dimensions of sitting male crew member in cockpit *(Roskam, 2011)*.

   The cockpit design must also take into account the visibility during takeoff, cruise, and landing. Figure 37 also illustrates the angles for line of sight. Roskam defines cockpit visibility as "the angular area obtained by intersecting the airplane cockpit with radial vectors emanating from the eyes of the pilot" (Roskam, 2011). The point C, in Figure 38, lies on the eyes of the pilot. Figure 39 demonstrates the minimum visbility pattern for transport aircraft, per FAR 25 specifications.
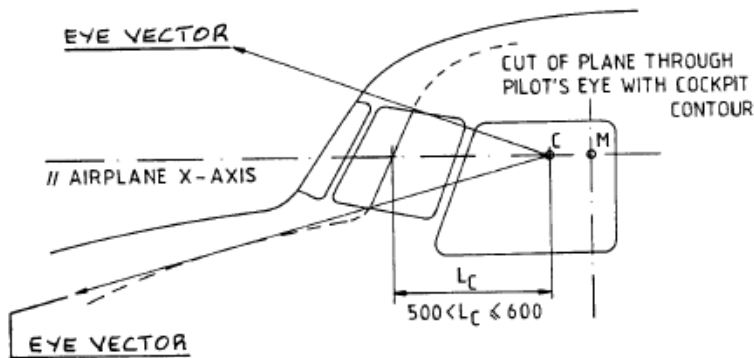
Figure 38. Radial eye vectors emanating from C. *(Roskam, 2011)*
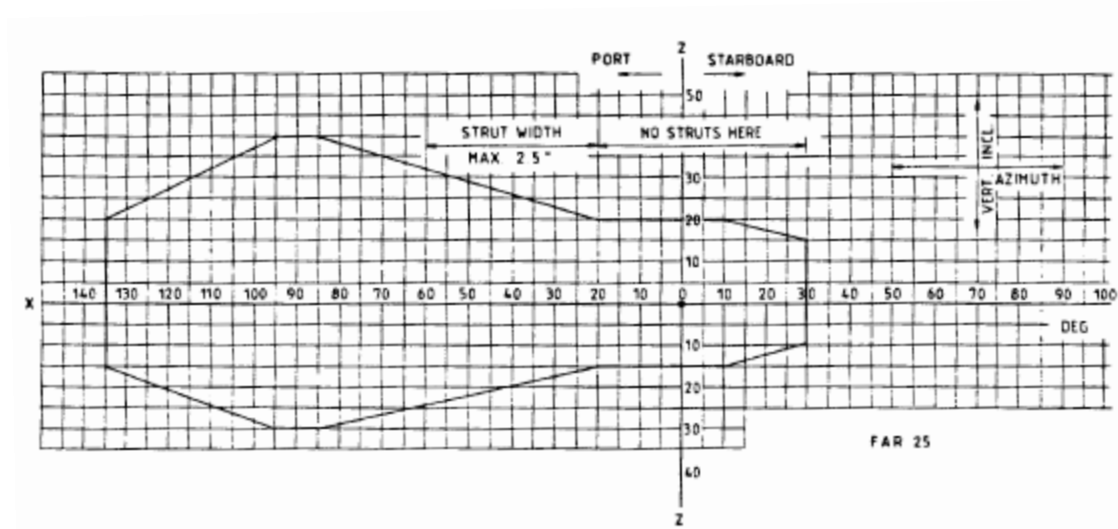
Figure 39. Ideal minimum visibility pattern for transport aircraft. *(Roskam, 2011)*

The cockpit layouts in section 5.1.1. meet the visibility requirements and height, width, and

weight requirements for the pilots. They are from the Boeing 737-100 model since the exchange

of the hybrid engine, and battery nacelles will not change the fuselage nor cockpit design.

5.1.1. Cockpit Layout Design
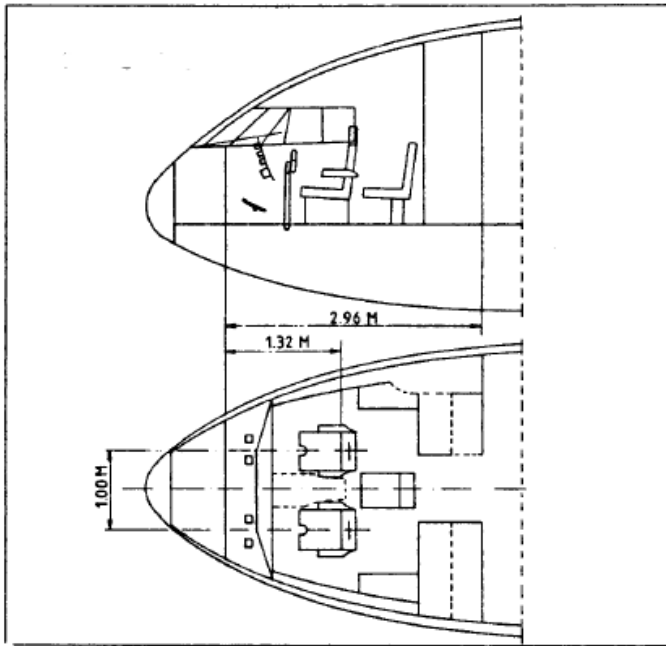
Figure 40. Side and top-down view of cockpit. Dimensions in meters *(Boeing Commercial Airplanes, 2013)*
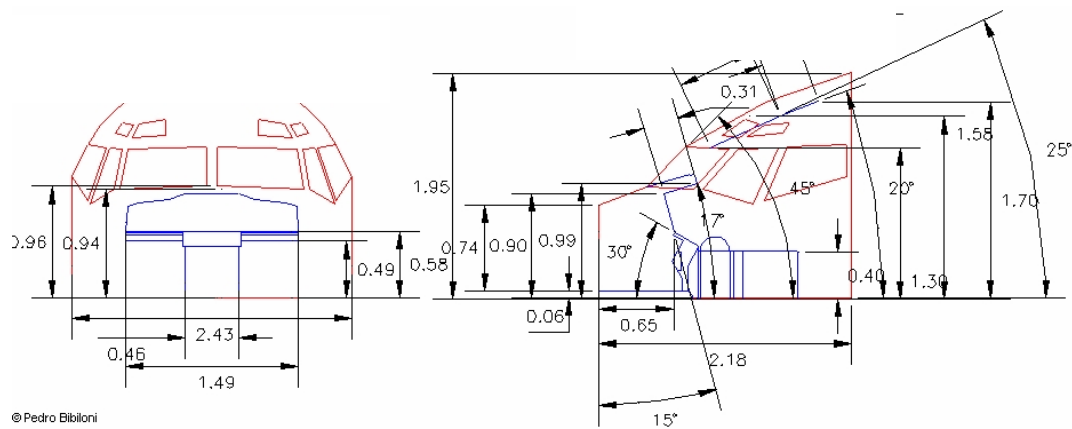
Figure 41. Front and side 3-D view of cockpit. Dimensions in meters *(Boeing Commercial Airplanes, 2013)*

Figure 42. Rear view of cockpit. *(Aircraft Technical Data and Specifications: Boeing 737-100/200, 2017)*

5.2. Fuselage Design

5.2.1. Fuselage Layout Design
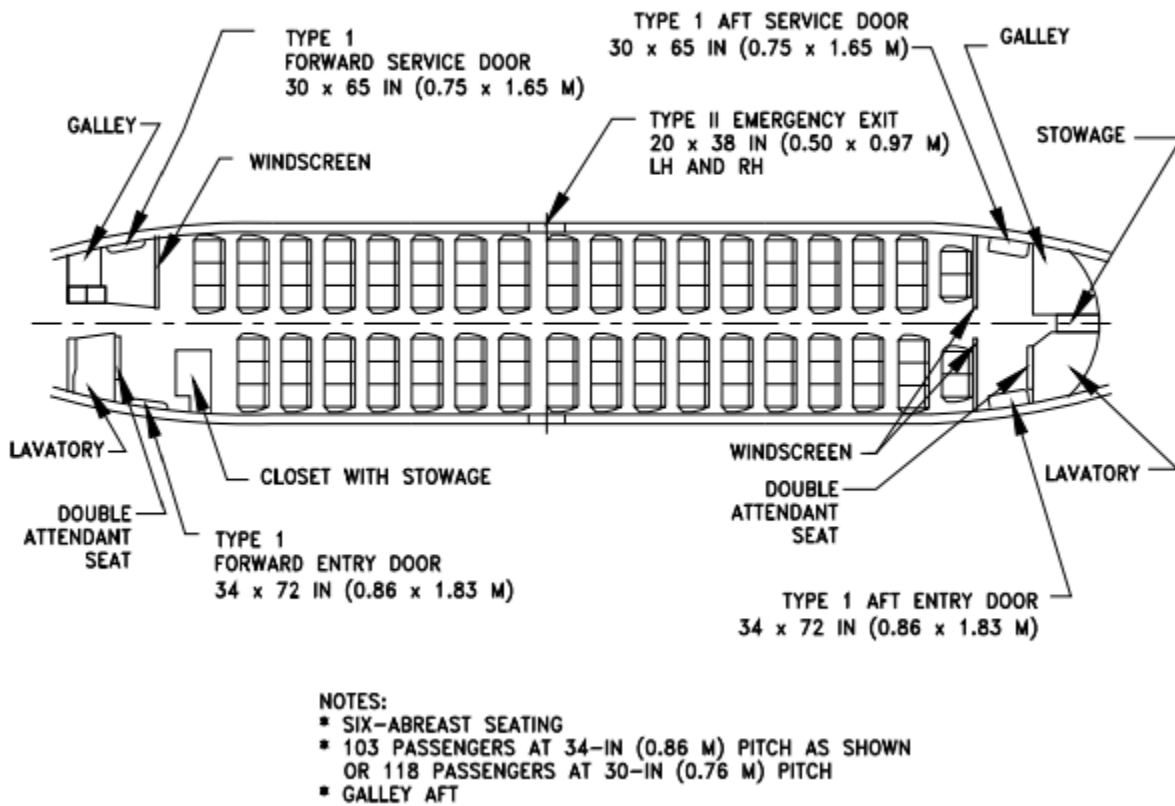
Figure 43. Top down view of the fuselage (Boeing Commercial Airplanes, 2013)
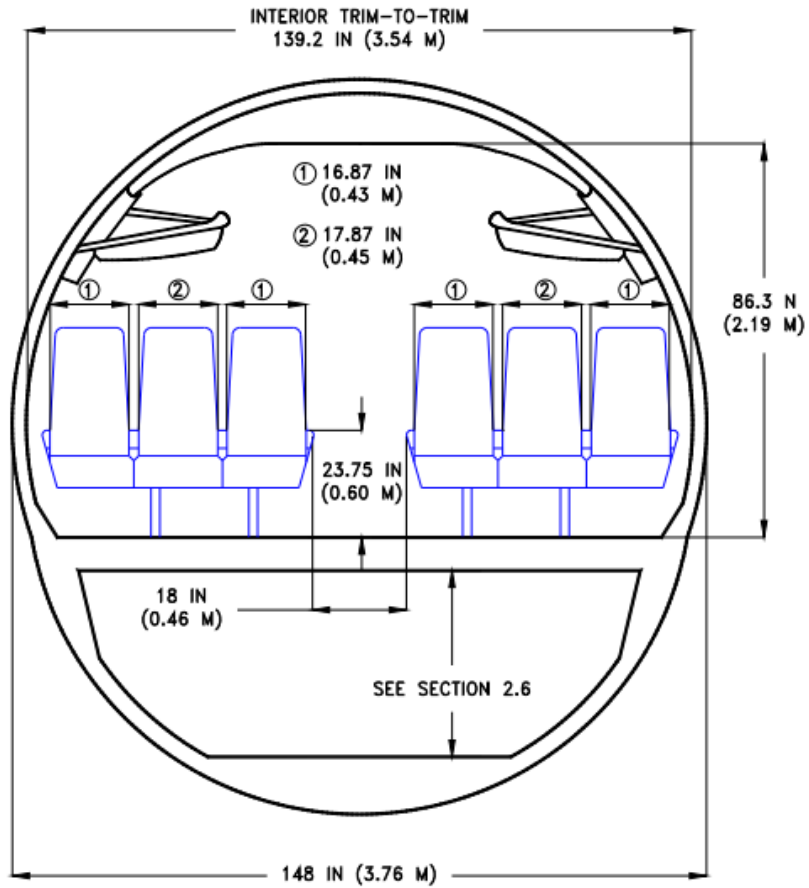
Figure 44. Front view of the fuselage (Boeing Commercial Airplanes, 2013)

Figure 45. Front 3-D view of the 6 abreast passenger seating in the fuselage (Creative Aviation Photography, 2017)

Figure 46. Rear 3-D view of the 6 abreast passenger seating in the fuselage (Creative Aviation Photography, 2017)
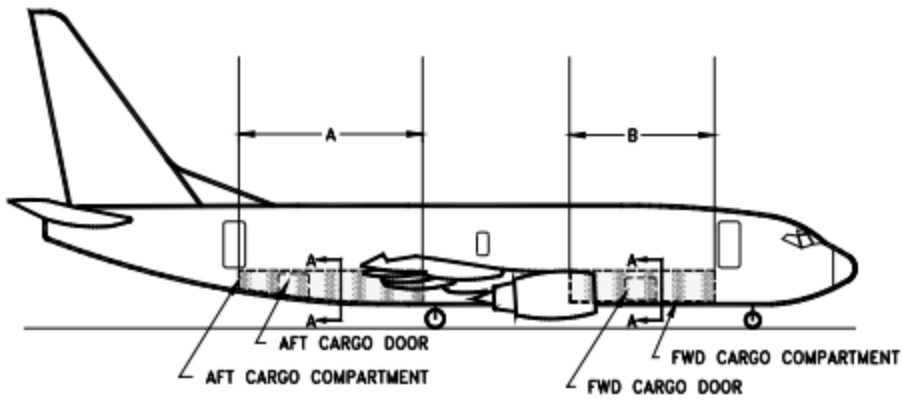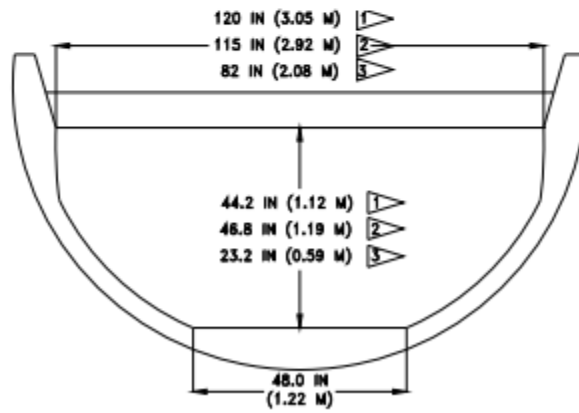
Figure 47. Side view of fuselage with cargo compartment visible *(Boeing Commercial Airplanes, 2013)*
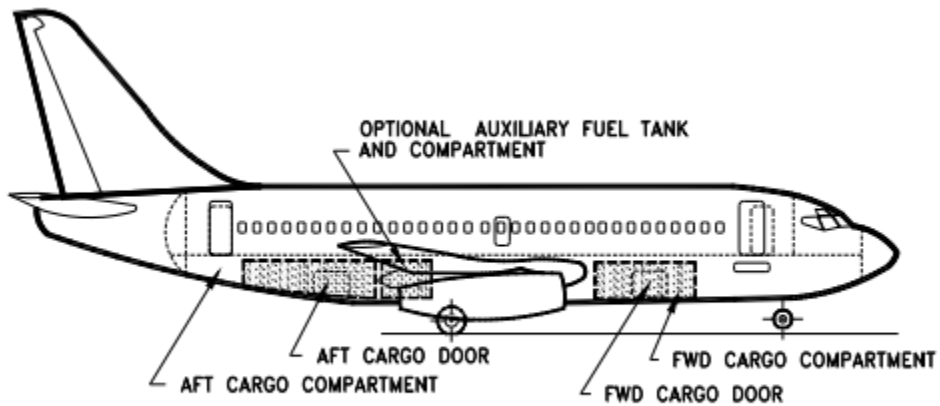
AIRPLANE MODEL	AFT CARGO COMPARTMENT			FORWARD COMPARTMENT BULK CARGO	TOTAL BULK CARGO
	BULK CARGO	AUXILIARY FUEL TANK CAPACITY	AUXILIARY FUEL TANK COMPARTMENT		
737-100	370 CU FT (10.48 CU M)	0	0	280 CU FT (7.93 CU M)	650 CU FT (18.41 CU M)

Figure 48. Side view of fuselage with cargo placement *(Boeing Commercial Airplanes, 2013)*

5.3. Recommendations and Conclusions

5.3.1. Recommendations

In general, the HTA is a hybrid version of the Boeing 737-100. Considering the 96 passenger payload, the 6 abreast seating allows for a smaller fuselage and lower takeoff weight. The standard cockpit design will work with two pilots, whether male or female. The fuselage design allows for flight attendant seating.

5.3.2. Conclusions

The current model of the 737-100 fuselage and cockpit meets FAR 25 requirements, visibility requirements, and provides the opportunity to exchange the engine and add batteries. To keep the takeoff weight a minimum, the minimum number of passengers will be considered, and the plane can be expanded length-wise in a future design.

6. Wing, High-Lift System and Lateral Control Design

6.1. Wing Planform Design

Using the known gross wing area, S, and aspect ratio, A, the remaining planform design characteristics of the wing will be chosen. These characteristics include the sweep angle, Λ, thickness ratio, t/c, airfoil type, taper ratio, λ, incidence angle i_w, twist angle, ε_w, dihedral angle, Γ_w, and the lateral control surface size and layout. Some of these will be calculated, and others will be chosen based on reference data. The HTA will feature conventional, cantilever low wing.

6.1.1. Sweep Angle-Thickness Ratio Combination

The 737-100 has a wing quarter chord sweep angle of 25º and is, therefore, aft swept. The HTA will feature the same 25 º sweep angle. This angle also matches well with other jet transport sweep angles, visble in the Figure 49 below.

Type	Dihedral Angle, Γ_w, deg.	Incidence Angle, i_w, root/tip deg.	Aspect Ratio, A	Sweep Angle, $\Lambda_{c/4}$, deg.	Taper Ratio, λ_w	Max. Speed, V_{max}, kts	Wing Type
DASSAULT/BREGUET							
Falcon 10	1.5	NA	7.1	27	0.36	492(25K)	ctl/low
Falcon 20F	2	1.5	6.4	30	0.31	465(25K)	ctl/low
Falcon 50	0	NA	7.6	24	0.32	475	ctl/low
CESSNA							
Citation I 500	4	2.5/-0.5	7.8	0	0.39	277(28K)	ctl/low
Citation II	4.7	NA	8.3	2	0.32	277(28K)	ctl/low
Citation III	2.8	NA	8.9	25	0.35	472(33K)	ctl/low
GATES LEARJET							
24	2.5	1	5.0	13	0.50	473(31K)	ctl/low
35A	2.5	1	5.7	13	0.50	464	ctl/low
55	2.9	NA	7.3	13	0.42	470(50K)	ctl/low
IAI							
1124 Westw. I	2	1/-1	6.5	5	0.33	471	ctl/mid
1125 Astra	2.6 (out)	NA	8.8	34/25 at LE	0.30	472(35K)	ctl/low
Canadair CL601	2.3	3	8.5	25	0.26	450	ctl/low
BAe 125-700	2	2.1/-0.3	6.3	20	0.28	436(28K)	ctl/low
GA Gulfst. III	3	3.5/-0.5	6.5	28	0.31	487	ctl/low
Nu Diamond I	2.7	3/-3.5	7.5	20	0.35	431(30K)	ctl/low
L. Jetstar II	2	1/-1	5.3	30	0.37	475(30K)	ctl/low

ctl = cantilever   (30K) = 30,000 ft altitude

Figure 49. Jet Transports Wing Geometric Data *(Roskam, Airplane Design Part II: Preliminary Configuration Design and Integration of the Propulsion System, 2011)*

The next values to select for the wing parameters are the taper ratio and the dihedral angle. The taper ratio consists of the ratio of the tip chord to root chord. The dihedral angel is the upward angle from the horizontal to the tailplane of the fixed-wing aircraft. These values will be modeled after the Boeing 737-100. λ=0.339 and Γ_w=6.

Since the airplane will be flying at high subsonic speeds, a trade study will be performed varying the sweep angle and the thickness ratio. This will facilitate the choice of the sweep angle and thickness ratio that allows for the minimum weight of the wing. The following equation:

$$\frac{M_{cc}^2 \cos^2 \Lambda}{\sqrt{1-M_{cc}^2 \cos^2 \Lambda}}\left[\left(\frac{\gamma+1}{2}\right)\left(\frac{2.64\left(\frac{t}{c}\right)}{\cos \Lambda}\right)+\left(\frac{\gamma+1}{2}\right)\left(\frac{2.64\left(\frac{t}{c}\right)(0.34C_l)}{\cos^3 \Lambda}\right)\right]+\frac{M_{cc}^2 \cos^2 \Lambda}{1-M_{cc}^2 \cos^2 \Lambda}\left[\left(\frac{\gamma+1}{2}\right)\left(\frac{1.32\left(\frac{t}{c}\right)}{\cos \Lambda}\right)^2\right]+M_{cc}^2 \cos^2 \Lambda\left[1+\right.$$
$$\left.\left(\frac{\gamma+1}{2}\right)\frac{(0.68c_l)}{\cos^2 \Lambda}+\left(\frac{\gamma+1}{2}\right)\frac{(0.34c_l)}{\cos^2 \Lambda}\right]-1=0 \qquad (39)$$

can be used to solve for the thickness ratio for varying sweep angles. The table and plot below demonstrate these results.

Table 28. Thickness Ratio and Wing Weight vs. sweep angle

Λ (deg)	t/c	W_w (lbs)
0	0.079	----------
5	0.081	436448.0332
10	0.086	81961.74273
15	0.095	44021.92291
20	0.108	29471.24401
25	0.124	21783.48296
30	0.145	17064.19453
35	0.169	13911.36935
40	0.197	11691.97308
45	0.227	10076.63814
50	0.259	8877.443908
55	0.291	7981.378457
60	0.319	7320.729094
65	0.338	6862.089862
70	0.337	6614.330935
75	0.295	6700.319668
80	0.142	8184.063457
85	-0.454	----------
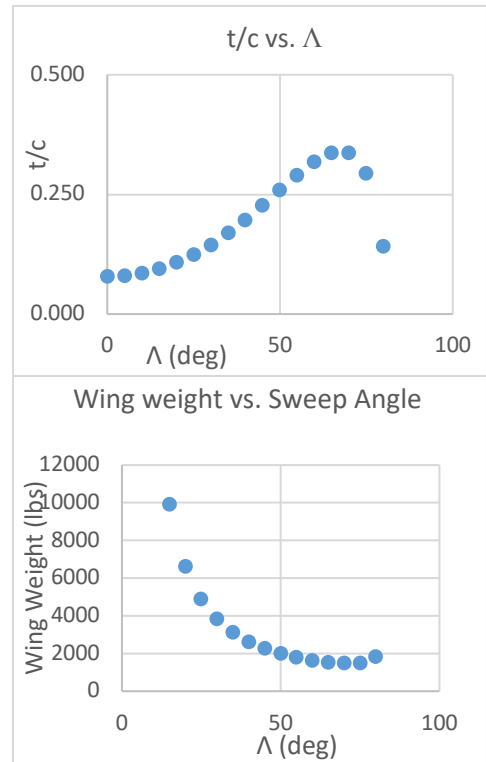
Figure 50. Plots of t/c and W_w vs. Λ

Using the wing weight as the figure of merit, the minimum wing weight occurs at a

sweep angle of 70º. This is not a reasonaible sweep angle, and therefore, the wing weight may

not be an appropriate figure of merit.

Besides using the weight of the wing as a figure of merit, there are other considerations

for selecting the thickness ratio. The thickness ratio should be greater than 0.1 to accommodate

the wing structure, fuel, batteries, and main landing gear when retracted. Additionally the

thickness ratio should not exceed 0.2 in order to prevent the drag profile from being too high.

Additionally, large sweep angles result in lower performance of the wing during low speed. As a

result, high lift systems may be necessary to improve this performance. Using these values for

the thickness ratio, a sweep angle between 20 and 40º would be appropriate. Thus, the 25º angle

will be selected and this results in a thickness ratio of 0.124.

6.2. Airfoil Selection

Selecting the airfoil involves considering the aircraft mission, along with properties of the

drag coefficient at the design lift coefficition, section critical Mach number, and section pitching

moment. The Boeing 737-100 used the Wing root- BAC 449/450/451 airfoil with Wing tip-

BAC 442 airfoil .   This will be selected as well for the HTA. The schematic, below, illustrates

the various airfoils for the root airfoil, two midspan airfoils, and outbard airfoil.
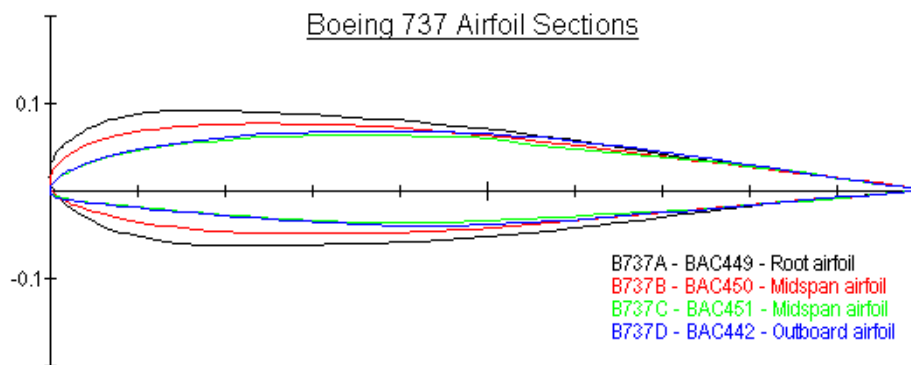
Figure 51. Boeing 737 Airfoil selections schematic *(Aircraft Technical Data and Specifications: Boeing 737-100/200, 2017)*

Based on Roskam's wing geometric data for transport aircraft, the incidence angle will be 1° (Aircraft Technical Data and Specifications: Boeing 737-100/200, 2017). Using the Boeing 737-100 model, the dihedral angle used will be 6°. Most aircraft have negative wash-out twist angles. Based on Roskam's discussion of designing wings for transport aircraft, a twist angle of -2° will be assumed.

6.3. Design of the High-Lift Devices

High lift devices are useful to help the aircraft meet its requirements for $C_{L_{\max\ TO}}$ and $C_{L_{\max L}}$. High lift devices include leading-edge devices and trailing-edge devices. Leading edge devices include VC Krueger flap, two-position slat, three-position slat, fixed slot, variable camber (VC) leading edge, hinged leading edge (or droop nose), folding bull-nose Krueger flap (Rudolph, 1996).   Trailing edge devices include split flap, plain flap, simple slotted flap, single-slotted Fowler flap, fized vain/main slotted flap, articulating vane/main double slopped flap, main/aft double slotted flap, triple-slotted flap (Rudolph, 1996).

The following sizing will determine which high lift devices would provide the HTA with enough lift to meet the takeoff and landing mission requirements. The HTA has $C_{L_{max_L}}$=2.73 and $C_{L_{max_{TO}}}$=2.25. These values were determined from the performance sizing in discussed in Chapter 4. According to Roskam, sizing the high lift devices involves determining the maximum lift coefficient capability of the wing, estimating $\Delta C_{L_{max_{TO}}}$ and $\Delta C_{L_{max_L}}$, accounting for the sweep of the wing, and then sizing the device using the desired ΔC_L.   Using the planform design characteristics of Λ=25°, t/c= 0.124, λ=0.339, i_w =2° , ε_w=, Γ=6°, S=1098 ft^2, b=93 ft, c_r=24.02 ft , and c_t= 5.2 ft, the high lift devices will be sized.

The $C_{L_{max}}$ can be obtained from the $C_{L_{max\ W}}$. To calculate the maximum lift coefficient of the wing, the following equation will be used:

$$C_{L_{max\,W}} = \frac{k_\lambda(C_{L_{max\,r}}+C_{L_{max\,t}})}{2} \qquad (40)$$

Thus, using $k_\lambda = 0.957$ and obtaining the root and tip maximum lift coefficients for the airfoil,

$C_{L_{max\,W}}$ can be calculated, with $C_{L_{max\,W}} = \frac{0.957(1.9+1.6)}{2} = 1.67$.
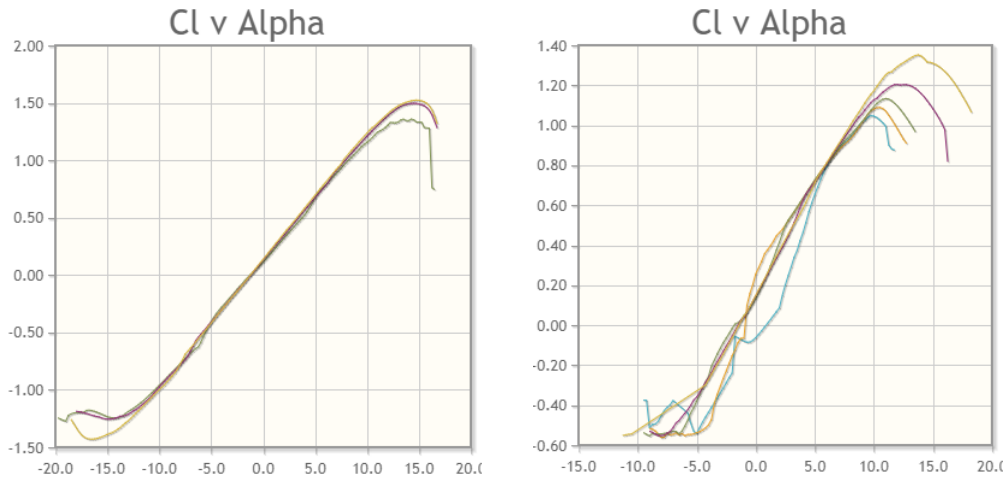
Figure 52. C$_l$ vs. angle of attack for maximum lift coefficient at root and midspan

$C_{L_{max\,W}} = 1.1$, and taking into account the quarter chord sweep angle, $C_{L_{max\,W}} = 1.8$.

Since the original 737-100 is a short-coupled airplane, the HTA will be assumed to be a short-coupled airplane. Therefore,

$$C_{L_{max\,W}} = 1.1 C_{L_{max}} \qquad (41)$$

and $C_{L_{max}} = 1.6$.

Using $C_{L_{max}} = 1.6$, the $\Delta C_{L_{max\,W}}$ and $\Delta C_{L_{max\,L}}$ can be calculated using the following two equations.

$$\Delta C_{L_{max\,TO}} = 1.05(C_{L_{max_{TO}}} - C_{L_{max}}) \qquad (42)$$

$$\Delta C_{L_{max\,L}} = 1.05(C_{L_{max_L}} - C_{L_{max}}) \qquad (43)$$

Therefore, $\Delta C_{L_{max\,TO}} = 1.05(2.25 - 1.1) = 1.2$ and $\Delta C_{L_{max\,L}} = 1.05(2.73 - 1.1) = 1.7$. The factor of 1.05 takes into account the trip penalties incurred when using flaps. To calculate the

$\Delta C_{L_{max}}$ values, with the sweep correction factor taken into consideration, the following table illustrates the various $\Delta C_{L_{max}}$ with three arbitrary flapped wing area to wing area ratios.

Table 29. $\Delta C_{L_{max\ TO}}$ and $\Delta C_{L_{max\ L}}$ using various S_{wf}/S

	Takeoff	Landing
S_{wf}/S	$\Delta c_{l_{max\ TO}}$	$\Delta c_{l_{max\ L}}$
0.60	0.83	1.18
0.80	1.11	1.57
0.90	1.25	1.77

In order to achieve the required flap lift increments, Fowler flaps will be used. The Fowler flaps have the following geometry: $\frac{c_f}{c} = 0.3, \delta_{f_{to}} = 35°, \delta_{f_L} = 40°$. (Roskam, Airplane Design Part II: Preliminary Configuration Design and Integration of the Propulsion System, 2011). The required incremental section lift coefficient, Δc_l will be calculated. This is the value that the trailing edge flaps must generate. The $\Delta c_{l_{max}}$ values have been estimated at takeoff and landing based on the S_{wf}/S ratio. Δc_l is related to $\Delta c_{l_{max}}$ through the following equation

$$\Delta c_l = \left(\frac{1}{K}\right) \Delta c_{l_{max}} \qquad (44)$$

K=0.94 is determined using , below, with $c_f/c = 0.3$ Thus the needed Δc_l values can be summarized in Table 30.
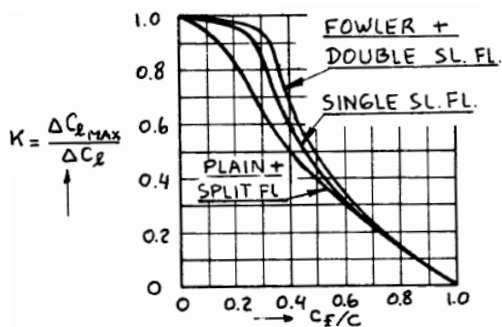
Figure 53. Effect of Flap Chord Ratio and Flap Type on K

Table 30. Calculated Δc_l for takeoff and landing

	Takeoff	Landing
S_{wf}/S	$\Delta c_{l_{to}}$	Δc_{l_l}
0.60	0.88	1.26
0.80	1.18	1.67
0.90	1.33	1.88

For Fowler flaps, the following equations hold:

$$\Delta c_l = c_{l_\alpha \alpha_{\delta_f}} \delta_f \tag{45}$$

$$c_{l_{\alpha_f}} = c_{l_\alpha(c'/c)} \tag{46}$$

$$\frac{c'}{c} = 1 + 2\left(\frac{z_{fh}}{c}\right) tan\left(\frac{\delta_f}{2}\right) \tag{47}$$

Therefore, $\Delta c_1 = 2\pi(0.53)\left(\frac{35}{57.29}\right) = 2.03$. Finally, using

$$\frac{S_{wf}}{S} = (\eta_0 - \eta_i)\{2 - (1-\lambda)(\eta_i + \eta_0)\}/(1+\lambda) \tag{48}$$

the following is a summary of the flap geometry: $\frac{S_{wf}}{S} = 0.83, \frac{c_f}{c} = 0.3, \delta_{f_{to}} = 35°, \delta_{f_L} = 40°$.

The Δc_1 supplied by the Fowler flaps satisfies the required Δc_1 for both takeoff and landing.

Thus, the Fowler flaps will be sufficient in providing additional lift.

6.3.1. AAA Calculation of Lift Coefficient

Using AAA, the clean maximum lift coefficient was found to be 1.541. Although this

value is lower than the original manual calculations, the increase in lift provided by the Fowler

Flaps is still substantial to provide the aircraft with lift.
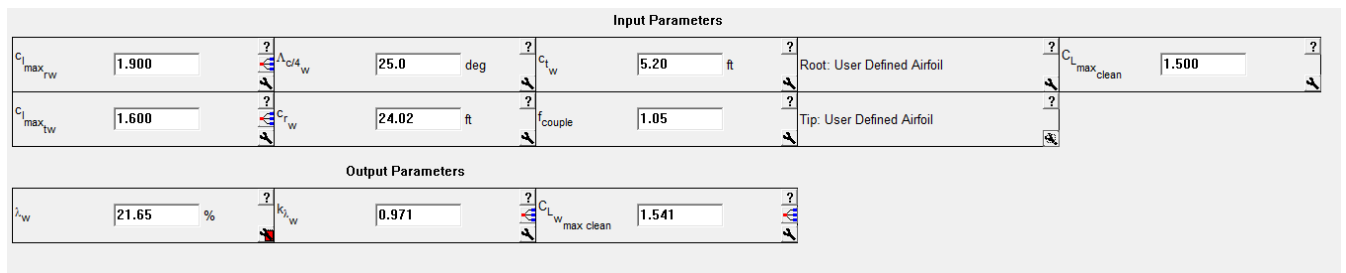
Figure 54. AAA Estimate of clean Lift Coefficient of the Wing

6.4. Design of the Lateral Control Surfaces

Roskam provides reference data for the lateral control surfaces. The data for jet transports is summarized in the table below. The aircraft will have a rudder area of 56.2 ft², a fin height of 20.2 ft, and a fin area of 224 ft² . The HTA will also have ailerons and spoilers with the ailerons composing 2.4% of the wing area.

In summary, the HTA will have the following wing parameters: b=93 ft, c_r=24 ft, c_t=5.2 ft, mac=12.5 ft, mgc=12.5 ft, Λ_{LE}=27.8° , Λ_{TE}= 16.625°, and (40.7, 43.8)= coordinates of the aerodynamic center measured in feet from the center of gravity.

The following figures will illustrate the wing planform and show these parameters.

Table 31. Jet Transport Lateral Control Surface Information

Table 8.7b) Jet Transports: Vert. Tail Volume, Rudder, Aileron and Spoiler Data

Type	Wing Area S ft²	Wing Span b ft	Vert. Tail Area S_v ft²	S_r/S_v	x_v ft	$\bar{V}_v$	Rudder Chord root/tip fr.c_v	S_a/S	Inb'd Ail. Span in/out fr.b/2	Inb'd Ail. Chord in/out fr.c_w
BOEING										
727-200	1,700	108	422	0.16	47.4	0.110	.29/.28	0.034	.38/.46	.17/.24
737-200	980	93.0	233	0.24	40.7	0.100	.25/.22	0.024	none	none
737-300	1,117	94.8	239	0.31	45.7	0.100	.26/.50	0.021	none	none
747-200B	5,500	196	830	0.30	102	0.079	0.30	0.040	.38/.44	.17/.25
747-SP	5,500	196	885	0.27	69.5	0.057	.31/.34	0.040	.38/.44	.17/.25
757-200	1,951	125	384	0.34	54.2	0.086	.35/.33	0.027	none	none
767-200	3,050	156	497	0.35	64.6	0.067	.33/.36	0.041	.31/.40	.23/.20
McDONNELL-DOUGLAS										
DC-9 S80	1,270	108	168	0.39	50.5	0.062	.49/.46	0.030	none	none
DC-9-50	1,001	93.4	161	0.41	46.2	0.079	.45/.44	0.038	none	none
DC-10-30	3,958	165	605	0.18	64.6	0.060	0.35	0.047	.32/.39	.20/.25
AIRBUS										
A300-B4	2,799	147	487	0.30	79.5	0.094	.35/.36	0.049	.29/.39	.23/.27
A310	2,357	144	487	0.35	68.5	0.098	.33/.35	0.027	.32/.40	.23/.27
Lockheed L1011										
-500	3,541	164	550	0.25	58.2	0.055	.29/.26	0.051	.40/.49	.22/.23
Fokker F-28										
-4000	850	82.3	157	0.16	37.9	0.085	.29/.31	0.034	none	none
Rombac/British Aerospace										
1-11 495	1,031	93.5	117	0.28	31.6	0.038	.39/.37	0.030	none	none
British Aerospace										
146-200	832	86.4	224	0.44	38.9	0.12	0.29	0.046	none	none
Tu-154	2,169	123	341	0.27	43.3	0.055	0.37	0.036	none	none

Table 32. Additional Jet Transport Lateral Control Surface Information

Table 8.7c) Jet Transports: Vert. Tail Volume, Rudder, Aileron and Spoiler Data
----

Type	Outb'd Ail. Span in/out fr.b/2	Outb'd Ail. Chord in/out fr.c$_w$	Inb'd Spoiler Span Loc. in/out fr.b/2	Inb'd Spoiler Chord in/out fr.c$_w$	Inb'd Spoiler Hinge Loc. in/out fr.c$_w$	Outb'd Spoiler Span Loc. in/out fr.c$_w$	Outb'd Spoiler Chord in/out fr.c$_w$	Outb'd Spoiler Hinge Loc. in/out fr.c$_w$
BOEING								
727-200	.76/.93	.23/.30	.14/.37	.09/.14	.79/.69	.48/.72	.16/.20	.65/.63
737-200	.74/.94	.20/.28	.40/.66	.14/.18	.66/.67	none	none	none
737-300	.72/.91	.23/.30	.38/.64	0.14	.64/.70	none	none	none
747-200B	.70/.95	.11/.17	.46/.67	.12/.16	0.71	none	none	none
747-SP	.70/.95	.11/.17	.46/.67	.12/.16	0.71	none	none	none
757-200	.76/.97	.22/.36	.41/.74	.12/.13	.73/.69	none	none	none
767-200	.76/.98	.16/.15	.16/.31	.09/.11	.85/.78	.44/.67	.12/.17	.74/.71
McDONNELL-DOUGLAS								
DC-9 S80	.64/.85	.31/.36	.35/.60	.10/.08	.69/.65	none	none	none
DC-9-50	.78/.95	.30/.35	.35/.60	.10/.08	.69/.65	none	none	none
DC-10-30	.75/.93	.29/.27	.17/.30	.05/.06	.78/.74	.43/.72	.11/.16	.75/.70
AIRBUS								
A300-B4	.83/.99	.32/.30	.57/.79	.16/.22	.73/.72	none	none	none
A310	none	none	.62/.83	.16/.22	.69/.66	none	none	none
Lockheed L1011								
-500	.77/.98	.26/.22	.13/.39	.08/.12	.82/.73	.50/.74	.14/.14	.67/.67
Fokker F-28								
-4000	.66/.91	.29/.28	no lateral control spoilers					
Rombac/British Aerospace								
1-11 495	.72/.92	0.26	.37/.68	.06/.11	.68/.63	none	none	none
British Aerospace								
146-200	.78/1.0	.33/.31	.14/.70	.22/.27	.76/.68	none	none	none
Tu-154	.76/.98	.34/.27	.43/.70	.14/.20	.62/.60	none	none	none

6.5. Drawings
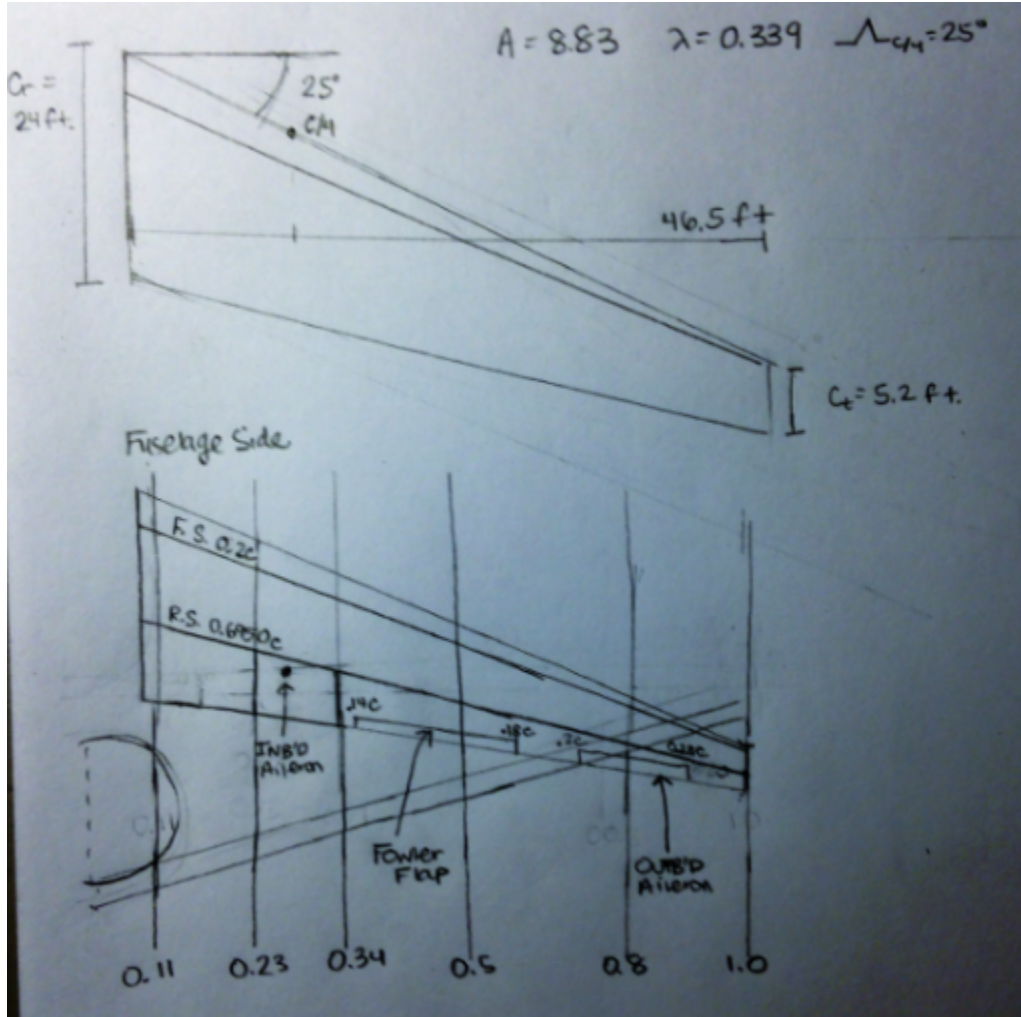
Figure 55. Wing Planform: flap and lateral control layout

6.6. Discussion

The HTA planform and lateral control layout illustrate the wing parameters. The Fowler flaps will be full span, and the spoilers will be used for lateral control. The spoilers will run from $0.4(\frac{b}{2})$ to $0.66(\frac{b}{2})$ with 0.14c to 0.18c. The outboard ailerons will run from $0.74(\frac{b}{2})$ to $0.94(\frac{b}{2})$ with 0.20c to 0.28c. Additionally, the drawings demonstrate the span of 93 feet, and the root and tip chord.

6.7. Recommendations and Conclusions

6.7.1. Recommendations

Based on the geometry of the wing and the flight parameters chosen, Fowler flaps are the recommended high lift device that will provide substantial lift. Additionally, the fuel can be stored in the wing without the risk of fire due to lightning strikes since the fuel in the HTA is less than the fuel in the 737-100. The batteries will additionally be suspended below the wing in nacelles, and this may change the aerodynamics surrounding the flaps and the nacelles.

6.7.2. Conclusions

The data in both tables from Roskam, along with pre-existing Boeing 737-100 specifications, provides benchmarks with which to compare the wing parameters. Although wing weight is usually a figure of merit for the thickness ratio, it proved to be a poor basis for the thickness ratio. Using a thickness ratio greater than 0.1 and less than 0.2 proved to provide optimal sweep angles of 25° at the quarter chord, along with a reasonable thickness ratio of 0.124. Additionally. The 25° sweep angle, which is the same as the original 737-100, yielded Λ_{LE}=27.8° , Λ_{TE}= 16.625°, from linear interpolation.

Through the analysis of the Boeing airfoil data, the $\Delta C_{L_{max}}$ was calculated, and the Fowler flaps were found to provide substantial lift, without any leading edge devices. The HTA has requirements for $C_{L_{max\,to}}$ = 2.25 and $C_{L_{max\,L}}$ = 2.73. The calculations demonstrated that an additional $\Delta C_{L_{max}}$ of 1.25 is needed for takeoff and $\Delta C_{L_{max}}$ of 1.77 is needed for landing. Since the Fowler flaps provide an additional $\Delta C_{L_{max}}$ = 2.03, they are substantial in providing lift.

Other high lift devices could be considered for the HTA. Given the geometry of the wing and the parameters chosen, the Fowler flaps provide adequate lift, and the wing geometry provides adequate storeage for the fuel.

7. Design of the Empennage and the Longitudinal and Directional Controls

7.1. Overall Empennage Design

The empennage design, which was initially introduced in the configuration design chapter is composed of the tail and stabilizing features organized in a tail aft arrangement. The HTA will feature a single vertical tail mounted to the fuselage along with a horizontal stabilizer.

For conventional configurations, the center of mass is generally near wing's aerodynamic center. This is the point at which the wing's pitching moment coefficient doesn't vary with changes in angle of attack. The empennage moment arms, x_h, x_v, x_c, will be located so as to create a maximum moment arm relative to the center of gravity (Roskam, Airplane Design Part III: Layout Design of Cockpit, Fuselage, Wing, and Empennage: Cutaways and Inboard Profiles, 2011). Besides creating a large moment arm, the placement of these locations minimizes the area of the empennage. This helps minimize the weight of the aircraft and the drag during flight. For the HTA, $x_h = 43.8\ ft\ and\ x_v = 40.7\ ft$. The in the table below summarizes the volume coefficients and control surface data.

Table 33. Summary of Comparable Volume Coefficients and Control Surface Data

Airplane Type	$\bar{V}_h$	S_e/S_h	$\bar{V}_v$	S_r/S_v
Boeing 737-200	1.28	0.27	0.100	0.24
Boeing 737-300	1.35	0.24	0.100	0.31
McDD DC-9-S80	0.96	0.34	0.062	0.39
McDD DC-9-50	1.32	0.38	0.079	0.41
Fokker F-28-4000	1.07	0.20	0.085	0.16
Rombac/BAe 1-11-495	0.86	0.27	0.038	0.28
Averages:	1.14	0.28	0.077	0.30

U

s

i

n

$$S_h = \bar{V}_h S\bar{c}/x_h \tag{49}$$

g

c

$$S_V = \overline{V_V} Sb / x_V \tag{50}$$

Together, these will compose the horizontal stabilizer and the vertical stabilizer.

7.2. Design of the Horizontal Stabilizer

The horizontal stabilizer area is 401 ft², and was calculated using equation 1:

$S_h = \frac{\overline{V_h} S \bar{c}}{x_h} = \frac{(1.28)(1098)(12.5)}{43.8} = 401 \ ft^2$. Additional parameters of the horizontal stabilizer

include the aspect ratio, quarter chord sweep angle, taper ratio, thickness ratio, airfoil, dihedral

angle, and incidence angle. The 737-100 model will be used as a reference for these parameters.

Therefore, the horizontal stabilizer aspect ratio will be 4.15. The thickness ratio will be 0.12.

The horizontal stabilizer will have a 7° dihedral angle, a taper ratio of 0.26, a quarter chord

sweep angle of 30° and a variable incidence angle (Aircraft Technical Data and Specifications:

Boeing 737-100/200, 2017).

The horizontal stabilizer will span 36 feet and will have a tailplan area of 312 ft² and an

elevator area of 70.5 ft². The elevator is 0.3 of the chord at the root and 0.32 of the chord at the

tip. The airfoil used is the BAC airfoil by Boeing (Aircraft Technical Data and Specifications:

Boeing 737-100/200, 2017).

7.3. Design of the Vertical Stabilizer

The vertical stabilizer, or fin, provides directional stability, and will have an area of

$S_V = \frac{\overline{V_V} Sb}{x_V} = \frac{(0.1)(1098)(93.011)}{40.7} = 250.9$ ft². Additionally, using the 737-100 for reference, the

design parameters of the vertical stabilizer will be chosen. These include the aspect ratio of 1.64,

the quarter chord sweep angle of 35°, a taper ratio of 0.288, a thickness ratio of 0.15, and a 0°

incidence angle. Additionally, the fin height of 20 feet and a rudder area of 56 ft². The airfoil

used is the BAC airfoil by Boeing (Aircraft Technical Data and Specifications: Boeing 737-

100/200, 2017).

7.4. Empennage Configuration Drawings

The figure below consists of the drawings of the empennage arrangement for the HTA. Included in this drawing are the elevator and rudder outlines. All dimensions are in feet and are illustrated below.
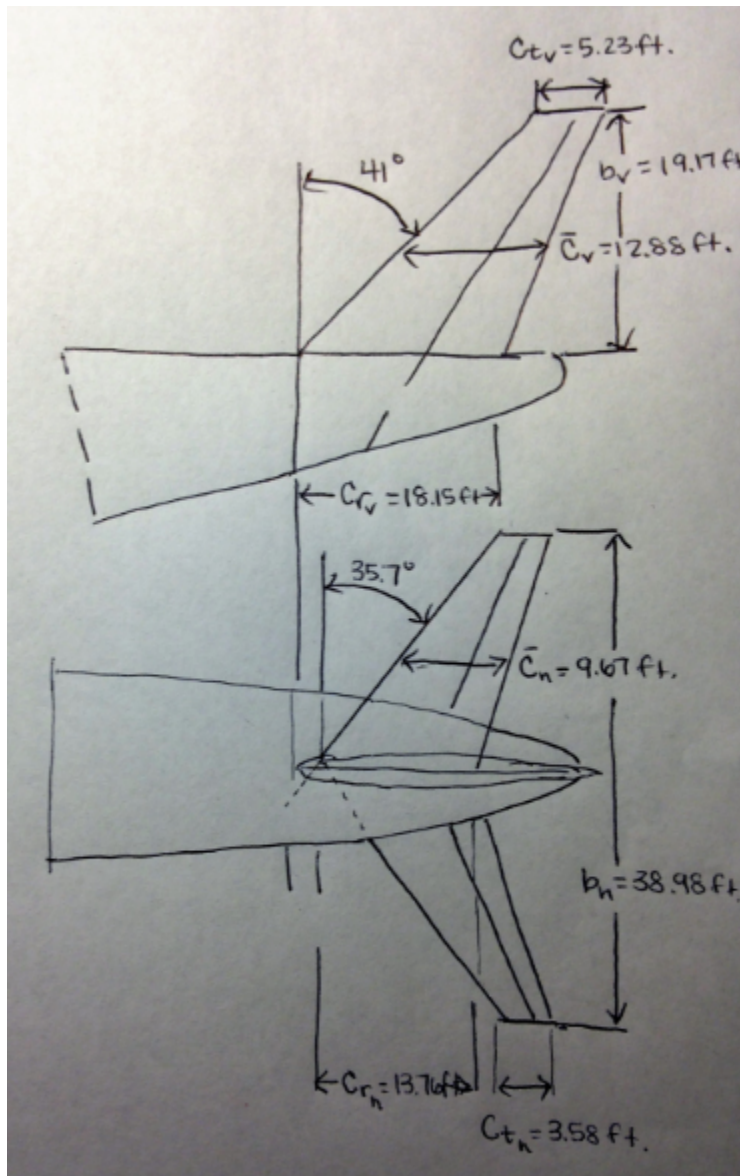
Figure 56. Empennage Configuration (units in feet)

7.5. Empennage Design Evaluation

AAA will be used to analyze the performance of the empennage horizontal and vertical stabilizers. Using the inputs of AP, λ, S, $\Lambda_{c/4}$, and the x, y, and z offset values, the output parameters were calculated. This provided the root and tip dimensions, span, mean geometric chord, leading edge and trailing edge sweep angle, and the positions for the mean geometric chord for both the vertical and horizontal tail. The outputs and inputs are presented below.
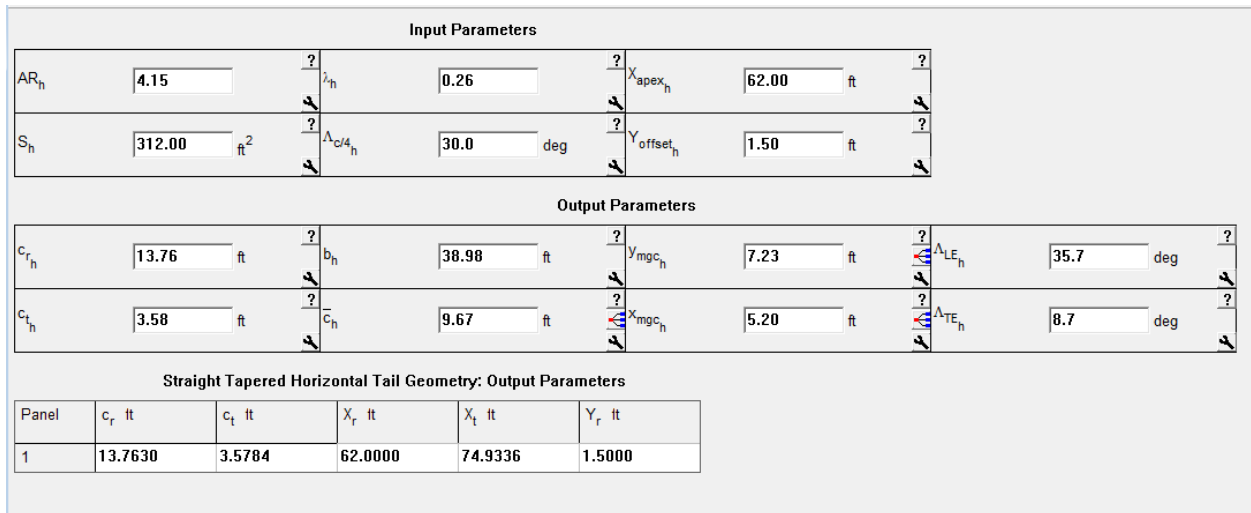
Figure 57. Horizontal Tail Geometry Calculations by AAA
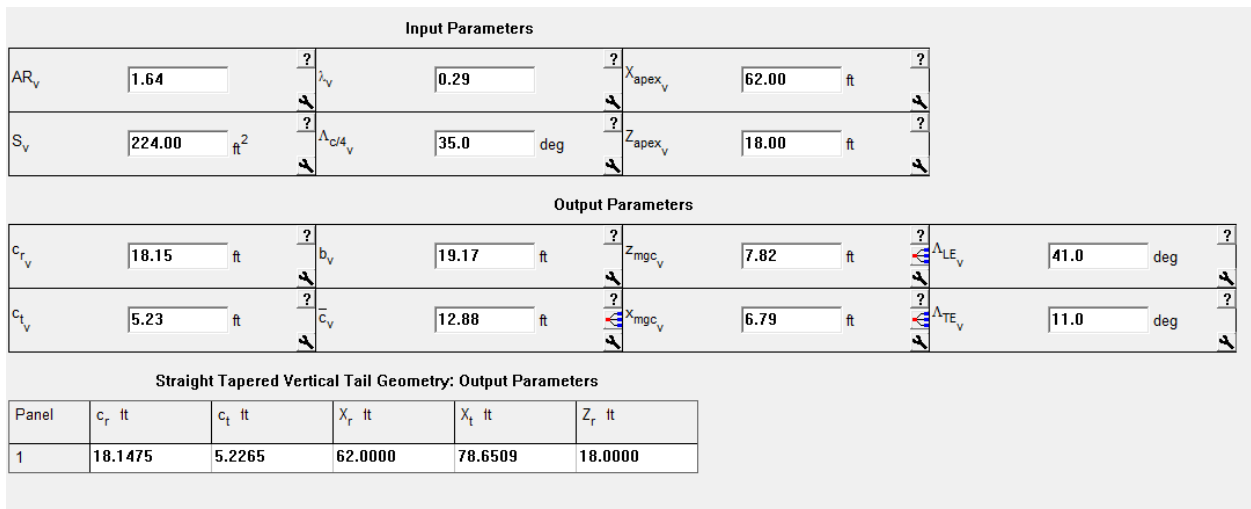
Figure 58. Vertical Tail Geometry Calculations by AAA

7.6. Discussion

Since the use of batteries during various stage of flight will not change the empennage, the 737-100 model was used as a reference for the HTA. This data, along with similar data provided by Roskam, provided the foundation for initial selections for the parameters. Additionally, the parameters chosen are consistent with the control surface ratios provided by Roskam. Thus, $S_e/S_h = 0.27$ for a 737-200 and $S_e/S_h = 0.24$ for a 737-300. Using the 737-100 parameters, $\frac{S_e}{S_h} = \frac{70.5}{401} = 0.18$. This value is lower, but comparable. For the rudder area to vertical stabilizer area, $\frac{S_r}{S_v} = 0.31 \ and \ 0.39$ for 737-200 and 737-300, respectively. For the HTA, $\frac{S_r}{S_v} = \frac{56}{250.9} = 0.22$. Again, although this is lower, it is comparable.

AAA additionally calculated very similar values to the original 737-100 aircraft. The tail geometry is consistent with previous aircraft, and will provide adequate stability for the HTA.

7.7. Recommendations and Conclusions

7.7.1. Recommendations

The HTA empennage will be modeled after the 737-100 airplane with slight changes. The moment arms have been estimated at $x_h = 43.8 \ ft \ and \ x_v = 40.7 \ ft$. These locations will be iterated to determine the aerodynamic center that provides the best stability and control.

7.7.2. Conclusions

The tail aft empennage arrangement provides a suitable conventional configuration design for the HTA. With the hybrid plane being modeled after the 737-100, the parameters have been chosen based on the fuel powered model. The distance from the cg to the ac will be established further when exploring the stability and control of the landing gear and may be adjusted, if necessary, after an iterative process. The figures below illustrate how the empennage fits in the aircraft.
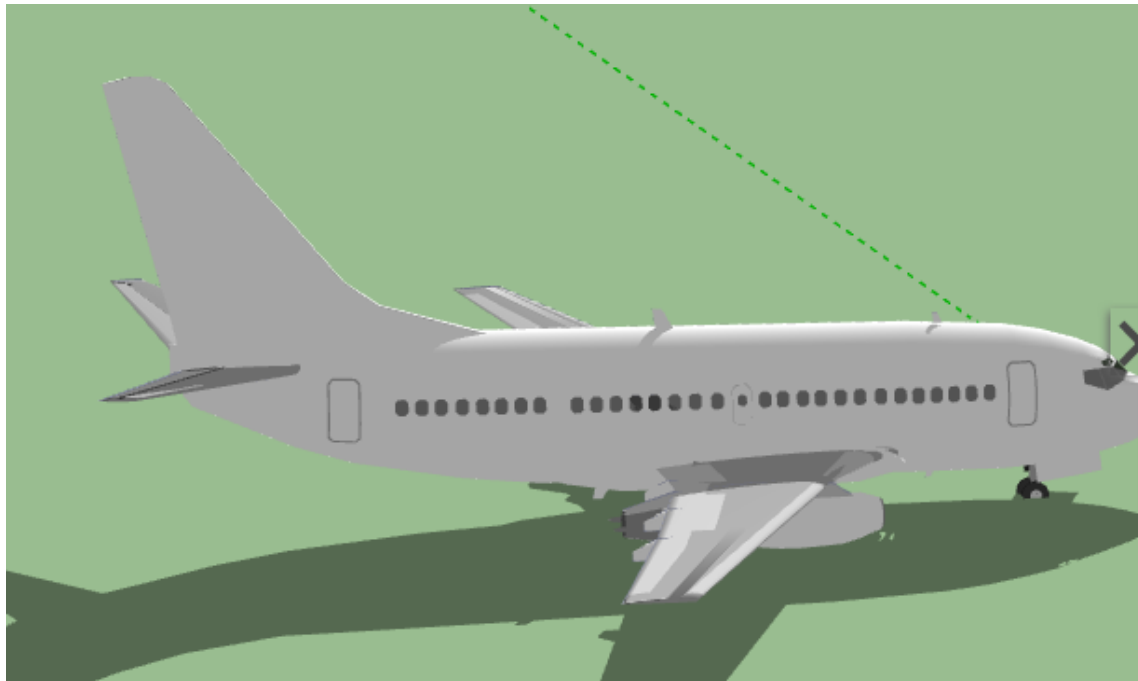
Figure 59. Vertical tail configuration in HTA
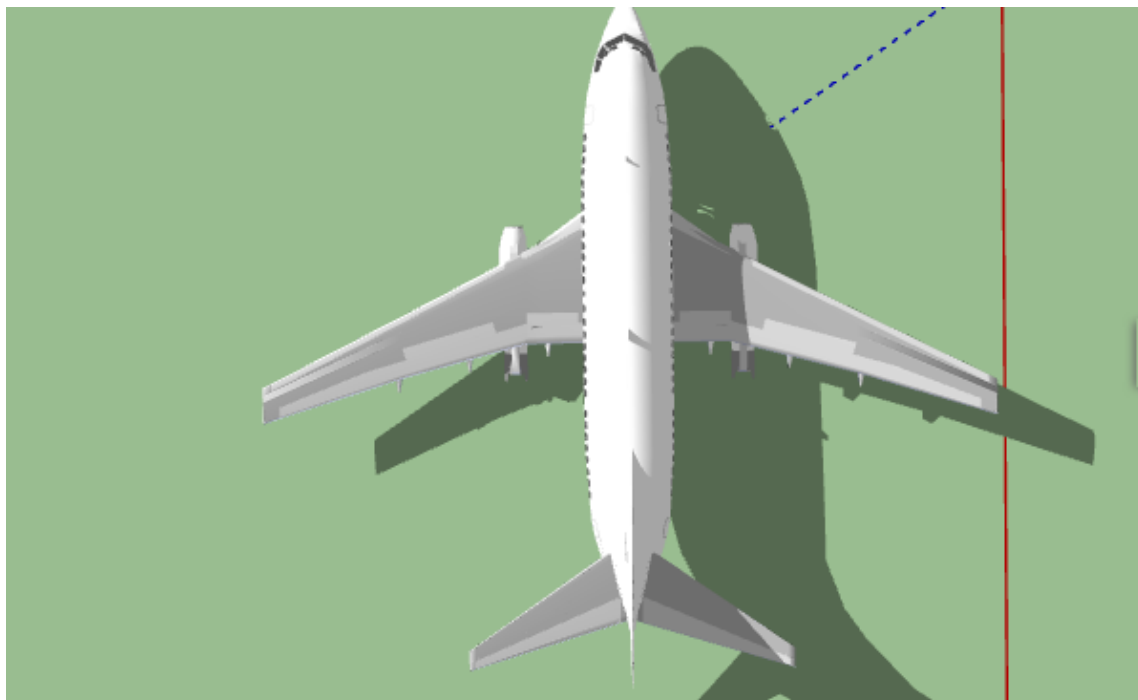
Figure 60. Horizontal tail configuration in HTA

8. Design of the Landing Gear and Weight and Balance Analysis

8.1. Introduction

The landing gear arrangement, previously introduced in the configuration chapter, will consist of retractable conventional tricycle landing gear. The main landing gear will retract into the fuselage, and the nose landing gear will retract into the nose. In order to size the landing gear, the center of gravity will need to be determined. From there, a weight and balance iteration will be performed to determine whether the cg of the proposed design is in the correct location. The cg excursion diagram will be used to illustrate the possible locations of the cg.

8.2. Estimation of the Center of Gravity

The following data consists of the component weight and coordinate data for the Class I component weight estimation Assuming a takeoff weight of 83,000 lbs and the weight fractions from Roskam's Part V. Component Weight Estimation, the weights and positions are summarized in the table below (Roskam, Airplane Design Part II: Preliminary Configuration Design and Integration of the Propulsion System, 2011).

The zero reference point will be located a distance well to the left and below the airplane. This allows the airplane to change size without changing the reference point. The x-axis will refer to x-coordinates called the fuselage stations (F.S.) and the y-axis coordinates will be referred to as the wing buttock lines (B.L.). For the HTA, the first F.S. point will be at 151 inches, and the first B. L. point will be at 78 inches.

The comcomponent weight and coordinate data for the HTA are summarized in Table 34, below. Note that the aircraft is symmetric, so the y coordinates will all be 0 inches.

Table 34. HTA Component Weight and Coordinate Data

No.	Type of Component	W_i (lbs)	x_i (in.)	W_ix_i (in lbs)	y_i (in.)	W_iy_i (in lbs)	z_i (in.)	W_iz_i (in lbs)
1	Fuselage Group	8,549	641	5,479,909	0	0	248	2,120,152
2	Wing Group	7,636	680	5,192,480	0	0	350	2,672,600
3	Empennage Group	1,992	1190	2,374,480	0	0	300	597,600
4	Engine Group	20,950	590	12,360,500	0	0	140	2,933,000
5a	Landing Gear Group:Nose Gear	500	390	195,000	0	0	130	74,750
5b	Landing Gear Group: Main Gear	2654	710	1,884,340	0	0	130	345,020
6	Fixed Equipment Group	10,707	680	7,280,760	0	0	200	2,141,400
7	Trapped Fuel and Oil	142.8	690	98,532	0	0	215	30,702
8	Crew	700	300	210,000	0	0	240	168,000
9	Fuel	4,500	690	3,105,000	0	0	430	1,935,000
10	Batteries	18,000	733	13,194,000	0	0	120	2,160,000
11	Passengers	16,800	680	11,424,000	0	0	200	3,360,000
12	Luggage	3,000	680	2,040,000	0	0	200	600,000
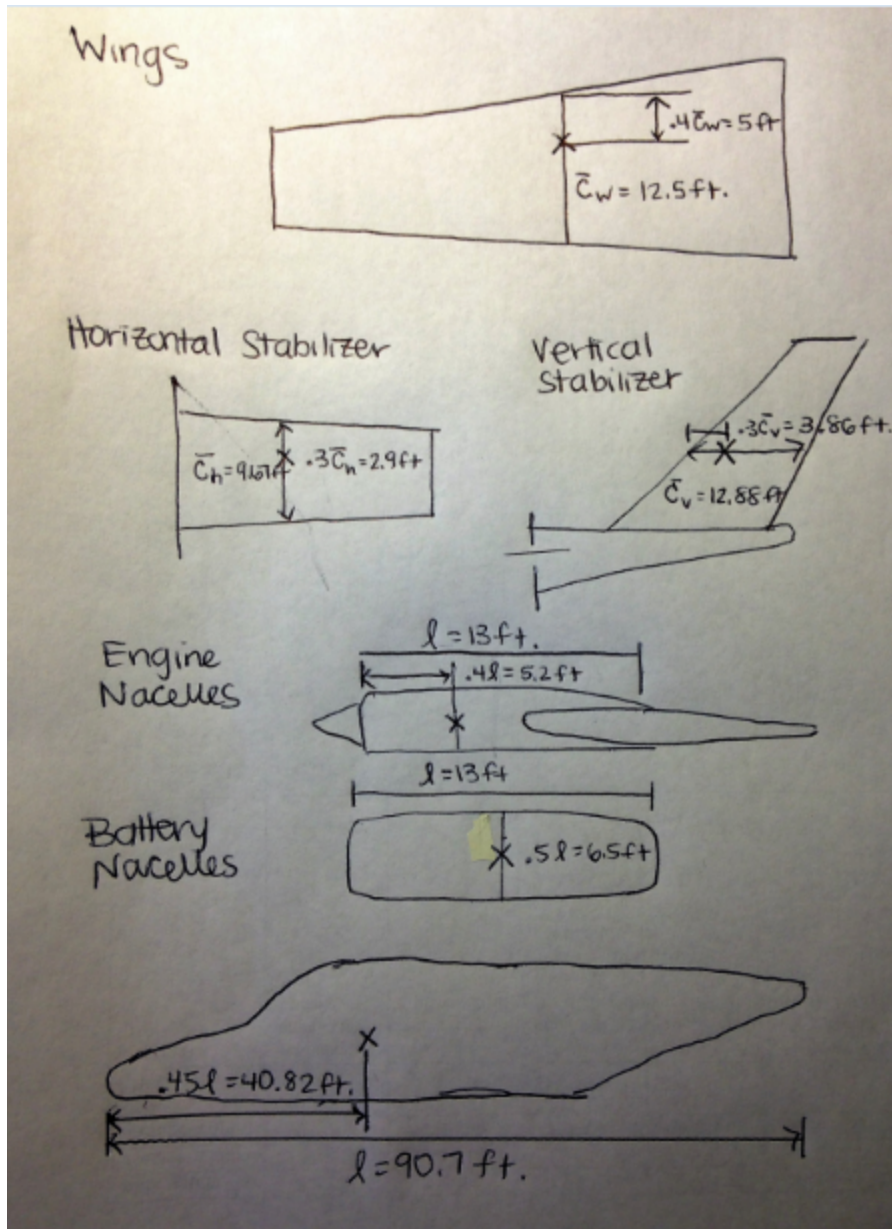
Figure 61. c.g. for various aircraft components
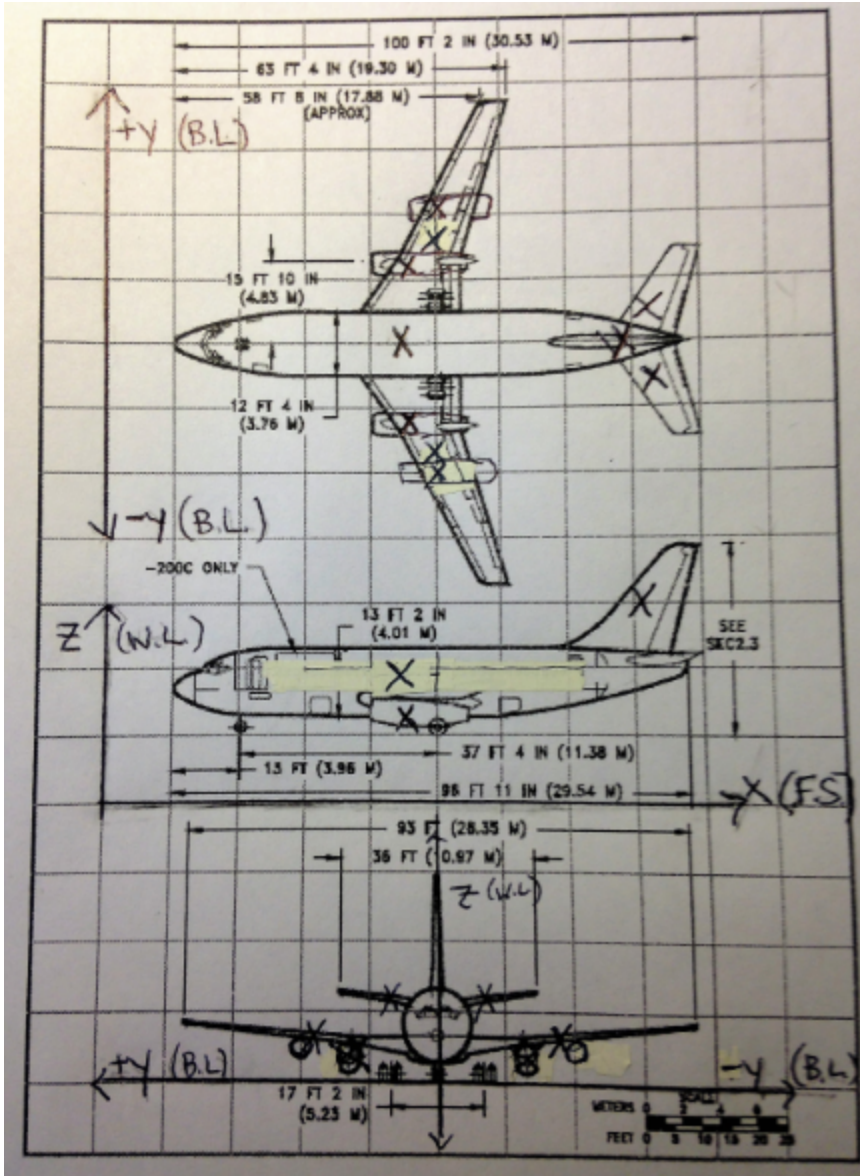
Figure 62. c.g. location for each component on the aircraft

Using the listed c.g. locations for the various components and their individual weights,

the c.g. excursion diagram was produced using Excel. The most forward c.g. is located at 46.91

ft. and the most aft c.g. is located at 66.08 ft. Although they have a very wide spread, AAA will

be used to check these calculations, and then after the landing gear placement, the weight and

balance will be performed again.
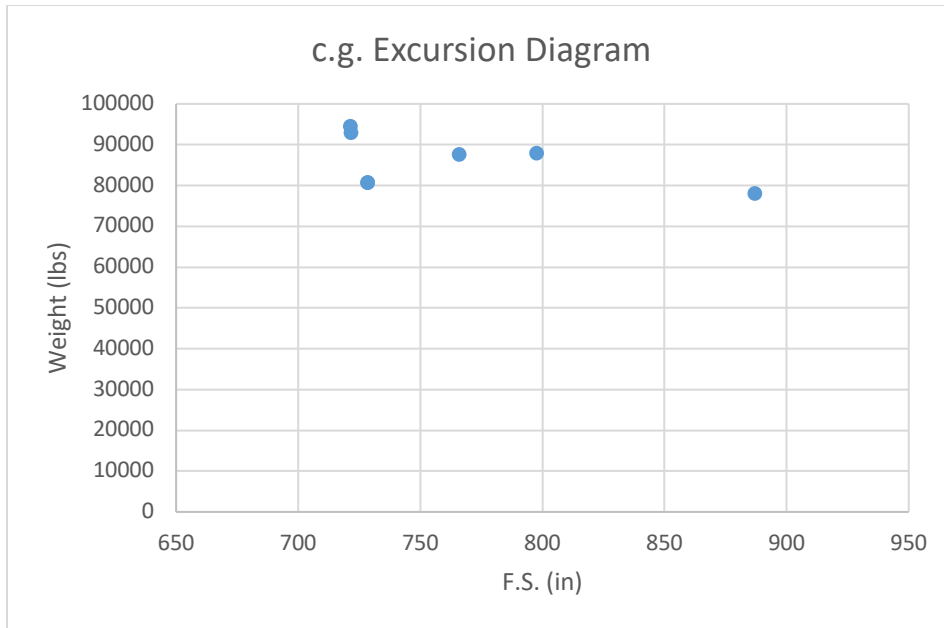
Figure 63. c.g. excursion plot produced using Microsoft Excel

Using the 737-200 airplane for comparison, the weight fractions were calculated for the

various components. The figure below illustrates the results from AAA.

Figure 64. Weight fractions referenced from the 737-200 from AAA

Using the empty weights, the c.g. positions for each of the empty weight components can

be determined, as well as the c.g. of the structure as a whole. These results, from AAA, are

summarized as follows.

Empty Weight Table

Component	Weight lb	X_{cg} ft	Y_{cg} ft	Z_{cg} ft
Fuselage Group	8826.6	4.45	0.00	1.72
Wing Group	7733.8	4.70	0.00	2.43
Empennage Group	1992.0	8.07	0.00	2.12
Landing Gear Group	3154.0	5.62	0.00	1.44
Nacelle Group	1008.8	4.59	0.00	1.08
Powerplant Group	5968.5	49.17	0.00	11.67
Fixed Equipment Group	10844.2	56.67	0.00	16.67

Output Parameters

$W_{structure}$ = 22715.2 lb, $X_{cg_{structure}}$ = 5.02 ft, $Y_{cg_{structure}}$ = 0.00 ft, $Z_{cg_{structure}}$ = 1.93 ft

W_E = 39593.8 lb, X_{cg_E} = 25.82 ft, Y_{cg_E} = 0.00 ft, Z_{cg_E} = 7.44 ft

Figure 65. c.g. locations produced using AAA

Using the outputted parameters as inputs, the c.g. of the HTA along with the c.g. locations for each component.

Input Parameters

W_E = 39593.8 lb, X_{cg_E} = 25.82 ft, Y_{cg_E} = 0.00 ft, Z_{cg_E} = 7.44 ft

Loading Table

Component	Weight lb	X_{cg} ft	Y_{cg} ft	Z_{cg} ft
Crew	760.0	25.00		20.00
Trapped Fuel and Oil	359.7	57.50	0.00	17.92
Mission Fuel Group 1	11554.0	58.33		17.08
Mission Fuel Group 2	0.0	0.00		0.00
Passenger Group 1	4200.0	56.67		16.67
Passenger Group 2	4200.0	56.67		16.67
Passenger Group 3	4200.0	56.67		16.67
Passenger Group 4	4200.0	56.67		16.67
Baggage	2880.0	56.67		16.67
Cargo	0.0	0.00	0.00	0.00
Military Load Group 1	0.0	0.00		0.00
Military Load Group 2	0.0	0.00		0.00

Output Parameters

$W_{current}$ = 71947.6 lb, X_{cg} = 39.63 ft, Y_{cg} = , Z_{cg} = 11.69 ft

Figure 66. c.g. location for MTOW aircraft

From here, the c.g. excursion diagram for the x and z directions can be plotted. The following information was used to plot the c.g. excursion diagram.

Input Parameters

W_{PL} 37680.0 lb	$X_{cg_{mg}}$ 59.17 ft	X_{mgc_w} 10.42 ft
$W_{PL_{exp}}$ 0.0 lb	X_{apex_w} 31.00 ft	$\bar{c}_w$ 12.69 ft

C.G. Excursion Table

Component	Weight lb	X_{cg} ft	Load (1-13)	Unload (1-13)
Empty Weight	39593.8	25.82	1	13
Crew	760.0	25.00	6	8
Trapped Fuel and Oil	467.6	57.50	2	12
Mission Fuel Group 1	15018.3	58.33	3	1
Mission Fuel Group 2	0.0	0.00	4	2
Passenger Group 1	4200.0	56.67	7	3
Passenger Group 2	4200.0	56.67	8	4
Passenger Group 3	4200.0	56.67	9	5
Passenger Group 4	4200.0	56.67	10	6
Baggage	2880.0	56.67	11	7
Cargo	18000.0	15.80	5	9
Military Load Group 1	0.0	0.00	12	10
Batteries	0.0	0.00	13	11

Output Parameters

$W_{current}$ 93519.7 lb	X_{cg} 35.76 ft

Figure 67. Loading Table from AAA for x-direction c.g. excursion diagram

Using the loading table and the valculated c.g. values, the x c.g. excursion plot illustrates

the possible c.g. locations depending on the loading scenario.
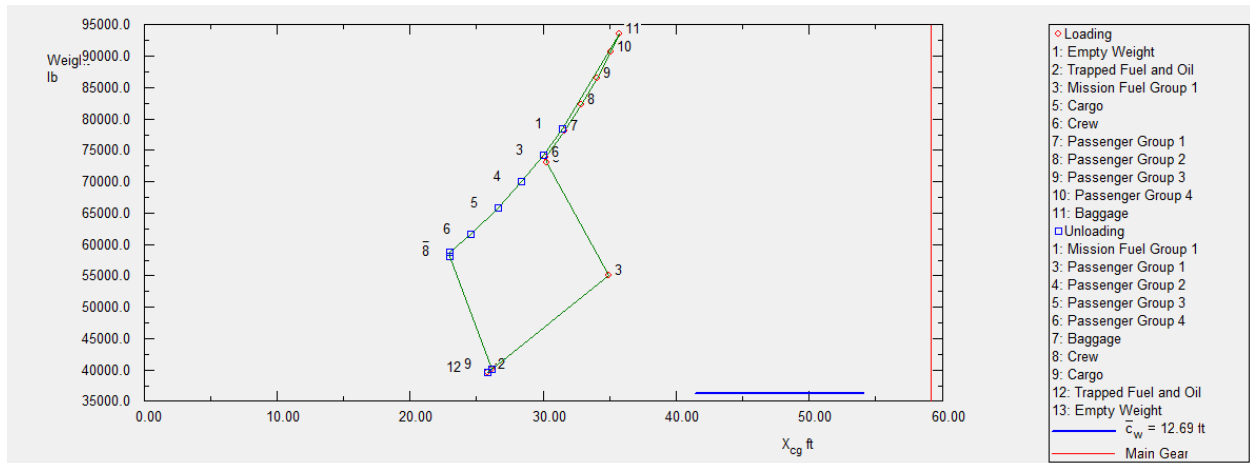
Figure 68. c.g. excursion diagram (x-direction)

The plot illustrates a variation in c.g. with the most forward c.g. being located at 22.9 ft

and the most aft c.g. being located at 35.7 ft. Note that the c.g. is left of the main landing gear,

which indicates that the HTA will not tip over with the current loading and unloading scenarios.

For reference, the z-direction c.g. excursion diagram has also been plotted. Note that for the

loading and unloading scenarios, the cargo represents the batteries.

Input Parameters

W_{PL}	37680.0	lb
$W_{PL_{exp}}$	0.0	lb

C.G. Excursion Table

Component	Weight lb	Z_{cg} ft	Load (1-13)	Unload (1-13)
Empty Weight	39593.8	7.44	1	13
Crew	760.0	20.00	6	8
Trapped Fuel and Oil	467.6	17.92	2	12
Mission Fuel Group 1	15018.3	17.08	3	1
Mission Fuel Group 2	0.0	0.00	4	2
Passenger Group 1	4200.0	16.67	7	3
Passenger Group 2	4200.0	16.67	8	4
Passenger Group 3	4200.0	16.67	9	5
Passenger Group 4	4200.0	16.67	10	6
Baggage	2880.0	16.67	11	7
Batteries	18000.0	10.00	5	9
Military Load Group 1	0.0	0.00	12	10
Military Load Group 2	0.0	0.00	13	11

Output Parameters

$W_{current}$	93519.7	lb
Z_{cg}	11.58	ft

Figure 69. Loading Table from AAA for z-direction c.g. excursion diagram
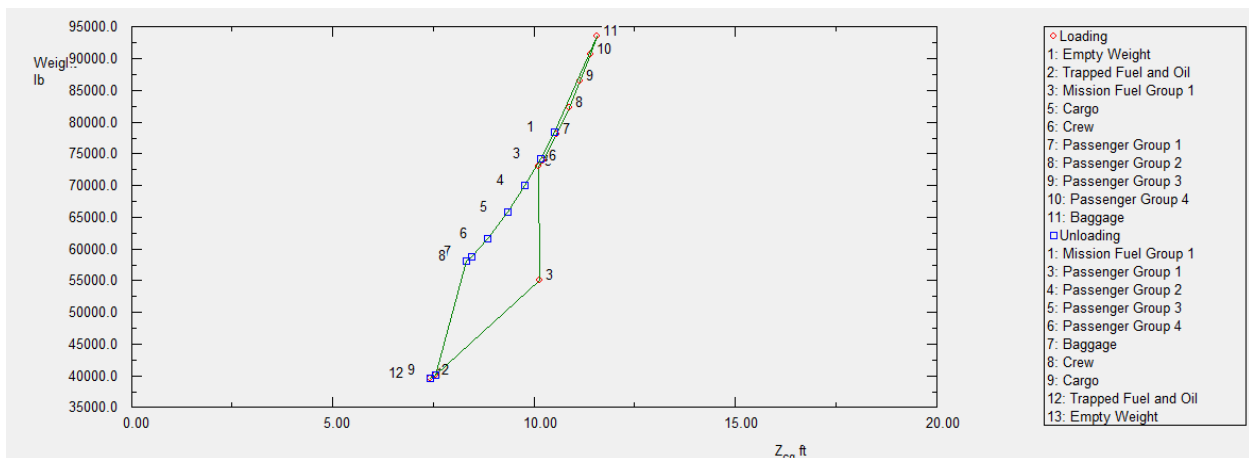
Figure 70. c.g. excursion diagram (z-direction)

8.3. Landing Gear Design

For the landing gear design, the following characteristics will be determined: number and size of tires, length and diameter of struts, preliminary disposition, and retraction feasibility. The HTA will have retractable tricycle landing gear. Preliminary decisions on placement of the wheels and struts will be made, and the placements will be checked to see that they meet the tip over criteria and ground clearance criteria.

The main landing gear must be behind the aft most c.g. Based on the c.g. excursion diagram, the most aft c.g. is located at 39.63 ft. By constructing a line parallel ot the sweep of the fuselage and a 7-15 degree angle to find the optimal ground clearance, the intersection of these two is the location of the main landing gear. This location, at 47.33 ft, which is the same as the location of the Boeing 737-100 model, is aft of the c.g. Thus, it meets the tip-over criteria.

To meet the ground clearance criteria, the main gear struts will be placed under the fuselage. The selection of the strut length will impact the weight of the landing gear, ground clearance of the aircraft, the tip-over characteristics, and stability during ground operation.

To determine the maximum static load per strut, the following equations will be used:

$$P_n = \frac{W_{TO} l_m}{l_m + l_n} \tag{51}$$

$$P_m = (W_{TO} l_n)/n_s (l_m + l_n) \tag{52}$$

Note that P_n and P_m, are the maximum nose wheel strut loading and main gear strut loading, and l_m and l_n, are the distance from the c.g. to the main landing gear and nose gear, respectively. For the HTA, the maximum load per strut for the main landing gear is 32,833 lbs, and the maximum load per strut for the nose gear is 27,852 lbs.

There will be two nose wheels and four main wheels. The nose wheel tires have a diamer of 24 inches and a wheel tread width of 7.75 inches. The main wheel tires have a diameter of 40 inches and a wheel tread width of 14.5 inches (Brady, 1999). Boeing oleo pneumatic shock

aborbers provide shock absorption. One main gear strut and one nose gear strut dampen the

vertical oscillations felt upon landing.
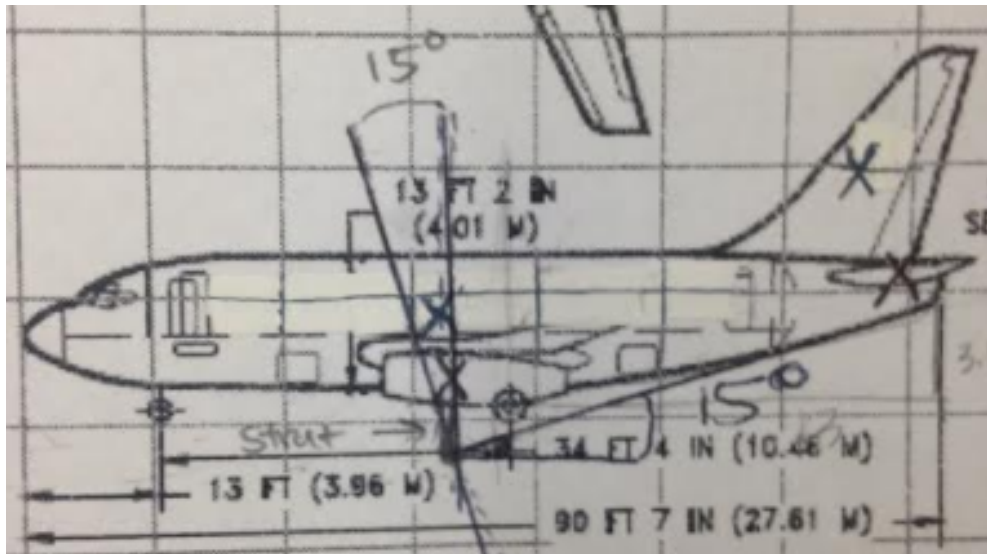
Figure 71. Landing gear and strut placement
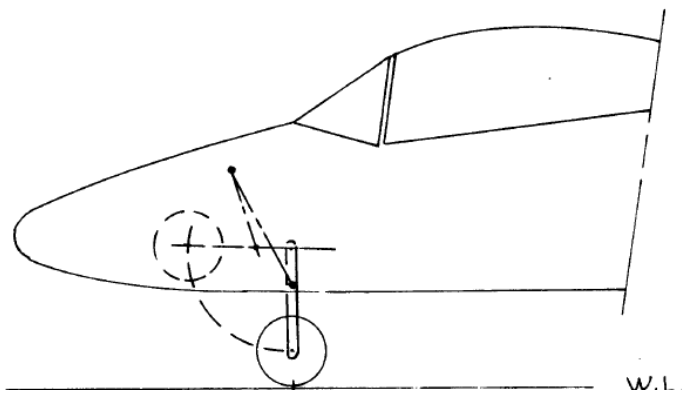
Figure 72. Nose gear retraction
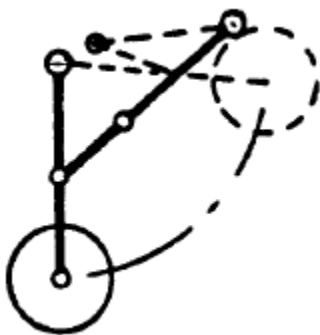
Figure 73. Stick Diagram for main gear retraction
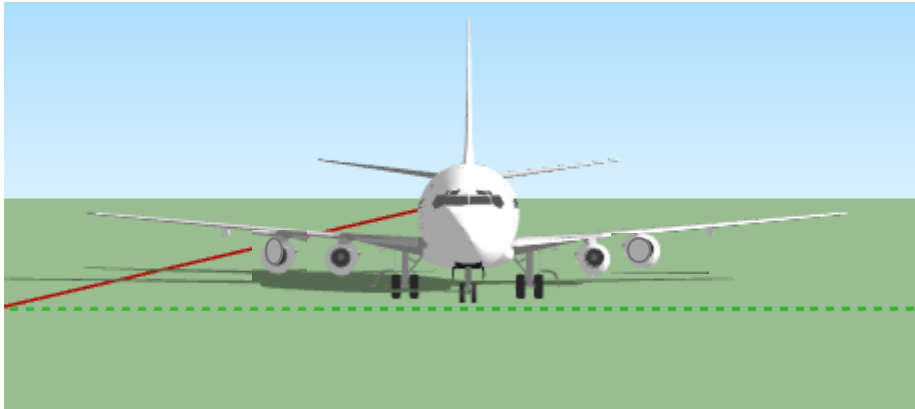
Figure 74. Illustration of the two nose tires and four main tires for the landing gear.

Figure 75. Landing Gear retracted into fuselage

8.4. Weight and Balance

Since the landing gear placement, at 47 feet from the nose, is aft of the most aft c.g., the weight and balance does not need to be repeated. The location of the main landing gear correlates with the location of the main landing gear in the 737-100 model.

8.5. Conclusion

Compared to the 737-100 model, the c.g. excursion diagram demonstrated the change in c.g. location due to the addition of the batteries. The location of the batteries did not change the location of the main landing gear, and, as a result, the HTA will not tip over in any loading scenario. The landing gear can support the weight of the plane, with the added weight due to the batteries, and the landing gear retracts directly into the fuselage.

9. Stability and Control Analysis

9.1. Introduction

The stability and control analysis will be performed by following Roskam's steps in Airplane Design Part II. This will allow the determination of the stability and control characteristics of the HTA. These characteristics include the static longitudinal stability, static directional stability, and minimum control speed with one engine out (Roskam, Airplane Design Part II: Preliminary Configuration Design and Integration of the Propulsion System, 2011)

Stability is the tendency of an object to return to equilibrium when displaced (Crawford, 2009). Static stability involves an object's initial tendency to return to equilibrium upon initial displacement. For aircraft, this requires a balance because the greater an aircraft's static stability, the greater its resistance in maneuvering. The center of gravity, or c.g., strongly determines the longitudinal static stability. Moving the c.g. aft reduces static stability and increases maneuverability.

Aircraft can have inherent stability, in which the stability is built into the aircraft's design, or de facto stability, where control systems provide feedback and provide stability requirements. Some aircraft have relaxed stability. This type of stability involves the aircraft changing its attitude and bank angle on its own. This, along with stability augmentation devices, allows for better cruise performance and better maneuverability at high altitudes. Many jet transport aircraft have relaxed stability. The HTA will also feature relaxed stability.

9.2. Static Longitudinal Stability

The longitudinal X-plot illustrates the rate at which the c.g. moves aft as a function of the horizontal tail area and the rate at which the aerodynamic center, or a.c., moves aft as a function of the horizontal tail area. This will be plotted for the HTA, which features a conventional configuration.

The a.c. leg of the plot will be calculated using the following equations:

$$\bar{x}_{ac_A} = \frac{\left[\bar{x}_{ac_{wf}} + \frac{\left\{C_{L_{\alpha h}}\left(1-\frac{d\varepsilon_h}{d\alpha}\right)\left(\frac{S_h}{S}\right)\bar{x}_{ach} - C_{L_{\alpha c}}\left(1+\frac{d\varepsilon_c}{d\alpha}\right)\bar{x}_{acc}\left(\frac{S_c}{S}\right)\right\}}{C} + C_{L_{\alpha wf}}\right]}{F} \qquad (53)$$

$$F = \frac{\left[1+\left(C_{L_{\alpha h}}\left(1-\frac{d\varepsilon_h}{d\alpha}\right)\left(\frac{S_h}{S}\right)+C_{L_{\alpha c}}\left(1+\frac{d\varepsilon_c}{d\alpha}\right)\left(\frac{S_c}{S}\right)\right)\right]}{C_{L_{\alpha wf}}} \qquad (54)$$

The figure below illustrates how to find the geometric quantities to perform these calculations. (Roskam, Airplane Design Part II: Preliminary Configuration Design and Integration of the Propulsion System, 2011)
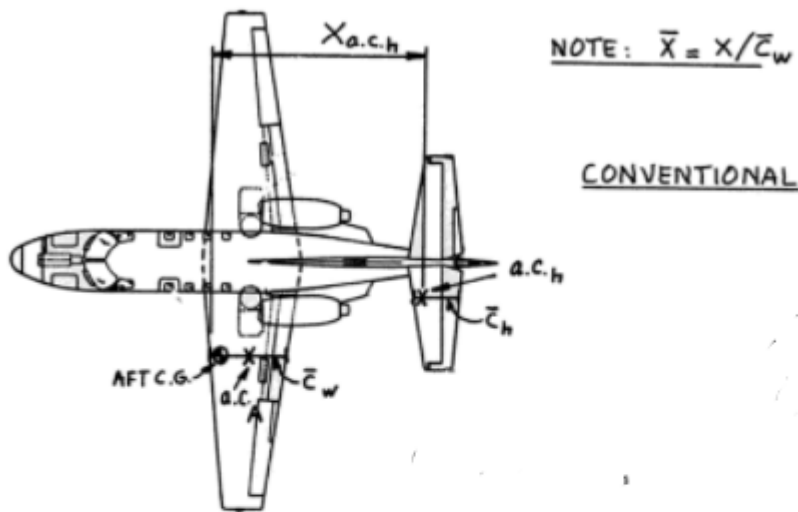
Figure 76. Geometric quantities for aircraft calculations
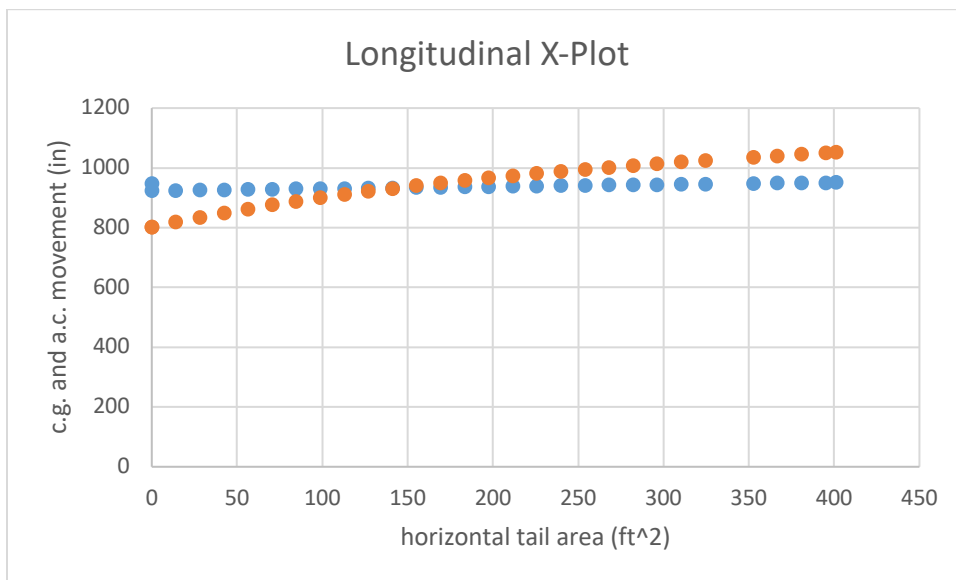
Figure 77. Longitudinal X-Plot for the HTA

The longitudinal x plot illustrates that as the tail plane area is increased, the c.g. moves aft, and the a.c. also moves aft, but more slowly. The 10% difference between the a.c. and c.g. location is the optimal area of the horizontal stabilizer.

The 10% static margin yields a horizontal stabilizer area of 380-401 ft². These results match the results from the wing design, where the horizontal stabilizer area was sized to 401 ft².

This yields a slightly larger wing area than the 737-100, but this is likely due to the extra battery weight being suspended below the wings.

The HTA has a level of instability of $0.085\bar{c}_w$, which has been chosen based on the instability levels of comparable jet transport. Using the aft c.g. leg of the longitudinal X-plot, the longitudinal stability augmentation system must generate a change in static margin of $\Delta SM = 0.085 + 0.05 = 0.135$, where the minimum static margin of $\bar{X}_{cg} - \bar{X}_{ac} = 0.05$ or 5%. The empennage area follows from these calculations. The original horizontal tail area of 401 ft^2 will be compared with the horizontal tail area obtained from the longitudinal X-plot. Since they are the same, 401 ft^2 will remain the design size.

9.3. Static Directional Stability

The directional X-plot illustrates the change in directional stability for various vertical tail areas.
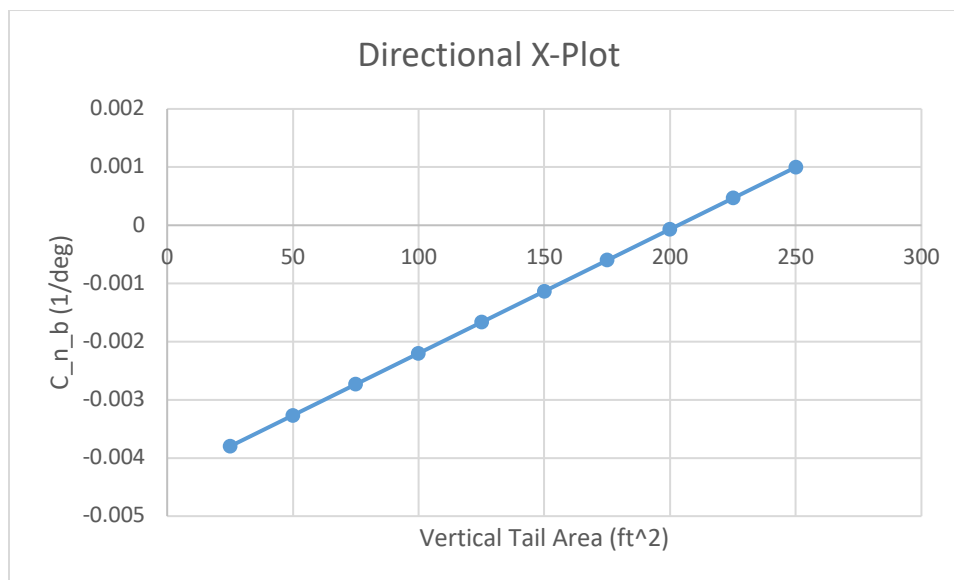
Figure 78. HTA Directional X-Plot

The desired de facto level of directional instability is $C_{n_\beta} = 0.0010$. From the plot, $C_{n_\beta} = -0.001$ and there is a difference of 0.002. The sideslip feedback system must support

this difference. To compute the required sideslip to rudder feedback gain, the following

equations will be used.

$$k_\beta = \frac{\Delta C_{n_\beta}}{C_{n_{\delta_r}}}, \text{ with } k_\beta < 5 \ deg/deg \tag{55}$$

$$\Delta C_{n_\beta} = 0.0010 - C_{n_\beta} \tag{56}$$

As a result, $k_\beta = \frac{\Delta C_{n_\beta}}{C_{n_{\delta_r}}} = \frac{0.0010 - 0.002}{-0.0012} = 0.833 \ deg/deg$. This is acceptable, and the

vertical tail is not critical for the HTA.

9.4. Minimum Control Speed with One Engine Inoperative

The critical one engine out yawing moment can be determined from the following

equation.

$$N_{t_{crit}} = T_{TO_e} Y_t \tag{57}$$

In this equation Y_t is the lateral thrust moment arm of the most critical engine, which equals 17.5

ft. T_{TO_e} is the thrust required by the engine at takeoff. The geometry for these calculations is

illustrated in the figure below.
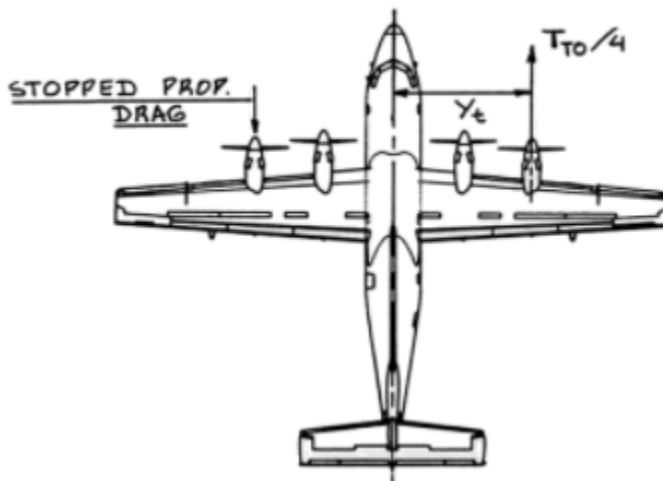
Figure 79. Geometry for one engine out V$_{mc}$ calculations

Using the geometry and the thrust at takeoff, $N_{t_{crit}} = T_{TO_e}Y_t = 21,000lb \cdot 17.5\ ft =$

$367,500\ ftlbs$. For a jet transport with a low bypass ratio, $N_D = 0.15N_{t_{crit}}$, and thus $N_D =$

$55,125\ ft\ lbs$. Therefore, the critical engine out yawing moment is 55,125 ft lbs.

The following equations can be used to calculate the maximum allowable V_{mc} and the

rudder deflection required to hold the engine out condition at V_{mc}. The rudder deflection angle

should not exceed 25 degrees. If it does, the vertical tail needs to be resized or the rudder needs

to be resized.

$$V_{mc} = 1.2\ V_s \tag{58}$$

$$\delta_r = (N_D + N_{t_{crit}})/\bar{q}_{mc}SbC_{n_{\delta_r}} \tag{59}$$

Using the lowest stall speed, which is the stall speed at landing, V_{mc} is calculated to be 1.2 $V_{s_L} =$

$1.2(54) = 64.8\ kts$. From the vertical tail and rudder geometry, the control power derivative is

equal to $C_{n_{\delta_r}} = -0.245\ rad^{-1}$. Thus, at $V_{mc} = 64.8$ kts, the rudder deflection angle is

calculated to be $\delta_r = \dfrac{T_{TO_e}Y_t}{-\bar{q}SbC_{n_{\delta_r}}}$.

$\delta_r = (N_D + N_{t_{crit}})/\bar{q}_{mc}SbC_{n_{\delta_r}} = (55,125\ ft\ lbs + 367,500\ ft\ lbs)(.5(7.38*$

$10^{-4})(109.37ft/s)^2(250\ ft^2)(93.011\ ft)\left(-\dfrac{0.0012}{deg}\right) = 43.6^{\circ}$. This is a large angle, and the

size of the vertical tail should be increased and the calculation performed again.

9.5. Empennage Design-Weight and Balance- Landing Gear Design- Longitudinal Static Stability and Control Check

The horizontal stabilizer area meets the 10% static margin difference, and the horizontal

stabilizer does not need to be resized. The vertical stabilizer needs to increase in order to provide

a smaller rudder deflection angle.

9.7. Conclusion

Overall, the sizing of the HTA is still comparable to the 737-100 model. The horizontal

stabilizer was increased to 401 ft^2, as determined in the wing sizing chapter, and this sizing will

be maintained based on the longitudinal X-plot.

The critical one engine out yawing moment has been determined to be 55,125 ft lbs, with

a minimum control speed of 64.8 kts.

Rudder deflection should not exceed 25 degrees, but was calculated to be 43.6°, whichi

necessitates an increase in size of the vertical stabilizer. This will be explored further during the

Class II sizing.

10. Drag Polar Estimation

10.1. Introduction

A drag polar is the relationship between the airplane's lift and its drag, where the lift

coefficient depends on the drag coefficient. The results of the HTA's comparison of its lift and

drag coefficients will be examined and displayed in a plot.

To perform the drag polar estimation, Roskam's method will be utilized. This involves

eight steps. Initially, the wetted area of the airplane components will be estimated. The airraft's

components will be analyzed individually. These include the fuselage, wings, empennage, and

engine and battery nacelles. Once these have been computed, the equivalent parasite area will be

calculated. From there, the compressibility drag increment will be found along with the flap

drag increment, and landing gear drag increment. The drag polars for cruise, takeoff, and

landing will be constructed, and the L/D critical values will be determined from the drag polars.

10.2. Airplane Zero Lift Drag

The following equations will be used to compute the wetted areas for each component.

$$S_{wet_{plf}} = 2S_{exp.plf}\{1 + 0.25\left(\frac{t}{c}\right)_r (1 + \tau\lambda)/(1 + \lambda) . \tag{60}$$

$$\tau = \left(\frac{t}{c}\right)_r / \left(\frac{t}{c}\right)_t \tag{61}$$

$$\lambda = c_t/c_R \tag{62}$$

$$S_{wet_{fus}} = \pi D_f l_f \left(1 - \frac{2}{\lambda_f}\right)^{\frac{2}{3}} (1 + 1/\lambda_f^2) \tag{63}$$

$$\lambda_f = l_f/D_f \tag{64}$$

$$S_{wet_{fan}} = l_n D_n \{2 + \frac{0.35 l_1}{l_n} + \frac{0.8 l_1 D_{h1}}{l_n D_n} + \frac{1.15\left(1 - \frac{l_1}{l_n}\right)D_{ef}}{D_n}\} \tag{65}$$

$$S_{wet_{gen}} = \pi l_g D_g \left[1 - \left(\frac{1}{3}\right)\left(1 - \frac{D_{eg}}{D_g}\right)\{1 - 0.18)\left(\frac{D_g}{l_g}\right)^{5/3}\}\right] \tag{66}$$

$$S_{wet_{plug}} = 0.7\pi l_p D_p \tag{67}$$

It's important to note that the wings, empennage, and nacelles usually intersect the fuselage or a nacelle, so the intersection of the wetted area will be subtract. In order to estimate the wetted area of the batteries, the calculated wetted area of the engine nacelles will be multipled by a factor of 1.5.

The wetted areas are as follows:

Table 35. Wetted Area Summary

Component	Wetted Area (ft²)
Wing	2,367
Intersection of wing and fuselage	-200
Vertical Tail	463
Horizontal Tail	642
Engine Nacelles	455
Battery Nacelles	455
Fuselage	4,000
TOTAL WETTED AREA	8,182

The wetted area compares fairly with the wetted area of a jet transport that weights approximately 90,000 lbs and has a wetted area of $6,000 ft^2$, as illustrated in the graph below (Roskam, Airplane Design Part II: Preliminary Configuration Design and Integration of the

Propulsion System, 2011). The HTA has a larger wetted area due to the battery nacelles. This

added area may impact the cruise L/D and the corresponding fuel consumption.
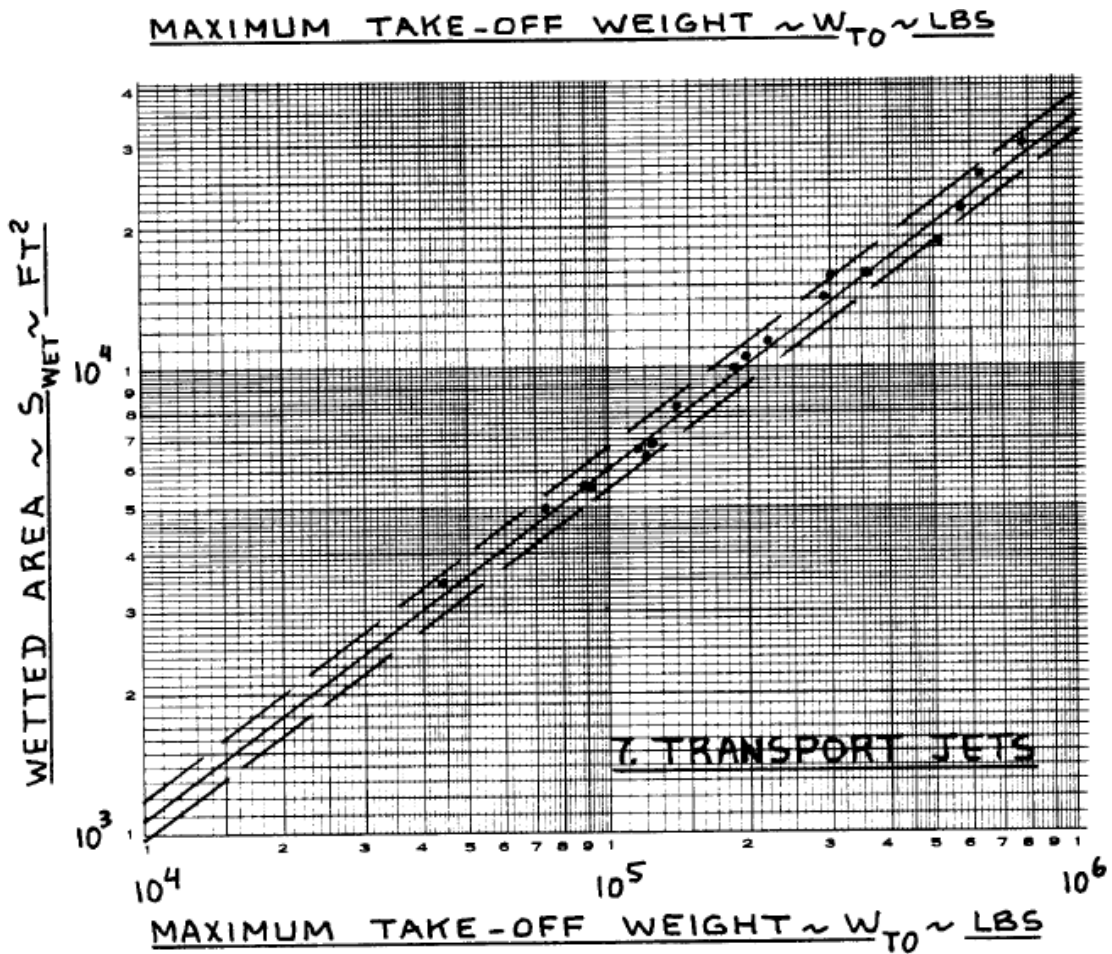
Figure 80. Maximum takeoff weight vs. wetted area for jet transports

Using the plot below, the equivalent parasite area of the HTA is approximately 22 ft^2.
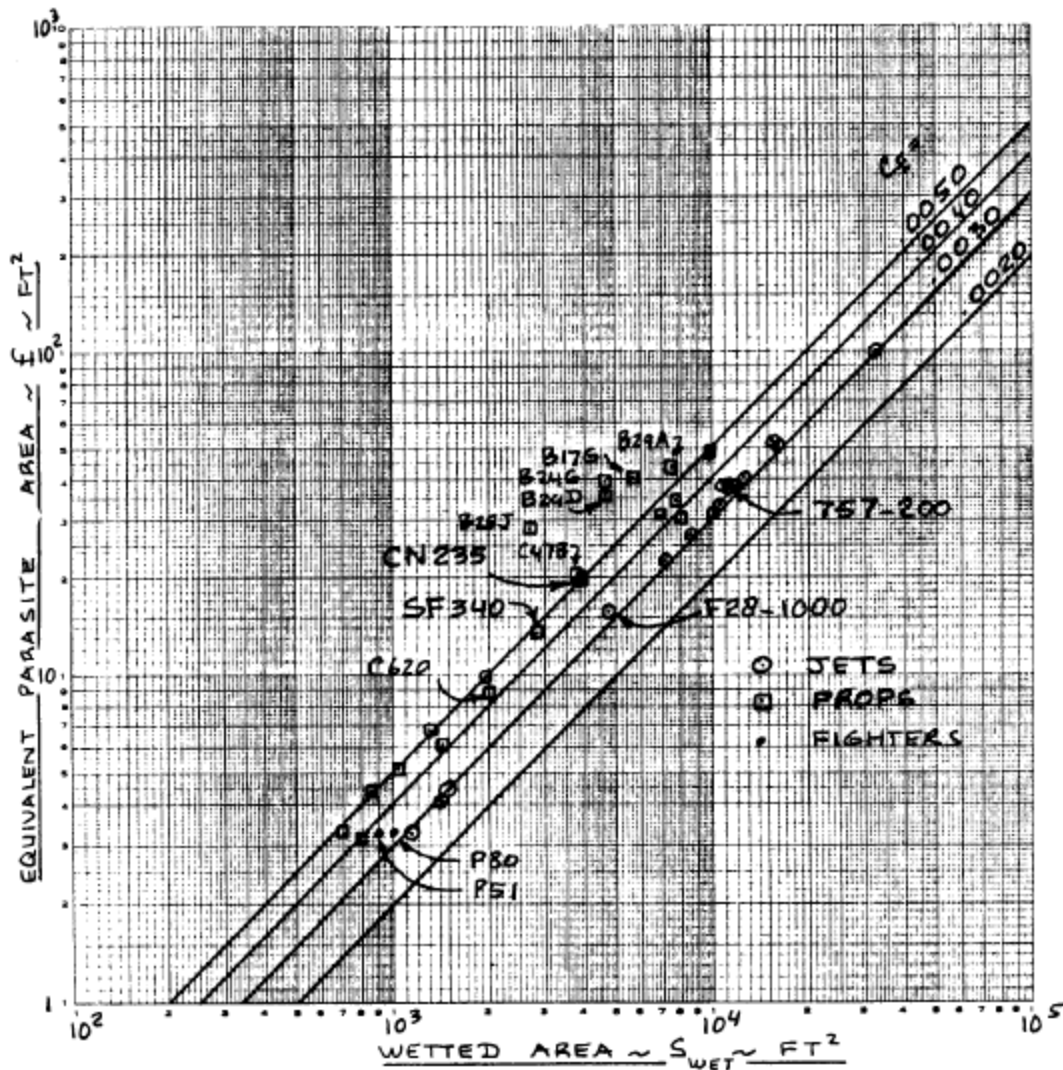
Figure 81. Wetted area vs. equivalent parasite area

10.3. Low Speed Drag Increments and Compressibility Drag

The clean zero lift drag coefficient at low speed is $C_{D_0} = \frac{f}{s} = \frac{22}{1098} = 0.02$. Using the

figure below, the compressibility drag increment is about 0.0005. Due to this low value the

cruise drag does not need to be re-evaluated. The cruise value of the zero lift drag coefficient

can be summarized as $C_{D_0} = 0.0005 + 0.02 = 0.0205$. The minimum lift to drag ratio can be

calculated and then compared to the previously determined L/D.

Originally, C_{D_0} was estimated to be:

Table 36. C_{D_0} summary

Configuration	C_{D_0}
Clean	0.014
Takeoff flaps	0.03
landing flaps	0.08
gear down	0.02

Using the clean C_{D_0} value and the newly calculated $C_{D_0} = 0.0205$, the (L/D)$_{max}$ values are equal

to 18.27 and 18.05, respectively. Based on the sensitivity calculation, for each increase in L/D,

there is a decrease of 856 lbs. Thus, for a change of 0.224, the weight will increase 192 lbs,

which is not substantial enough to change the structure.
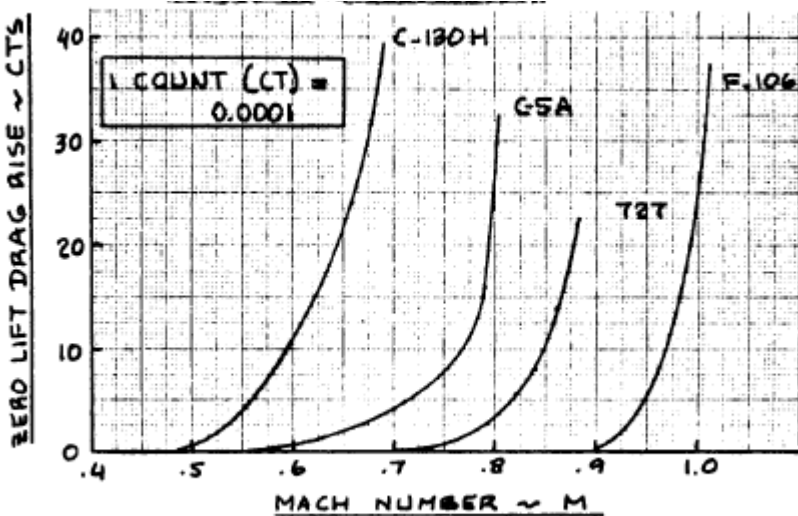
Figure 82. Typical Compressibility Drag Behavior

10.3.1. High Lift Device Drag Increments for Takeoff and Landing Gear Drag

Table 37. First Estimates for Drag with flaps and gear down

Configuration	ΔC_{D_0}	e
Clean	0	0.80 – 0.85
Take-off flaps	0.010 – 0.020	0.75 – 0.80
Landing Flaps	0.055 – 0.075	0.70 – 0.75
Landing Gear	0.015 – 0.025	no effect

The values in table 2 will be used to produce the drag polar plot based on the change in C_{D_0} for various configurations, including clean, takeoff flaps, landing flaps, and landing gear.

10.5. Airplane Drag Polars
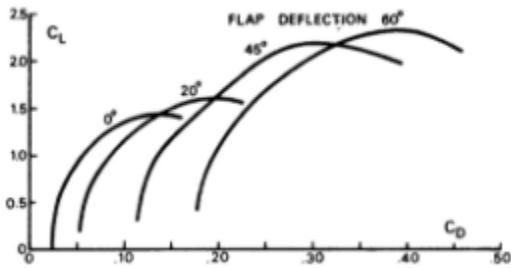
Figure 83. Low speed polars for transport
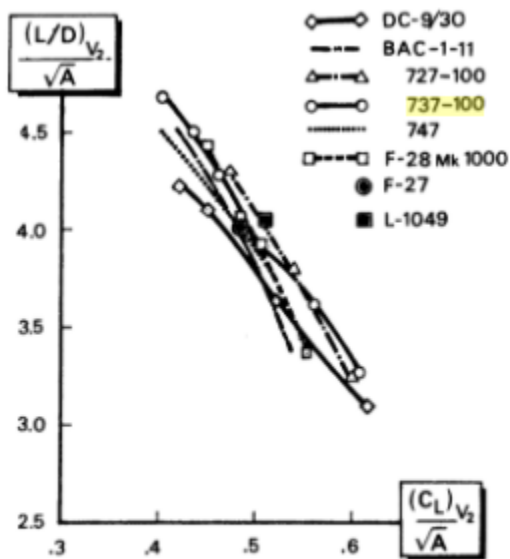
Figure 84. L/D Ratios

10.6. Discussion

The HTA will not be resized. Although it is heavier than anticipated, it is within 10%, and was expected, due to the battery weight. A more thorough estimation would probably include subtracting more overlapping wetted areas, as well as more accurately sizing the battery nacelles.

10.7. Conclusion

The HTA is ready to commence Class II sizing following an analysis of the economic,

safety, and environmental tradeoffs.

11. Environmental and Economic Tradeoffs

11.1. Important Design Parameters

The HTA three view drawing that reflections the iterations of the design is illustrated in
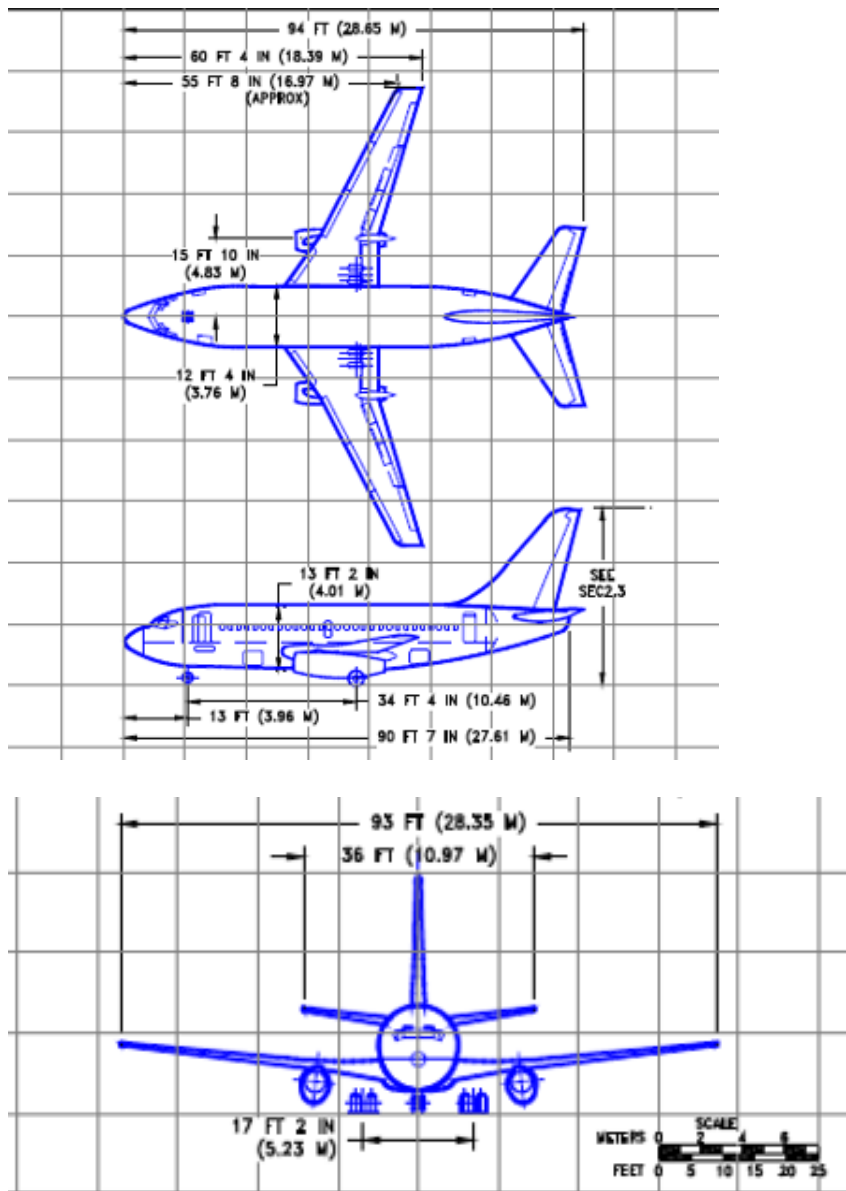
Figure 85. 3-view of HTA

The most important feature of this aircraft is the implementation of lithium ion batteries for battery powered cruise, loiter, descent, and landing. These batteries changed the weight analysis and overall sizing of the aircraft, but many of the features, such as the fuselage design, remained the same as the original 737-100. The following will summarize economic and environmental tradeoffs, as well as safety tradeoffs for the HTA.

11.2. Recommendations

To further support this design concept, more research needs to be done for the overall battery weight and volume sizing. The sizing summarized in the reports reflected conceptual designs and sizings that have been done for both similar sized aircraft, such as Boeing's conceptual SUGAR designs, and small aircraft, through the work of Riboldi. Additionally, more research could be done with lithium ion batteries to determine if the battery specific energy could be increased further. In terms of design, the vertical stabilizer size needs to increase as well. This is to support a lower rudder deflection angle.

11.2.2. Einvironmental/Economic Tradeoffs

12. Preliminary Design Sequence II

This chapter commences the Class II sizing of the HTA. The systems that have the largest impact on the HTA include the propulsion system, specifically engines and the fuel and battery power to support the system; aerodynamic control systems, including the ailerons, elevator, and rudder; and aircraft structural system, which include the wings, fuselage, horizontal tail, and vertical tail. These systems have a significant impact on the empty weight of the aircraft, and will be thoroughly analyzed during the weight and balance analysis. Additionally, a ghost view of the aircraft, presented in Figure 86, illustrates the aircraft systems and their current locations.
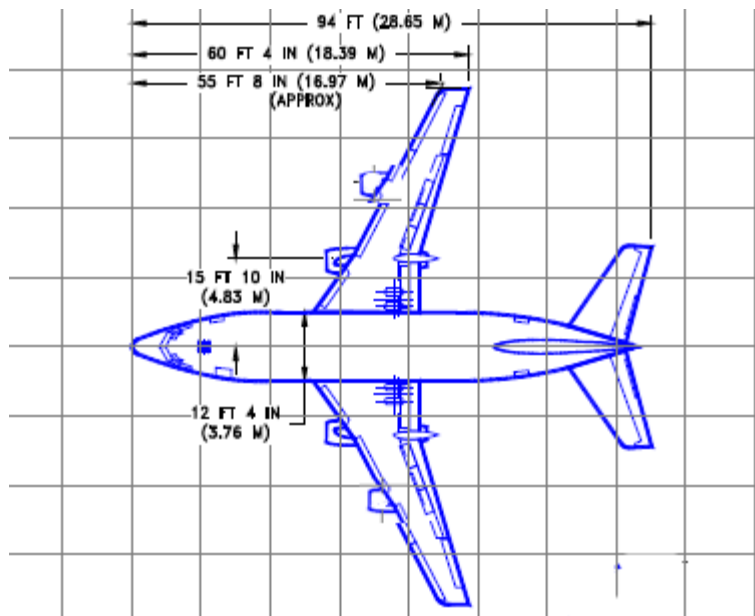
Figure 86. Ghost View of Aircraft

Initially, a V-n diagram will be constructed, and then the Class II weight and balance analysis will be performed. From there, the Classs II stability and control analysis will be conducted, followed y the Class II drag polar analysis. The power computation and installation will follow, analyzing power for the aircraft along with factors that change the power output, such as altitude. Finally, a cost analysis will be performed to predict the acquisition cost of the airplane. This will be performed based on statistical data and equations for cost.

13. V-n Diagram

A V-n diagram is a graph of the velocity vs. load factor, which illustrates the aircraft performance limits. These limits include the design ultimage load factors and the speed to which each of the airplane's parts have been designed (Roskam, Airplane Design Part V: Component Weight Estimation, 2003). This will be used with the Class II weight estimation and will be considering the case where flaps are up.

For the calculations, the following nomenclature will be used: V_C =design cruise speed, V_D=design diving speed, V_M =design maneuvering speed, V_S=+1g stall speed or minimum speed at which airplane is controllable, and V_B= design speed for maimum gust intensity.

13.1. Calculation of V_S

To determine the minimum controllable speed of the FAR 25 aircraft, the following equation will be used: (Roskam, Airplane Design Part V: Component Weight Estimation, 2003)

$$V_S = \left\{ \frac{2\left(\frac{GW}{S}\right)}{\rho C_{N_{max}}} \right\}^{1/2} \tag{68}$$

Note that GW is the flight design gross weight, measured in lbs; S is the wing area in square feet; the air density is measured in slugs/cubic feet; and $C_{N_{max}}$ is defined as:

$$C_{N_{max}} = \left\{ \left(C_{L_{max}}\right)^2 + \left(C_{D_{at\ C_{L_{max}}}}\right)^2 \right\}^{1/2} \tag{69}$$

Another way to calculate $C_{N_{max}}$ is using the following:

$$C_{N_{max}} = 1.1 C_{L_{max}} \tag{70}$$

Solving these equations gives $C_{N_{max}} = 1.56$ and $V_S = 129.8$ kts.

13.2. Calculation of V_C

The design cruise speed must be greater than the design speed for maximum gust intensity in the event that there are severe atmospheric turbulences that could cause speed increases. To determine V_B, consider the intersection of the $C_{N_{max}}$ line and the V_B gust line. The value of V_B may not be less than the value at the intersection. From there, using the equation below, V_C=290 kts.

$$V_C \geq V_B + 43\ kts \tag{71}$$

13.3. Calculation of V_D

To calculate the design driving speed, the following equation will be used:

$$V_D \geq 1.25 V_C \qquad (72)$$

As a result, $V_D \geq 368.75$ kts.

13.4. Calculation of V_M

The design maneuvering speed is given by the following condition:

$$V_M \geq V_{S_1}(n_{lim})^{\frac{1}{2}} \qquad (73)$$

Therefore, $V_M = 205.23\ kts$. The limit maneuvering load factor at V_C depends on the more critical requirement of either the positive limit maneuvering load factor or the gust load factor lines. The positive maneuvering load factor, $n_{lim_{pos}}$. Where the following equation determines the positive limit maneuvering load factor.

$$n_{lim_{pos}} \geq 2.1 + \left\{ \frac{24,000}{W+10,000} \right\} \qquad (74)$$

The only exception to this is that the limit maneuvering load factor must be greater than or equal to 2.5 at all times, but not greater than 3.8 at the takeoff weight. Thus, although $n_{lim_{pos}}$ is equal to 2.4, following the exception, $n_{lim_{pos}}$=2.5. The negative maneuvering load factor has two specifications. This value is greater than or equal to -1 up to the design cruise velocity and from the cruise speed design to the the design diving speed, the negative maneuvering load varies linearly.

To determine the negative stall speed line, the following equations will be used:

$$V_{S_{neg}} = \left\{ \frac{2\left(\frac{GW}{S}\right)}{\rho C_{N_{maxneg}}} \right\}^{1/2} \qquad (75)$$

$$C_{N_{maxneg}} = \left\{ \left(C_{L_{maxneg}} \right)^2 + \left(C_{D_{at\ C_{Lmaxneg}}} \right)^2 \right\}^{1/2} \qquad (76)$$

$$C_{N_{max_{neg}}} = 1.1 C_{L_{max_{neg}}} \tag{77}$$

It will be assumed that $C_{L_{max_{neg}}} = -1.0$, from similar transport aircraft. As a result, $C_{L_{max_{neg}}} =$

-1.1 and $V_{S_{neg}} = 154$ kts.

The design maneuvering speed depends on the construction of the gust load factor lines if

they are more critical. Thus the derived gust velocities will be determined. To plot the gust

lines, the following equations will be used (Roskam, Airplane Design Part V: Component Weight

Estimation, 2003).

$$n_{lim} = 1 + \left(K_g U_{de} V C_{l_\alpha}\right)/(498 GW/S) \tag{78}$$

$$K_g = 0.88\mu_g/(5.3 + \mu_g) \tag{79}$$

$$\mu_g = 2\left(\tfrac{GW}{S}\right)/(\rho(mgc)gC_{l_\alpha}) \tag{80}$$

In these equations, K_g is the gust alleviation factor, and the gust load factor for the lines is

defined using n_{lim}. Note that V is the true airspeed, and that is the variable. Since n_{lim} also

depends on U_{de}, those values, for each of the gust lines, for $V_B, V_C,$ and V_D, can be determined

using the equations below (Roskam, Airplane Design Part V: Component Weight Estimation,

2003).

$$V_{B_{U_{de}}} = \begin{cases} 66 \ fps \ for \ 0 \le h \le 20{,}000 \ ft \\ 84.67 - 0.000933h \ for \ 20{,}000 \le h \le 50{,}000 \ ft \end{cases} \tag{81}$$

$$V_{C_{U_{de}}} = \begin{cases} 50 \ fps \ for \ 0 \le h \le 20{,}000 \ ft \\ 66.67 - 0.000833h \ for \ 20{,}000 \le h \le 50{,}000 \ ft \end{cases} \tag{82}$$

$$V_{D_{U_{de}}} = \begin{cases} 25 \ fps \ for \ 0 \le h \le 20{,}000 \ ft \\ 33.34 - 0.000417h \ for \ 20{,}000 \le h \le 50{,}000 \ ft \end{cases} \tag{83}$$

Assuming a cruise height of 35,000 feet, the gust lines in Figure 88, below, were graphed based

on the equations:

$$V_B = 1 + 0.004835V \tag{84}$$

$$V_C = 1 + 0.003487V \tag{85}$$

$$V_D=1+0.001742V \tag{86}$$

The negative gust lines had negative slopes, but still started at 1.

13.5. V-n Maneuver Diagram and V-n Gust Diagram

The following graphs summarize the design limits, by illustrating the V-n Maneuver Diagram and the V-n Gust Diagram for the HTA.
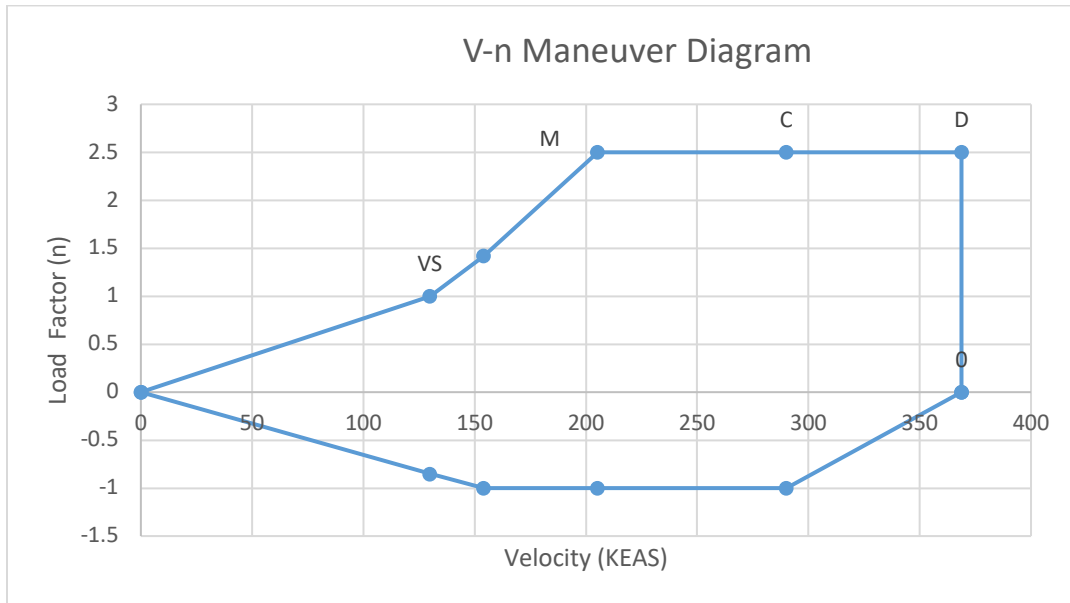
Figure 87. V-n Maneuver Diagram
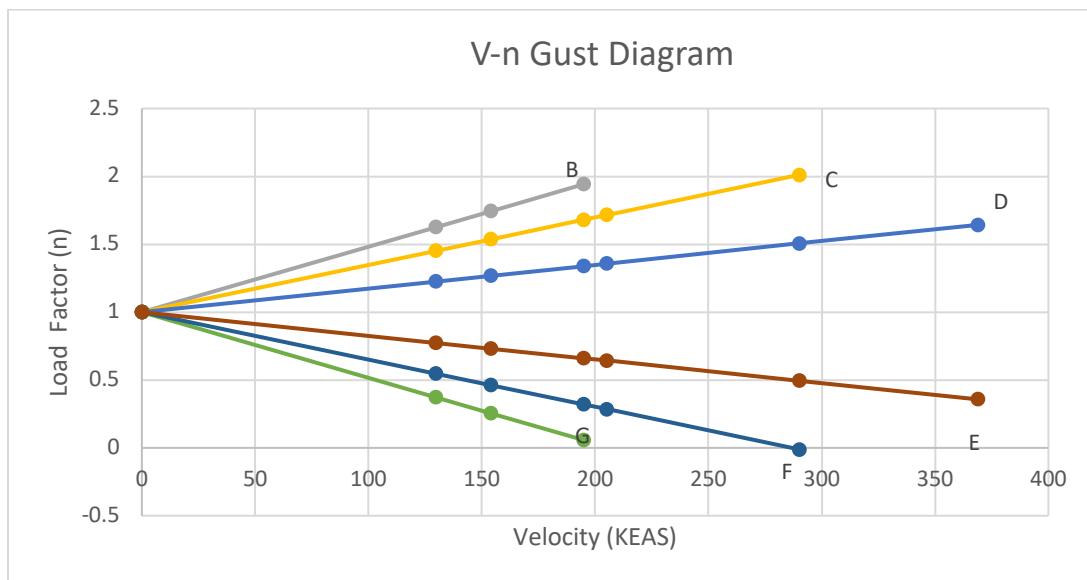
Figure 88. V-n Gust Diagram

According to the diagrams in Figure 87 and Figure 88, the positive load factor that can be safely achieved at varying airspeeds ranges from 0 to 2.5, while the negative load factor cannot go below -1. Any velocity and load factor combination that lies outside of the line would result in a stall; whereas, any point inside the lines is within the flight envelope, and is possible. These diagrams were constructed assuming symmetrical loading. This chart has been plotted for 35,000 feet, but can be plotted at various altitudes to illustrate the loading factor achieveable. The gust lines fall within the maneuvering V-n diagram.

14. Class II Weight and Balance

From the Class I analysis, the following weights are already known: payload, crew, fuel, batteries, trapped fuel and oil, and engine weight. The remaining weights will need to be estimated. The weight of the structure consists of the wing, fowler flaps, empennage, fuselage, nacelles, and landing gear. The weight of the powerplant consists of the engines, fuel system, propulsion system, accessory drives, and thrust reversers. The fixed equipment weight consists of flight controls, electrical system, instrumentation, avionics, electronics, airconditioning, pressurization syste, de-icing system, oxygen, APU, furnishings, baggage and cargo handling, operational items, and paint. Equations used in Roskam's fifth volume will be used to compute the weights of the structure, power, and fixed equipment. From there, the Class II empty weight will be compared to the Class I empty weight. Iterations will be performed if there is a discrepancy between the two weights.

14.1. Class I Weights

The following table summarizes the known weight values from the Class I sizing.

Table 38. Class I Weights

Item	Nomenclature	Weight (lbs)
payload	W_{pl}	19,680
Crew	W_{crew}	820
Fuel	W_F	4,140
Trapped Fuel and Oil	W_{tfo}	150
Batteries	W_{bat}	10,300

14.2. Weight Estimate Calculations

14.2.1. Structural Weight

The structural weight, W_{struct}, consists of the wing, W_w, fowler flaps, empennage, W_{emp}, fuselage, W_{fus}, nacelles, W_n, and landing gear, W_g. Both the GD Method and the Torenbeck method will be used to compute the weight of the wing. Both methods, which can be used for transport aircraft, consider the weight of normal high lift devices and ailerons.

14.2.1.1. Wing Weight

The GD method will use the equation, below, where the maximum Mach number at sealevel should be between 0.4 to 0.8 and the maximum wing thickness ratio should range from 0.08 to 0.15 (Roskam, Airplane Design Part V: Component Weight Estimation, 2003). The HTA cruises at Mach 0.75 and has a thickness ratio fo 0.124. As a result, the GD Method can be applied for estimation and the equation can be used.

$$W_w = \{0.00428(S^{0.48})(A)(M_H)^{0.43}(W_{to}n_{ult})^{0.84}\lambda^{0.14}\} / \left[\left\{100\left(\tfrac{t}{c}\right)_m\right\}^{0.76}\left\{cos\Lambda_{\tfrac{1}{2}}\right\}^{1.54}\right] \quad (87)$$

Additionally, the aircraft meets specifications for the Torenbeek sizing, as it is a transport with a take-off weight greater than 12,500 lbs. The following equation presents Torenbeek's method (Roskam, Airplane Design Part V: Component Weight Estimation, 2003).

$$W_w = 00017 W_{MZF} (b / \cos\left(\Lambda_{\frac{1}{2}}\right))^{0.75} (1 + \left(\frac{6.3\cos\left(\Lambda_{\frac{1}{2}}\right)}{b}\right)^{0.5} (n_{ult}^{0.055}) \left(\frac{bs}{t_r W_{MZF}\cos\Lambda_{\frac{1}{2}}}\right)^{0.3} \tag{88}$$

The GD Method gives an estimation of 4,872 lbs, and the Torenbeek Method gives an estimation

of 8,038. The Class I sizing provided an estimate of 7,636 lbs. Averaging the three weights

gives 6,849 lbs. However, considerations must be made for the number of engines and Fowler

flaps. With 2 suspended engines and 2 suspended battery nacelles, the weight will initially be

reduced by 10%, and with the Fowler flaps, the weight is increased by 2%. The resulting Class

II estimate of the wing weight is 6,287 lbs.

14.2.1.2. Empennage Weight

The Empennage consists of the sum of the horizontal tail and vertical tail. For

commercial transport jets, like the HTA, the GD Method and the Torenbeek Method will be

applied to estimate. From there, comparisons will be made to the Class I estimate and a final

Class II estimate will be established.

Using the GD Method, the horizontal tail and vertical tail can be estimated using the

following two equations (Roskam, Airplane Design Part V: Component Weight Estimation,

2003).

$$W_h = 0.0034((W_{to}n_{ult})^{0.813}(s_h)^{0.584}\left(\frac{b_h}{t_{r_h}}\right)^{0.033}\left(\frac{mgc}{l_h}\right)^{0.28})^{0.915} \tag{89}$$

$$W_v = 0.19((1 + \frac{z_h}{b_v})^{0.5}(W_{to}n_{ult})^{0.363}(S_v)^{1.089}(M_H)^{0.601}(l_v)^{-0.726}\left(1 + \frac{S_r}{S_v}\right)^{0.217}(A_v)^{0.337}\ (1 +$$

$$\lambda_v)^{0.363}\left(\cos\Lambda_{\frac{1}{4}}\right)^{-0.484})^{1.014} \tag{90}$$

Torenbeek's Method involves the following equations (Roskam, Airplane Design Part V:

Component Weight Estimation, 2003).

$$W_h = K_h S_h (3.81(S_h)^{0.2} V_D)/(1000 \cos \Lambda_{\frac{1}{2}h})^{\frac{1}{2}}) - 0.287 \tag{91}$$

$$W_v = K_v S_v (3.81(S_v)^{0.2} V_D)/(1000 \cos \Lambda_{\frac{1}{2}v})^{\frac{1}{2}}) - 0.287 \tag{92}$$

For fixed incidence stabilizers, $K_h = 1$, and for fuselage mounted horizontal tails, $K_v = 1$.

The GD Method yields a horizontal tail weight of 831.649 lbs; while the Torenbeek Method

produces a horizontal tail weight of 1,169 lbs. The GD Method provides a vertical tail area of

2,797 lbs, and the Torenbeek Method calculated 1,093 lbs. The total empennage weight from

GD is 3,628 lbs, and the total empennage weight from Torenbeek is 2,263 lbs. The Class I

estimate had an empennage weight of 1,992 lbs. Taking the average of the three yields 2,627 lbs

for the Class II estimate of the empennage.

14.2.1.3. Fuselage Weight

For commercial transport aircraft, the fuselage weight can be calculated using the GD

Method and the Torenbeek Method. Again, both calculations will be performed to assess the best

estimate for Class II fuselage weight.

The GD Method provides the following equation (Roskam, Airplane Design Part V:

Component Weight Estimation, 2003).

$$W_{fus} = 10.43(K_{inl})^{1.42} \left(\frac{\bar{q}}{100}\right)^{0.283} \left(\frac{W_{TO}}{1000}\right)^{0.95} \left(\frac{l_{fus}}{h_{fus}}\right)^{0.71} \tag{93}$$

In the above quation, K_{inl} is the factor that takes into account whether there are inlets on the

fuselage for buried engines. Since the engines are suspended and not buried, $K_{inl} = 1$, and $\bar{q}$ is

the design dive dynamic pressure in psf.

The Torenbeek Method, which applies to jet transport aircraft with dive speeds above 250

kts, provides the following equation (Roskam, Airplane Design Part V: Component Weight

Estimation, 2003).

$$W_{fus} = 0.021 \, K_f \left\{ \left(\frac{V_D l_h}{w_{fus} + h_{fus}} \right)^{\frac{1}{2}} (S_{fgs})^{1.2} \right. \tag{94}$$

S_{fgs} is the fuselage gross shell area in feet. $K_f = 1.08$ for a pressurized fuselage. The weight of

the fuselage is a function of the dive speed, width and height of the fuselage, and the distance

from the wing root quarter cord to the the tail root quarter cord in feet.

Using the GD Method, the fuselage weight is 4024 lbs. The Torenbeek Method calculates

the fuselage weight to be 7425 lbs, and the Class I estimated 8,549 lbs. Since the GD Method is

significantly different, I will use the average of the Torenbeek Method and the Class I estimate.

The Class II fuselage weight estimate is 7,987 lbs.

14.2.1.4. Nacelle Weight

The nacelle weight consists of the podded engines and the structural weight associated

with engine external ducts. The pylon weight is included. The nacelle weight also consists of

the battery nacelles. The GD Method and the Torenbeek Method will be used to calculate the

nacelle weight.

The GD Method for turbojet engines gives the nacelle weight as a function of the capture

area per inlet in square feet, the number of inlets, the nacelle length, and the maximum static

pressure at engine compressor face in psi (Roskam, Airplane Design Part V: Component Weight

Estimation, 2003).

$$W_n = 7.435(N_{inl})\{(A_{inl})^{0.5}(l_n)(P_2)\}^{0.731} \tag{95}$$

Using the hFan geometry, the fan diameter is 89 inches and the length is 156 inches (Bradley &

Droney, Subsonic Ultra Green Aircraft Research: Phase I Final Report, 2011). I will assume that

the maximum static pressure at the engine compressor face is 20 psi based on similar jet

transport data. The GD Method estimates the nacelles to weigh 3,495 lbs.

The Torenbeek Method, which estimates the nacelle weight based on the turbofan engine thrust at takeoff estimates a nacelle weight of 1,564 lbs using the following equation (Roskam, Airplane Design Part V: Component Weight Estimation, 2003).

$$W_n = 0.065 T_{TO} \tag{96}$$

Taking into consideration the two estimation, along with the Class I estimation of 2,082 lbs, the Class II estimation of the nacelle weight is 2,381 lbs.

14.2.1.5. Landing Gear Weight

The landing gear weight for commercial transport aircraft is a function of the takeoff weight, for the GD Method calculation. For the Torenbeek Method, the landing gear is calculated considering constants in the landing gear weight equation. These constants are summarized in Table 39, below (Roskam, Airplane Design Part V: Component Weight Estimation, 2003). The GD Method equations and Torenbeek Method equations are:

$$W_g = 62.21 \left(\frac{W_{TO}}{1000}\right)^{0.84} \tag{97}$$

$$W_g = K_{g_r}(A_g + B_g(W_{TO})^{\frac{3}{4}} + C_g W_{TO} + D_g(W_{TO})^{3/2} \tag{98}$$

Table 39. Constants in Landing Gear Weight Equation

Airplane Type	Gear Type	Gear Comp.	A_g	B_g	C_g	D_g
Jet Trainers and Business Jets	Retr.	Main	33.0	0.04	0.021	0.0
		Nose	12.0	0.06	0.0	0.0
Other civil airplanes	Fixed	Main	20.0	0.10	0.019	0.0
		Nose	25.0	0.0	0.0024	0.0
		Tail	9	0.0	0.0024	0.0
	Retr.	Main	40.0	0.16	0.019	1.5×10^{-5}
		Nose	20.0	0.10	0.0	2.0×10^{-6}
		Tail	5.0	0.0	0.0031	0.0

The GD Method calculates the landing gear weight to be 2,406 lbs. Using the constants for retractable landing gear for a jet transport, the Torenbeek Method calculates the landing gear to

be 3,111 lbs. From the Class I estimate, landing gear was 2,654 lbs. The average results in 2,724

lbs for the Class II estimate.

14.2.1.6. Structure Weight Summary

The total structure weight is summarized by the following table:

Table 40. Class II Estimation of Structure Weight

Component	GD Method Estimate (lbs)	Torenbeek Method Estimate (lbs)	Class I Estimate (lbs)	Class II Estimate (lbs)
Wing	4,872	8,038	7,636	6,287
Empennage	3,628	2,263	1,192	2,627
Fuselage	4,024	7,424	8,549	7,987
Nacelle	3,495	1,564	2,082	2,381
Landing Gear	2,406	3,111	2,654	2,724
TOTAL	18,425	22,400	22,113	22,006

14.2.2. Powerplant Weight

The powerplant weight, W_{pwr}, of the HTA consists of the following: weight of the

engines, including the exhaust, cooling, supercharger, and lubrication systems; air induction

system, which includes the inlet ducts, ramps, spikes, and controls; fuel system; and the

propulsion system, which includes engine controls, starting systems, and provisions for engine

installation (Roskam, Airplane Design Part V: Component Weight Estimation, 2003). Since the

HTA will be using the hFan engine, which is a hybrid electric system, allowing the HTA to be

able to use a gas turbine for some stages of the mission and batteries for other stages of the

mission, while providing sufficient thrust for the aircraft with the added battery weight, the

specifications of the propulsion system are available. A schematic of the hFan propulsion system

is illustrated in the figure below (Bradley & Droney, Subsonic Ultra Green Aircraft Research:

Phase I Final Report, 2011).
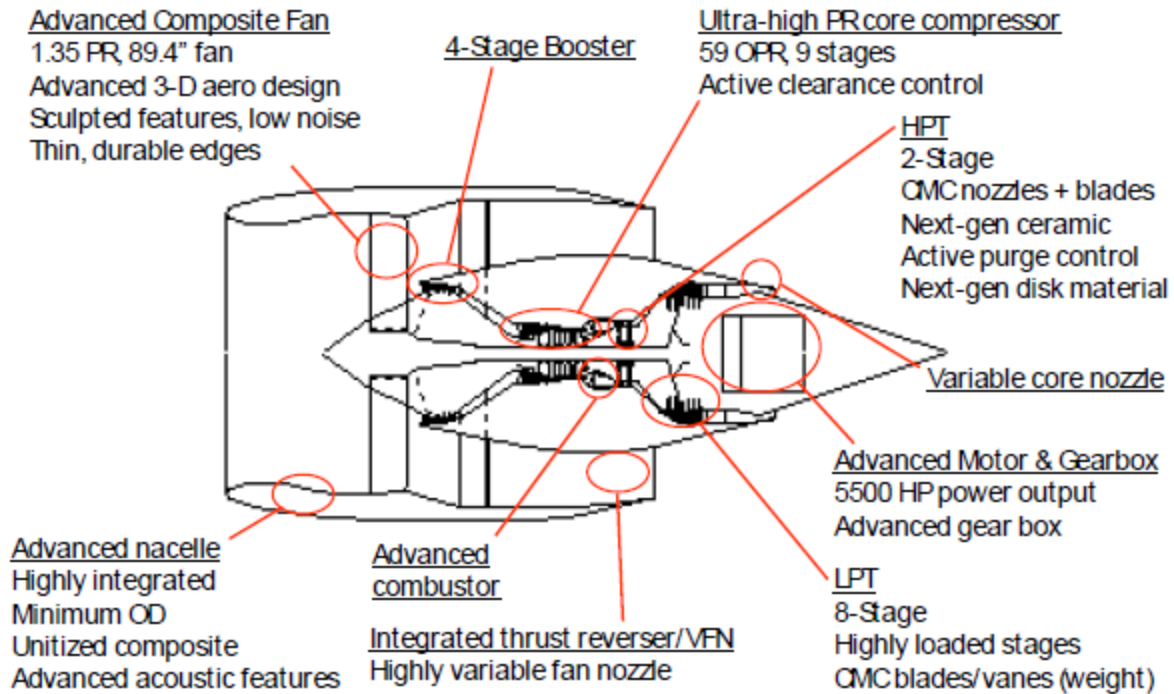
Figure 89. hFan engine overview

The HTA will require 2 suspended engines. Thus, from the manufacturers of the propulsion system, the weight of the propulsion system, which includes the advanced composite fan, 4-stage booster, ultra-high PR core compressor, combustor, thrust reverser, variable core nozzle, low and high pressure turbo, air induction system, fuel system, nacelles, and pylons, is 21,778 lbs (Bradley & Droney, Subsonic Ultra Green Aircraft Research: Phase I Final Report, 2011).

14.2.3. Fixed Equipment Weight

The fixed equipment weight, W_{feq}, consists of the weights of the flight control system, W_{fc}, hydraulic system, W_{hs}, the electric system, W_{els}, instrumentation, avionics, and electronics, W_{iae}, air-conditioning, pressurization, anti- and de-icing system, W_{api}, oxygen system, W_{ox}, auxiliary power unit (APU), W_{apu}, furnishings, W_{fur}, baggage and cargo handling equipment, W_{bc}, operational items, W_{ops}, and paint, W_{pt} (Roskam, Airplane Design Part V: Component Weight Estimation, 2003). Therefore, $W_{feq} = W_{fc} + W_{hps} + W_{els} + W_{iae} + W_{api} + W_{ox} +$

$W_{apu} + W_{fur} + W_{bc} + W_{ops} + W_{pt}$. The Torenbeek Method and GD Methods can be used to estimate the subsystem weights for the transport aircraft. The weights for each method will be compared to the weight estimated from similar data, and a Class II estimate will be formed.

14.2.3.1. Flight Control System Weight

The GD Method to estimate commercial transport aircraft flight control system weight involves the following equation (Roskam, Airplane Design Part V: Component Weight Estimation, 2003).

$$W_{fc} = 56.01 \left\{ \frac{(W_{TO})(\bar{q})}{100000} \right\}^{0.576} \tag{99}$$

For the GD Method, the flight control system weight is a function of the design dive dynamic pressure in psf, $\bar{q}$ and the takeoff weight. Using this method, $W_{fc} = 56.01 \left\{ \frac{(77602.6)(450)}{100000} \right\}^{0.576} =$ 1633.4 lbs.

The Torenbeek Method estimates the flight control system weight for a jet transport with powered flight controls using the following equation (Roskam, Airplane Design Part V: Component Weight Estimation, 2003).

$$W_{fc} = 0.64(W_{TO})^{2/3} \tag{100}$$

Thus, the Tornbeek Method estimate is $W_{fc} = 1164.4$ lbs.

The SUGAR aircraft 765-093, 765-094, 765-095, and 765-096, which range from fully fuel-powered to hybrid powered aircraft, provide a database of additional weight data, including the flight control system data with which to compare the HTA flight control system weights (Bradley & Droney, Subsonic Ultra Green Aircraft Research: Phase I Final Report, 2011). The average flight control system weight is 2,932.5 lbs, which is about 1.8% of the takeoff weight. Using this ratio, the HTA is estimated to have a flight control system weight of 1,432 lbs.

Table 41. SUGAR Flight Control System Weight Data

SUGAR A/C	A/C number	W_{TO} (lbs)	W_{fc} (lbs)	$\dfrac{W_{fc}}{W_{TO}}$
SUGAR Free	765-093	175,635.000	3,084.000	0.018
Refined SUGAR	765-094	136,412.000	2,900.000	0.021
SUGAR High	765-095	163,853.000	2,873.000	0.018
SUGAR Volt	765-096	164,375.000	2,873.000	0.017
		Average	2,932.500	0.018

Thus, combining the three methods of estimation, the Class II estimate of the flight control system weight is the average, 1,410 lbs.

14.2.3.2. Hydraulic System Weight

The hydraulic system weight can be estimated by using Roskam's recommended range of $0.0060W_{TO} - 0.120W_{TO}$, giving a range of 466-931 lbs for the HTA (Roskam, Airplane Design Part V: Component Weight Estimation, 2003). Additional comparisons can be performed, comparing the HTA to similar aircraft. When comparing to similar size aircraft, such as the 737-200, the Hydraulic system weight is 873 lbs, and using the ratio $\frac{W_{hs}}{W_{TO}}$=0.0076, an estimate for the HTA's W_{hs} is 587 lbs.

. When comparing to similarly powered aircraft, such as the SUGAR aircraft, the average for the SUGAR 765-093, 765-094, and 765-095 is 846 lbs (Bradley & Droney, Subsonic Ultra Green Aircraft Research: Phase I Final Report, 2011). For the SUGAR aircraft, the ratio of the hydraulic system weight to the takeoff weight is approximately 0.0053. Using this ratio and the takeoff weight of the HTA, an additional estimate for the HTA's hydraulic system weight is 413 lbs.

Table 42. SUGAR Hydraulic System Weight Data

SUGAR A/C	A/C number	W_{TO} (lbs)	W_{hs} (lbs)	$\dfrac{W_{hs}}{W_{TO}}$
SUGAR Free	765-093	175,635.000	894.000	0.005
Refined SUGAR	765-094	136,412.000	836.000	0.006
SUGAR High	765-095	163,853.000	827.000	0.005
SUGAR Volt	765-096	164,375.000	827.000	0.005
		Average	846.000	0.005

Combining the estimates of 466 lbs, 931 lbs, 413 lbs, and 587 lbs, gives a Class II estimate of 600 lbs for the weight of the hydraulic system.

14.2.3.3. Electrical System Weight

The Torenbeek Method to estimate the electrical system weight uses an equation that is a function of the passenger cabin volume in cubic feet, V_{pax}. This equation is as follows (Roskam, Airplane Design Part V: Component Weight Estimation, 2003).

$$W_{els} = 10.8(V_{pax})^{0.7}\{1 - 0.018(V_{pax})^{0.35}\} \tag{101}$$

The Torenbeek Method gives an estimate of 831 lbs.

The weight of the electrical system can be estimated from weights of similar electrical systems, as well (Bradley & Droney, Subsonic Ultra Green Aircraft Research: Phase I Final Report, 2011). The SUGAR aircraft electrical systems average 2362 lbs. Compared to their takeoff weight, the ratio of electrical system weight to takeoff weight is 0.015. Using this ratio, an estimate, from the SUGAR aircraft, for the electrical system weight of the HTA is 1152 lbs. Using the 737-200 data from Roskam, the ratio of electrical system weight to takeoff weight is 0.009, and the resulting weight for the HTA's electrical system is 716 lbs.

Table 43. SUGAR Electrical System Weight Data

SUGAR A/C	A/C number	W_{TO} (lbs)	W_{es} (lbs)	$\dfrac{W_{es}}{W_{TO}}$
SUGAR Free	765-093	175,635.000	2,557.000	0.015
Refined SUGAR	765-094	136,412.000	2,297.000	0.017
SUGAR High	765-095	163,853.000	2,297.000	0.014
SUGAR Volt	765-096	164,375.000	2,297.000	0.014
		Average	2,362.000	0.015

Averaging the resulting estimates from Torenbeek, SUGAR aircraft, and the 737-200, $W_{es} = 900$ lbs for the Class II estimate.

14.2.3.4. Instrumentation, Avionics, and Electronics Weight

The GD Method calculates the weight of the instruments as the sum of the flight instruments, engine instruments, and other instruments as a function of the number of engines and the number of pilots (Roskam, Airplane Design Part V: Component Weight Estimation, 2003).

$$W_i = N_{pil}\left\{15 + 0.032\left(\frac{W_{TO}}{1000}\right)\right\} + N_e\left\{5 + 0.006\left(\frac{W_{TO}}{1000}\right)\right\} + 0.15\left(\frac{W_{TO}}{1000}\right) + 0.012W_{TO} \tag{102}$$

This method resulst in an estimate of 989 lbs.

The Torenbeek Method for jet transports is a function of the empty weight and the maximum range in nautical miles (Roskam, Airplane Design Part V: Component Weight Estimation, 2003).

$$W_{iae} = 0.575W_e^{0.556}R^{0.25} \tag{103}$$

The Torenbeek Method estimates W_{iae} to be 1,475 lbs.

These two methods can now be compared to the data gathered from the SUGAR aircraft

(Bradley & Droney, Subsonic Ultra Green Aircraft Research: Phase I Final Report, 2011). The

SUGAR aircraft, have a ratio of $\frac{W_{iae}}{W_{TO}}$ =0.014, and therefore provide the HTA estimate for W_{iae} to

be 1,107 lbs. The Class II estimate for W_{iae} is 1,050 lbs.

Table 44. SUGAR Data for Instrumentation, Avionics, and Electronics Weight

SUGAR A/C	A/C number	W_{TO} (lbs)	W_{iae} (lbs)	$\dfrac{W_{iae}}{W_{TO}}$
SUGAR Free	765-093	175,635.000	2,219.000	0.013
Refined SUGAR	765-094	136,412.000	2,277.000	0.017
SUGAR High	765-095	163,853.000	2,277.000	0.014
SUGAR Volt	765-096	164,375.000	2,277.000	0.014
		Average	2,262.500	0.014

14.2.3.5. Air-Conditioning, Pressurization, and Anti- and Deicing Systems Weight

For pressurized commercial jet airplanes, the air-conditioning, pressurization system, and

the anti- and deicing systems weight, W_{api} can be estimated using the GD method. The GD

Method is a function of the passenger cabin volume in cubic feet, V_{pax}, the number of crew

members, N_{cr}, and the number of passengers, N_{pax}. The equation below provides the estimate

(Roskam, Airplane Design Part V: Component Weight Estimation, 2003).

$$W_{api} = 469 \left\{ \frac{V_{pax}(N_{cr}+N_{pax})}{10,000} \right\}^{0.419} \tag{104}$$

The resulting GD Method estimate for W_{api} is 1,019 lbs.

The Torenbeek Method is a function of the length of the passenger cabin in feet, and is

summarized by the following equation (Roskam, Airplane Design Part V: Component Weight

Estimation, 2003).

$$W_{api} = 6.75(l_{pax})^{1.28} \tag{105}$$

The Torenbeek Method estimate is 1,496 lbs.

Compared to similar aircraft, such as the 737-200, with W_{api} = 1,416 lbs, and SUGAR

aircraft, which would give a ratio $\frac{W_{api}}{W_{TO}}$ = 0.01, provides a low estimate of 792 lbs (Bradley &

Droney, Subsonic Ultra Green Aircraft Research: Phase I Final Report, 2011). For the Class II

estimate, the SUGAR aircraft data will be neglected, and W_{api} is estimated as the average of the

GD and Torenbeek Methods along with the 737-200 data and SUGAR A/C data as 1,181 lbs.

Table 45. SUGAR API Weight Data

SUGAR A/C	A/C number	W_{TO} (lbs)	W_{api} (lbs)	$\dfrac{W_{api}}{W_{TO}}$
SUGAR Free	765-093	175,635.000	1,796.000	0.010
Refined SUGAR	765-094	136,412.000	1,549.000	0.011
SUGAR High	765-095	163,853.000	1,582.000	0.010
SUGAR Volt	765-096	164,375.000	1,582.000	0.010
		Average	1,627.250	0.010

14.2.3.6. Oxygen System Weight

The weight of the oxygen system can also be estimated using both the GD Method and

Torenbeek Methods. The two equations, from Roskam are:

$$W_{ox} = 7(N_{cr} + N_{pax})^{0.702} \tag{106}$$

$$W_{ox} = 30 + 1.2N_{pax} \tag{107}$$

As a result, the GD Method gives an estimate of W_{ox} = 175 lbs, while the Torenbeek

Method gives an estimate of W_{ox} = 145 lbs for short flights above 25,000 ft, and W_{ox} =

270 *lbs* for extended flights overwater. Since the HTA is a short to medium range transport

aircraft, to determine a Class II estimate, $W_{ox} = 160$ lbs.

14.2.3.7. Auxiliary Power Unit Weight

The Auliary Power Unit (APU) weight will be taken into account, since the jet transport

requires one. Although a specific APU has not been determined, the weight will be estimated

using Roskam's estimate of the takeoff weight, along with comparisons for the 737-200 and the

SUGAR aircraft APU weights (Bradley & Droney, Subsonic Ultra Green Aircraft Research:

Phase I Final Report, 2011).

According to Roskam, $W_{apu} = 0.004W_{TO} - 0.013W_{TO}$ (Roskam, Airplane Design Part

V: Component Weight Estimation, 2003). This range is 310-1008 lbs, with an average of 660 lbs.

The SUGAR aircraft data gives an average APU weight of 1018.5 lbs, which is 0.6% of the

takeoff weight. Using this data gives a low estimate of $W_{apu} = 498$ lbs. Taking the average of

these values gives a Class II estimate of 450 lbs.

Table 46. SUGAR APU Weight Data

SUGAR A/C	A/C number	W_{TO} (lbs)	W_{apu} (lbs)	$\frac{W_{apu}}{W_{TO}}$
SUGAR Free	765-093	175,635	1,032	0.006
Refined SUGAR	765-094	136,412	1,014	0.007
SUGAR High	765-095	163,853	1,014	0.006
SUGAR Volt	765-096	164,375	1,014	0.006
		Average	1,018.5	0.006

14.2.3.8. Furnishings Weight

Furnishings include cabin furniture and accessory items, like seats, insulation, trim

panels, sound-proofing, instrument panels, control stands, lighting, and wiring. Furnishings also

include galley provisions and the structure, the lavatory system, overhead luggage containers,

escape provisions, and fire-fighting equipment (Roskam, Airplane Design Part V: Component

Weight Estimation, 2003). The Torenbeek Method and GD Method will provide initial

estimates, with the SUGAR data and the 737-200 data providing additional support for the Class

II Estimate.

The GD Method and Torenbeek Method provide the following equations, respectively to

calculate W_{fur}.

$$W_{fur} = 55N_{fdc} + 32N_{pax} + 15N_{cc} + k_{lav}(N_{pax})^{1.33} + k_{buf}(N_{pax})^{1.12} + 109\left\{\frac{N_{pax}(1+P_c)}{100}\right\}^{0.505} + 0.771\left(\frac{W_{TO}}{1000}\right) \tag{108}$$

$$W_{fur} = 0.211(W_{TO} - W_F)^{0.91} \tag{109}$$

These two equations yield W_{fur} = 3,918 and 5,655 lbs, respectively. The 737-200 aircraft gives

an estimate of W_{fur} = 4,463 lbs, and using the ratio provided by the Sugar aircraft data, below,

W_{fur} = 4,651 lbs.

Table 47. SUGAR Aircraft Furnishings Weight Data

SUGAR A/C	A/C number	W_{TO} (lbs)	W_{fur} (lbs)	$\dfrac{W_{fur}}{W_{TO}}$
SUGAR Free	765-093	175,635.000	10,866.000	0.062
Refined SUGAR	765-094	136,412.000	9,115.000	0.067
SUGAR High	765-095	163,853.000	9,115.000	0.056
SUGAR Volt	765-096	164,375.000	9,115.000	0.055
		Average	9,552.750	0.060

Nikolai also provides a method to determine the weight of the furnishings. It is the sum

of the crew seats, passenger seats, miscellaneous furniture, and the cabin windows. The

equations that provide these, respectively are as follows (Nikolai, 1984).

$$W_{cs} = 34.5(N_{cr})q^{0.25} \tag{110}$$

$$W_{ps} = 32.03(N_{pax}) \tag{111}$$

$$W_m = 0.771(W_{TO} * 10^{-3}) \tag{112}$$

$$W_{cw} = 109.33\left(N_{pax}(1 + P_c) * 10^{-2}\right)^{0.505} \tag{113}$$

$W_{cs}, N\_cr, q, W_{ps}, N_{pax}, W_m, W_{cw}, P_c$ are the weight of the crew's seats, the number of crew, the

dynamic pressure, weight of the passenger's seats, number of passengers, weight of

miscellaneous furnishings, weight of the cabin windows, and th ultimate fabin pressure in Psi,

respectively. Using these equations, results in the following weights: $W_{cs} = 318\ lbs, W_{ps} =$

$3,075\ lbs, W_m = 60\ lbs, and\ W_{cw} = 539$ lbs, with a total of 3991 lbs.

The Class II weight estimate for furnishings weight will be 3,991 lbs.

14.2.3.9. Baggage and Cargo Handling Equipment Weight

According to Roskam, the baggage and cargo containers' weight can be estimated using

$$W_{bc} = 1.6 * lbs/ft^3 \tag{114}$$

There will be 3 containers at 80 ft³ each, for a total of 240 ft³, which gives the total weight to be

384 lbs, as the Class II estimate for W_{bc}.

14.2.3.10. Operational Items Weight

The operational items include food, water, drinks, china, and lavatory supplies. Using the

SUGAR aircraft database, below, the Class II estimate of the HTA's operational items weight

will be calculated (Bradley & Droney, Subsonic Ultra Green Aircraft Research: Phase I Final

Report, 2011). Assuming the operational items weight as 4.6% the takeoff weight, the HTA's

estimate for operational items weight from SUGAR A/C data is $W_{ops} = 3,540$ lbs.

Table 48. SUGAR Data for Operational Items Weight

SUGAR A/C	A/C number	W_{TO} (lbs)	W_{ops} (lbs)	$\dfrac{W_{ops}}{W_{TO}}$
SUGAR Free	765-093	175,635.000	7,342.000	0.042
Refined SUGAR	765-094	136,412.000	7,207.000	0.053
SUGAR High	765-095	163,853.000	7,207.000	0.044
SUGAR Volt	765-096	164,375.000	7,207.000	0.044
		Average	7,240.750	0.046

According to Nikolai's Fundamental's of Aircraft Design,

$$W_{lav} = 1.11 * N_{pax}^{1.33} \tag{115}$$

$$W_{food} = K_{BUF} * N_{pax}^{1.12} \tag{116}$$

where W_{lav} is the weight of the lavatories and water provisions, W_{food} is the weight of the food

provisions, and $K_{BUF} = 5.68 \: or \: 1.02$ for long range flights and short range flights, respectively

(Nikolai, 1984). Combining these weights for 96 passengers give an estimate for the operational

weight of 650 lbs. This is significantly less than the data from the SUGAR A/C. Differences

include the number of passengers, and the length of the flight.

The calculated value of 650 lbs will be used as the estimate for the Class II operational

weight.

14.2.3.11. Weight of Paint

Roskam provides the following equation to estimate the weight of paint for a well painted

airplane to be:

$$W_{pt} = 0.003W_{TO} - 0.006W_{TO} \tag{117}$$

This gives a range of 233-466 lbs and an average of 349 lbs. The 737-700 uses approximately

350 lbs of paint (Hansen, n.d.). The Class II estimate will use an equivalent ratio of paint equal

to 260 lbs.

14.2.3.12. Fixed Equipment Weight Summary

Table 49. Fixed Equipment Weight Summary

Component	GD Method (lbs)	Torenbeek Method (lbs)	Roskam Method (lbs)	Estimate from 737 A/C (lbs)	Estimate from SUGAR A/C (lbs)	Estimate from Nikolai (lbs)	Class II Estimate (lbs)
Flight Control System	1633.4	1164.4	----------	----------	1432	--------	1,410
Hydraulic System	---------	-------------	466-931	873	413	--------	600
Electrical System	----------	831	---------	716	1,152	-------	900
Instrumetation, Avionics, and Electronics	989	1,475	---------	----------	1,107	--------	1,050
Air-Conditioning, Pressurization, Anti and De-icing	1,019	1,496	--------	1,416	793	--------	1,181
Oxygen System	175	145-208	------	-------	-----------	--------	160
APU	----------	---------	310-1008	------------	498	--------	450
Furnishings	3,919	5,655	---------	4,463	4,652	3,991	3,991
Baggage and Cargo	---------	----------	384	-----------	-------------	-------	384
Operational Items	---------	----------	-----------	-----------	3,540	650	650
Paint			233-466	350		-------	260
TOTAL							11,036

14.2.4. Empty Weight Discussion

The empty weight is the sum of the structural weight, powerplant weight, and fixed

equipment weight. $W_e = W_{struct} + W_{pwr} + W_{feq}$. Combining the totals from each of these

sections gives a total estimate of 52,439 lbs for the empty weight. Note that the nacelle weights were accounted for in the powerplant weight calculations, and the structural nacelle weight estimate will be neglected, since the manufacturer's data is available for the powerplant.

For the HTA, which uses fuel only in stages 1-4, and is battery powered for the remaining stages, the Class I estimate for the empty weight is 48,379 lbs. This difference of 4,060 lbs is fairly close to the Class I estimate, and gives a 7.7% difference.

The Class II weight sizing will need to be iterated if the weight savings criteria that follows does not provide a convergence. The weight savings criteria involve manufacturing the fuselage from composites, which would save 15% of the weight, manufacturing parts of the wing and fuselage under low stress from composites, which would save about 5%, and using a quadruplex digital flight control system and fly-by-wire as opposed to mechanical flight controls, which would save 15%, and replacing the primary wing and fuselage structure with lithium aluminum, which would give a 6% weight savings (Roskam, Airplane Design Part II: Preliminary Configuration Design and Integration of the Propulsion System, 2011). Thus, the empennage weight could be reduced by 394 lbs; the wing and fuselage low-stress composite replacement could be reduced by 713 lbs; the flight controls system could be reduced by 212 lbs; and the lithium aluminum would reduce the wing and fuselage structure by 857 lbs. Thus, the estimated empty weight has been lowered to 50,263 lbs, now only a 3.7% difference. Considering the percent difference is small, and the Class I weight sizing will continue to be used.

14.3. Component Centers of Gravity

The c.g. locations for the structural components, powerplant, and fixed equipment components will be presented using Roskam's guidelines. The table below illustrates the c.g.

location of the structural components, powerplant, and fixed equipment (Roskam, Airplane

Design Part V: Component Weight Estimation, 2003).

Using the revised Class II weights and the c.g. locations for both the x and z direction

gives the following weights summary.

Table 50. Class II Weights and CG locations

No.	Type of Component	Wi (lbs)	xi (in.)	Wixi (in lbs)	yi (in.)	Wiyi (in lbs)	zi (in.)	Wizi (in lbs)
1	Fuselage Group	7,130	641	4,570,330	0	0	248	1,768,240
2	Wing Group	5,568	680	3,786,240	0	0	350	1,948,800
3	Empennage Group	2,233	1190	2,657,270	0	0	300	669,900
4	Engine Group	21,778	590	12,849,020	0	0	140	3,048,920
5a	Landing Gear Group:Nose Gear	500	390	195,000	0	0	130	65,000
5b	Landing Gear Group: Main Gear	2224	710	1,579,040	0	0	130	289,120
6	Fixed Equipment Group	10,824	680	7,360,320	0	0	200	2,164,800
7	Trapped Fuel and Oil	34.4	690	23,736	0	0	215	7,396
8	Crew	700	300	210,000	0	0	240	168,000
9	Fuel	3,440	690	2,373,600	0	0	430	1,479,200
10	Batteries	12,000	733	8,796,000	0	0	120	1,440,000
11	Passengers	16,800	680	11,424,000	0	0	200	3,360,000
12	Luggage	3,000	680	2,040,000	0	0	200	600,000

The x c.g. location is located at 55.9 ft, and the z c.g. location is located at 16.4 ft based on the

equations from Roskam (Roskam, Airplane Design Part V: Component Weight Estimation,

2003).

$$x_{cg} = \sum_{i=1}^{n} \frac{W_i x_i}{W} \tag{118}$$

$$z_{cg} = \sum_{i=1}^{n} \frac{W_i z_i}{W} \tag{119}$$

If any of the components are moved, then the c.g. location moves according to the following

equation (Roskam, Airplane Design Part V: Component Weight Estimation, 2003).

$$\Delta x_{cg} = \frac{\Delta x_i (W_i)}{\sum_{i=1}^{n} W_i} \tag{120}$$

The most likely movement could be the batteries, but since they are suspended below the wings,

they do not have a wide range of movement available.

The c.g. excursion plot, based on the Class II data, is illustrated in the figure below. The

plot illustrates that the most forward c.g. location is at 57.33 ft and the most aft c.g. location is at

72.11 ft. This was plotted by varying the number of passengers, luggage, and fuel. The

conditions included a fully loaded aircraft, an aircraft with half passenger and full fuel, all

passengers and half the luggage, zero passengers and full luggage, no passengers and no cargo,

zero fuel, passengers only, and cargo only.
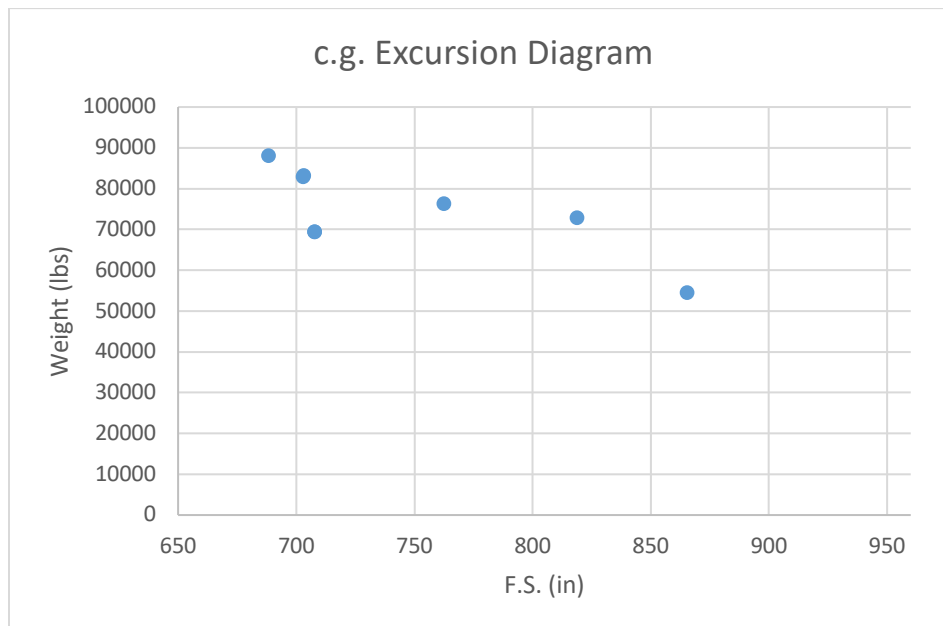
Figure 90. Class II cg excursion diagram

14.4. Airplane Inertias

To estimate the moments and products of inertia for the HTA, the weights from the Class II sizing and the c.g. locations in feet will be used. The engine group will be one weight and c.g. location, and will therefore be a 'lumped mass' assumption. This is also true for the passengers and fuel systems. The structural components will also be assumed to have uniform mass distributions. The following table summarizes the moments and products of inertia.

Table 51. Moments and products of Inertia

I_{xx}	I_{yy}	I_{zz}	I_{xy}	I_{yz}	I_{zz}
111,166.12	314,123.14	202,957.02	0	0	-52,406.14

The table was computed using the following equations (Roskam, Airplane Design Part V: Component Weight Estimation, 2003).

$$I_{xx} = \sum_{i=1}^{n} m_i \left\{ (y_i - y_{cg})^2 + (z_i - z_{cg})^2 \right\} \tag{121}$$

$$I_{yy} = \sum_{i=1}^{n} m_i \left\{ (z_i - z_{cg})^2 + (x_i - x_{cg})^2 \right\} \tag{122}$$

$$I_{zz} = \sum_{i=1}^{n} m_i \left\{ (x_i - x_{cg})^2 + (y_i - y_{cg})^2 \right\} \tag{123}$$

$$I_{xy} = \sum_{i=1}^{n} m_i \left\{ (x_i - x_{cg})(y_i - y_{cg}) \right\} \tag{124}$$

$$I_{yz} = \sum_{i=1}^{n} m_i \left\{ (y_i - y)(z_i - z_{cg}) \right\} \tag{125}$$

$$I_{zx} = \sum_{i=1}^{n} m_i \left\{ (z_i - z_{cg})(x_i - x_{cg}) \right\} \tag{126}$$

15. Cost Analysis

The life cycle cost consists of the research and development costs, production and construction costos, operations and maintenance costs, and retirement and disposal costs. For typical aircraft, the operating costs composes nearly 94% of the life cycle cost (Ploetner,

Schmidt, Baranowski, Isikveren, & Hornung, 2013). Thus, the preliminary cost analysis for the

HTA will consider the operating cost (Roskam, Airplane Design Part II: Preliminary

Configuration Design and Integration of the Propulsion System, 2011).

In order to estimate the program operating cost, C_{ops}, direct operating cost, DOC, and

indirect operating cost, IOC, mission data will be reviewed. These calculations will require the

block distance, R_{bl}, block time, T_{bl}, block speed, V_{bl}, and annual utilization in block hours,

$U_{ann_{bl}}$. The block distance can be considered the door to door distance. This distance will be the

1,720 nm established for the HTA. The block time is the door to door time from the departure

gate to the parking spot. The block time is calculated through the following equations (Roskam,

Airplane Design Part VIII: Airplane Cost Estimation: Design, Development, Manufacturing, and

Operating, 2015).

$$T_{bl} = T_{gm} + T_{cl} + T_{cr} + T_{de} \qquad (127)$$

$$T_{gm} = 0.51(10)^{-6}(W_{TO}) + 0.125 \qquad (128)$$

$$T_{cr} = (1.06R_{bl} - R_{cl} - R_{de} + R_{man})/V_{Cr} \qquad (129)$$

$$R_{cl} = (V_{cl})(T_{cl}) \qquad (130)$$

$$R_{man} = (V_{man})(T_{man}) \qquad (131)$$

$$T_{man} = 0.25(10^{-6})W_{TO} + 0.0625 \qquad (132)$$

The times consisting of the time spent on ground maneuvers, T_{gm}, such as leaving the gate,

taxiing to the runway, time on the takeoff run, on the landing ground run, and taxiing to the

destination, time spent in climb, T_{cl}, time spent in cruise, T_{cr}, and time spent in descent, T_{de}. The

ground maneuver time dependso n the takeoff weight, and the time for cruise depends on the

block distance, R_{bl}, distance for climb, R_{cl}, distance for descent, R_{de}, maneuvering distance,

R_{man}, and the cruise velocity, V_{cr}. The distance for climb depends on the climb velocity and the

time to climb. The distance for maneuvering depends on the maneuvering velocity, which will

be 250 kts, and time spent doing the maneuver. The results of the calculations are as follows:

Table 52. Block Time Results

Time segment	T_{bl}	T_{gm}	T_{cr}	T_{de}	T_{cl}	T_{man}
Time (hrs)	**4.485**	0.165	3.554	0.267	0.5	0.082

Table 53. Block Speed Results

	V_{bl}	V_{de}	V_{man}	V_{cr}	V_{de}
Speed (kts)	**383.478**	250	250	500	250

Table 54. Block Distance Results

	R_{bl}	R_{de}	R_{man}
Distance (nm)	**1720**	66.667	20.475

Thus, the annual utilization in block hours can be calculated using the following equation

(Roskam, Airplane Design Part VIII: Airplane Cost Estimation: Design, Development,

Manufacturing, and Operating, 2015).

$$U_{ann_{bl}} = 10^3 \left[3.4546 \cdot T_{bl} + 2.994 - (12.289(T_{bl})^2 - 5.6626(T_{bl}) + 8.964)^{\frac{1}{2}} \right] \qquad (133)$$

The annual utilization is approximately 3,297 hours, which is equivalent to about 9 hours of

daily utilization. These results are comparable to other aircraft, including 727-200, 737, 757, and

DC-8. For these medium range aircraft, with $2 < T_{bl} < 5$, the annual utilization numbers in

block hours ranges from 2,100-3,300 block hours. The HTA falls in this range. Now that these

parameters have been calculated, the direct operating cost can be calculated.

15.1. Direct Operating Cost

The direct operating cost is the sum of the direct operating cost of flying, maintenance,

depreciation, landing fees, and financing, abbreviated as $DOC, DOC_{flt}, DOC_{maint}, DOC_{depr},$

DOC_{lnr}, and DOC_{fin}, respectively. Each of these direct operating costs will be measured in

USD/nm. Each of these will be calculated and summed to find the total direct operating cost.

15.1.1. Direct Operating Cost of Flying

The direct operating cost of flying consists of the sum of the cost of the crew, C_{crew}, cost

of the fuel and oil, cost of the batteries, and cost of the airframe insurance.

15.1.1.1. Cost of the Crew

The cost of the crew depends on the number of crew members, n_{c_j},the type of crew

member, with n_{c_1} being the captain and n_{c_2} being the co-pilot, the factor, k_j, which accounts for

vacation pay, cost of training, crew insurance and premiums, and payroll tax, the block speed,

V_{bl}, the annual salaries of the crew members, SAL_j, the number of flight hours per year for a

crew member, AH_j, and the travel expense factor, TEF_j.

$$C_{crew} = \Sigma_{i=1}^{j} \left[n_{c_j} \left\{ \frac{1+k_j}{V_{bl}} \right\} \left(\frac{SAL_j}{AH_j} \right) + \left(\frac{TEF_j}{V_{bl}} \right) \right] \tag{134}$$

All the of the costs are for 2018. They have been scaled using the cost escalation factor,

CEF, which is

$$CEF_{year} = 6.008930 + 0.10280(year - 2014) \tag{135}$$

There will be two crew members for the HTA, a captain and co-pilot. The salaries of each

fo the respective crew members will be assumed to be \$158,686 and \$102,679. Flight crew will

be assumed to fly an average of 800 flight hours per year. The travel expense factor for each of

the crew is 13.06 per block hour. Thus, the total cost of the crew is 1.14 USD/nm.

15.1.1.2. Cost of the Fuel and Oil

The cost of fuel and oil, C_{pol}, depends on the mission fuel weight, the price of the fuel,

FP, and the density of the fuel, FD.

$$C_{pol} = 1.05 \left(\frac{W_{f_{bl}}}{R_{bl}}\right)\left(\frac{FP}{FD}\right) \tag{136}$$

The current fuel price is \$2.20 per gallon (Jet Fuel Daily Price, 2018). The fuel density is 6.74

lbs/gallon (Roskam, Airplane Design Part VIII: Airplane Cost Estimation: Design, Development,

Manufacturing, and Operating, 2015). Using a mass fuel fraction of 0.955696, the weight of the

fuel, and thus the weight of the block fuel is 3,438 lbs. The total cost of fuel and oil in USD per

nautical mile is 0.69 USD/nm.

15.1.1.3. Cost of the Batteries

To determine the direct operating cost fo the batteries, DOC_{bat}, measured in USD/nm, the

following assumptions will be made. The flight will require 35,314 kWh for the flight.

Generally, the cost per charge per kWh is \$0.0085. Thus the rate in USD/nm for the batteries

charge is 0.17 USD/nm. Note that the initial cost of the battery is not included in this.

15.1.1.4. Summary of Direct Operating Cost of Flying

The direct operating cost of flying, DOC_{flt}, can be calculated using the following

equation (Roskam, Airplane Design Part VII: Determination of Stability, Control and

Performance Characteristics: FAR and Military Requirements, 2006).

$$DOC_{flt} = C_{crew} + C_{pol} + C_{ins} + C_{bat} \tag{137}$$

Since the cost of insurance is 2% of the direct operating cost, the direct operating cost of flying if

a function of the direct operating cost. $DOC_{flt} = 2.10 + 0.02(DOC)$ USD/nm.

15.1.2. Direct Operating Cost of Maintenance

The direct operating cost of maintenance is calculated using the following equation, from

Roskam. The direct operating cost of maintenance is the sum of the labor cost of the airframe

and systems maintenance, labor cost of the engine maintenance, cost of maintenance materials

for the airframe and system, cost of maintenance materials for the engines, and applied

maintenance burden, all measured in USD/nm. The following equations summarize the

calculations necessary to determine the direct operating cost of maintenance (Roskam, Airplane

Design Part VIII: Airplane Cost Estimation: Design, Development, Manufacturing, and

Operating, 2015).

$$DOC_{maint} = C_{lab/ap} + C_{lab/eng} + C_{mat/ap} + C_{mat/eng} + C_{amb} \qquad (138)$$

$$C_{lab/ap} = 1.03(MHR_{map_{bl}})(R_{l_{ap}})/(V_{bl}) \qquad (139)$$

$$C_{lab/eng} = 1.03(1.3)N_e(MHR_{meng_{bl}})(R_{l_{eng}})/(V_{bl}) \qquad (140)$$

$$C_{mat/ap} = 1.03(C_{mat/apblhr})V_{bl} \qquad (141)$$

$$C_{mat/eng} = 1.03 * 1.3 * N_e * C_{mat/engblhr}/V_{bl} \qquad (142)$$

$$C_{amb} = 1.03\left\{(f_{amb/lab})\left[(MHR_{map_{bl}})(R_{l_{ap}}) + (N_e)(MHR_{eng_{bl}})(R_{l_{eng}})\right] + (f_{amb/lab})[C_{mat/apblhr} + (N_e)C_{mat/engblhr}]\right\}/V_{bl} \qquad (143)$$

The maintenance labor cost for the airframe and system depends on the number of

maintenance manhours per blockhour for airframe systems, which is 6.35 hours, the weight of

the airframe, which is 26,601 lbs, and the airplane maintenance labor rate per manhour, of 16

USd/nm. These inputs produce $C_{lab/ap} = 0.3142$ USD/nm.

The cost of the maintenance labor for the engines depends on the number of engines, the

number of engine maintenance hours per engine, which will be assumed to be 5 hours, the hourly

labor rate for engine maintenance, at $18.40, and the block speed of 383.5 kts. This produces

$C_{lab/eng} = 0.64$ USD/nm.

The cost of maintenance materials for the airframe and systems, other than the engines,

depends on the airframe price, and the cost of the maintenance materials per blockhour, at 100

USD/nm. Thus, $C_{mat/ap} = 0.27$ USD/nm.

The cost of maintenance materials for the engines depends on the number of engines, the

cost of the maintenance materials per blockhour, which is 90.34 USD/blockhour, and the block

speed of 383.5 kts. $C_{mat/eng} = 0.63$ USD/nm.

Finally, the cost of the applied maintenance burden per nm is a function of overhead

distribution factors for labor and material cost, the time of flight, the block time, and the cost of

the maintenance man hours per flight for the materials. This amounts to 1.053 USD/nm.

Taking the sum of these costs gives the direct operating cost of maintenance to be 2.91

USD/nm.

15.1.3. Direct Operating Cost of Depreciation

The direct operating cost of depreciation is composed of the cost of the airplane

depreciation without engines, avionics systems, the cost of the engine depreciation, the cost of

the avionics system depreciation, the cost of the depreciation of the spare parts, and the cost of

the depreciation of the engine spare parts (Roskam, Airplane Design Part VIII: Airplane Cost

Estimation: Design, Development, Manufacturing, and Operating, 2015).

$$DOC_{depr} = C_{dap} + C_{deng} + C_{dav} + C_{dapsp} + C_{dengsp} \qquad (144)$$

The airframe depreciation per nautical mile is calculated using the following equation.

$$C_{dap} = \frac{(F_{dap})[(AEP)-(N_e)(EP)-(N_p)(PP)-(ASP)]}{(DP_{ap})(U_{ann_{bl}})(V_{bl})} \qquad (145)$$

This cost depends on the airframe depreciation factor, which is 0.85, the airplane estimated price

of $33,354,004 for 2018, the number of engines, 2, the engine price, which will be assumed to be

$1,558,607, since the price of the hFan engine is not available, but this price is comparable to

other engines, the avionics system price of $2,670,000, the depreciation period off the airplane of

10 years, the annual utilization in block hours, calculated as 3,297 hours, and the block speed,

383.5 kts. This gives $C_{dap} = 1.85$ USD/nn.

The cost of engine depreciation per nautical mile is calculated using:

$$C_{deng} = \frac{(F_{deng})N_e(EP)}{(DP_{eng})(U_{ann_{bl}})(V_{bl})}$$

(146)

This equation depends on the engine depreciation factor of 0.85, the engine depreciation period

of 7 years, which may change when using the new hybrid engines, and other previously

established factors of engine price, annual utilization in block hours, and block speed. The result

is that $C_{deng} = 0.299$ USD/nm.

The cost of the depreciation of the avionics sytem in USD per nautical mile is calculated

using:

$$C_{dav} = \frac{(F_{dav})ASP}{(DP_{av})(U_{ann_{bl}})(V_{bl})}$$

(147)

Thus, $C_{dav} = 0.42$ USD/nm with an avionics system depreciation factor of 1 and the

depreciation time to be 5 years.

The cost of the depreciation of airplane spare parts in USD/nm is calculated using:

$$C_{dapsp} = \frac{(F_{dapsp})(F_{apsp})(AEP-(N_e)(EP))}{(DP_{apsp})(U_{ann_{bl}})(V_{bl})}$$

(148)

Thus C_{dapsp} is a function of the airplane spare parts depreciation factor of 0.85, the airplane

spare parts factor of 1, the airplane spare parts depreciation period of 10 years, and other

previously calculated values. $C_{dapsp} = 0.20$ USD/nm.

The cost of the depreciation of engine spare parts is given by:

$$C_{dapsp} = \frac{(F_{dengsp})(F_{engsp})(N\_e)(EP)(ESPPF)}{(DP_{engsp})(U_{ann_{bl}})(V_{bl})}$$

(149)

$C_{dapsp} = 0.23$ USD/nm, and is based on the engine spare parts depreiciation factor of 0.85, the

engine spare parts factor of 0.5, the engine spare parts price factor of 1.50, the depreciation

period for the engine spare parts, which is 7 years, and the block speed and annual utilization.

Summarizing, $DOC_{depr} = C_{dap} + C_{deng} + C_{dav} + C_{dapsp} + C_{dengsp} = 1.85 + 0.299 + 0.42 + 0.20 + 0.23 = 3.01$ USD/nm.

15.1.4. Direct Operating Cost of Landing Fees, Navigation Fees, and Registry Taxes

The direct operating cost of landing fees, navigation fees, and registry taxes is given by the following equations (Roskam, Airplane Design Part VIII: Airplane Cost Estimation: Design, Development, Manufacturing, and Operating, 2015).

$$DOC_{lnr} = C_{lf} + C_{nf} + C_{rt} \qquad (150)$$

$$C_{lf} = (C_{aplf})/(V_{bl}T_{bl}) \qquad (151)$$

$$C_{nf} = (C_{apnf})/(V_{bl}T_{bl}) \qquad (152)$$

$$C_{rt} = f_{rt}(DOC) \qquad (153)$$

The landing fee cost is 0.09 USD/nm, with the airplane landing fee per landing being 155.21 USD/nm. The cost of navigation fee will be assumed to be $0 USD/nm as the plane will not fly internationally. The cost of financing will be assumed to be 0.58 USD/nm, and the cost of registry taes is 0.01 USD/nm. Thus, the resulting sum is 0.099 USD/nm.

15.1.5. Direct Operating Cost of Financing

The direct operatinc cost of financing, DOC_{fin} is 7% of the DOC. Thus, this amounts to approximately 0.34 USD/nm.

15.1.5. Direct Operating Cost Discussion

The direct operating cost, totals 8.45 USD/nm. The following chart illustrates the breakdown of the DOC for a jet transport aircraft.
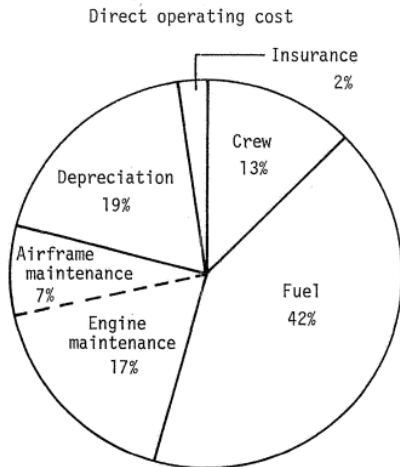
Figure 91. DOC for a Jet Transport

Based off of the calculations for the direct operating cost for the HTA, the figures below illustrates the breakdown of the DOC for both the HTA and a fuel version of the HTA. There is a significant decrease in fuel usage, but higher maintenance due to the batteries. Additionally, there is an increase in the depreciation with batteries due to the life cycles.
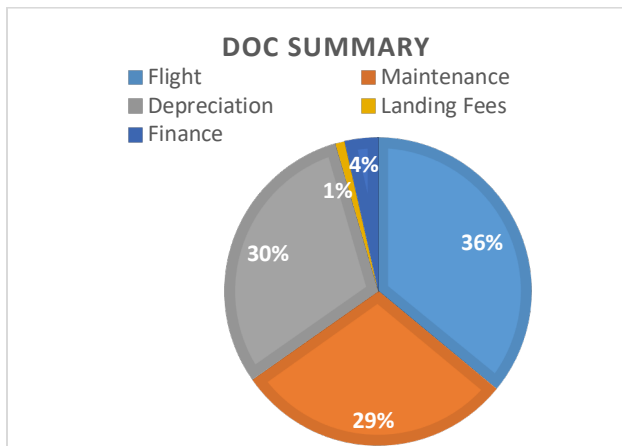
Figure 92.HTA DOC with batteries and fuel
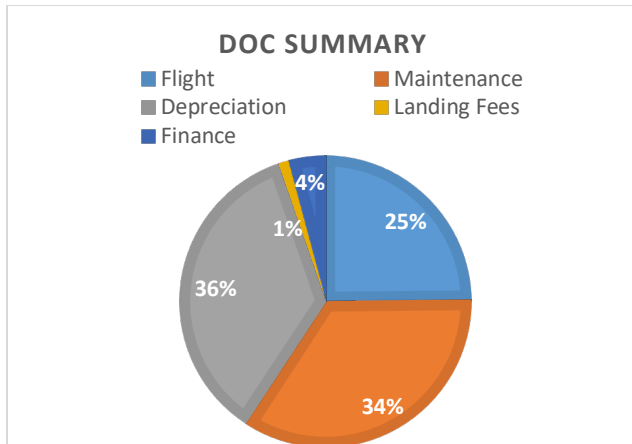
Figure 93. HTA DOC for all fuel

Additionally, the figure below illustrates the decrease in the direct operating cost over the years of the flight (Maddalon, Molloy, & Neubauer, Jr., 1980). This figure is a a jet transport. For a hybrid aircraft, the DOC should decrease more quickly as there will be less fuel to purchase. Note that this chart extends for 15 years. Many of these calculations were performed assuming a 10 year life of the airplane. However, many aircraft last longer than 10 years, which only increases the profit over the years.
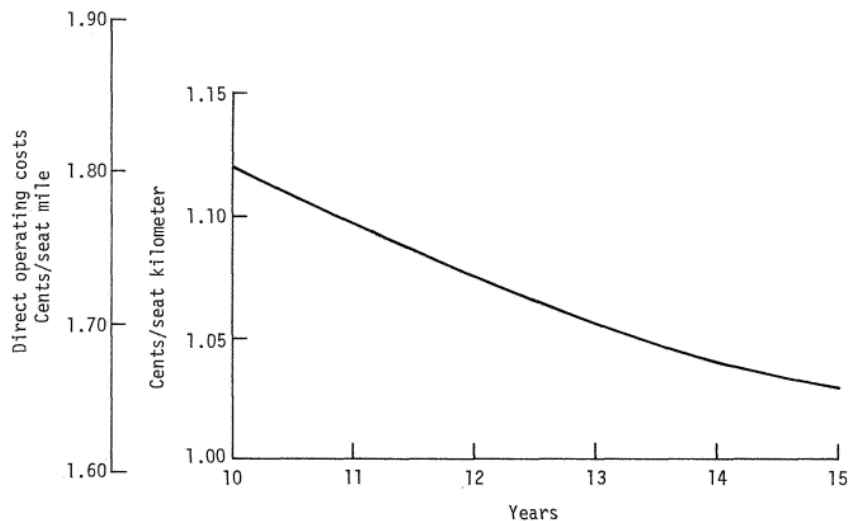
Figure 94. Effect of variable depreciation period on DOC

Sensitivity studies on a fully electric jet transport demonstrate that fuel price and electricity price have the strongest impact of the DOC. The study shows that with a 10%

increase in fuel costs, there is a 3% increase in DOC. Additionally, a reduction in the number of

cycles of battery use, less than the typical 2000 cycles, combined with battery installation costs

also produces higher DOCs (Ploetner, Schmidt, Baranowski, Isikveren, & Hornung, 2013).

15.2. Indirect Operating Cost

The indirect operating cost, IOC, is composed of the indirect operating cost for passenger

services, maintaining depreciating ground equipment and facilitiesm airplane and traffic

servicing, promotions sales, and entertainment, and general administrative expenses. Its units are

in USD/nm. The costs for these services can be estimated through the equation:

$$IOC = F_{ioc}(DOC) \tag{154}$$

F_{ioc} is the factor extrapolated from the 737 data from Roskam. This factor is 0.5. Thus, the

indirect operating cost is 4.14 USD/nm.

15.3. Program Operating Cost

The program operating cost depends on the indirect program operating costs, the direct

program operating costs, and the number of aircraft acquired. Due to the fact that operating costs

vary between customers, the program operating costs depends on the number of customers. For

the purposes of these calculations, 1,200 aircraft will be assumed to be in acquisition (Sales,

2018). As of January 1, 2018, Boeing has orders for more than 4,300 737- MAX aircraft. Since

the HTA has similar mission specifications, a high volume will be assumed for acquisition. Then

the program operating cost can be estimated using the following equations (Roskam, Airplane

Design Part VIII: Airplane Cost Estimation: Design, Development, Manufacturing, and

Operating, 2015).

$$C_{ops} = \sum_{i=1}^{i=n} \left[(C_{ops_{dir}})_i (N_{acq})_i + (C_{ops_{ind}})_i (N_{acq})_i \right] \tag{155}$$

$$(C_{ops_{dir}})_i = (DOC)_i (R_{bl\,ann})_i (N_{yr})_i \tag{156}$$

$$\left(C_{ops_{ind}}\right)_i = (IOC)_i\left(R_{bl_{ann}}\right)_i(N_{yr})_i \tag{157}$$

Assuming the aircraft are in use for 10 years, the operating cost is $190,835,543,254.38. The early design has a significant impact on the ultimate cost of the aircraft. In the future, trade studies can be performed on the number of years in service and the number of aircraft acquired per year to determine the effect on the operating cost.

15.3. Hybrid Power Cost Analysis

Although the price of jet fuel fluctuates per gallon, the general trend illustrates an increase in fuel costs and an increase in the number of general aviation aircraft, as discussed in the introduction. The price of electricity to recharge the batteries is significantly cheaper than jet fuel and has the added benefit of drastically reducing carbon dioxide and other harmful emittants. Electricity costs approximately 8.5 cents per kilowatt hour. For a fully-fuel powered version of the HTA, which requires 17,888 lbs or 2,670 gallons of jet fuel, this would reduce the cost of the total fuel per flight from $5,874 to $1,129.

15.3.1. Sample Battery Specifications

Although battery technology is not yet at its peak in power, companies are selling advanced lithium ion batteries for aviation power. True Blue Power is one such company.

For aviation, True Blue has a 46 amp hour battery, which at an output voltage of 26.4 Volts, and weight of approximately 23.4 kg, gives approximately 51.7 Wh/kg of energy. The low specific energy density would result in more batteries and higher weight, further illustrating the need for increased battery energy density. However, with the promise of better battery technology and the capabilities of lithium ion batteries, these batteries may provide future capabilities.

This battery has a life expectancy of 8 years with a 2 year maintenance interval. It weighs 51.7 lbs and has superior performance at extreme temperatures, including -40ºF to 158ºF and at pressures up to 35 Psi. Its dimensions are 10.9 in by 10.5 in by 10.1 in, making it easily fit in small spaces and configure with other batteries (True Blue Power, 2018). Each battery costs approximately $16,400 (True Blue Power, 2018). Though the batteries may initially be expensive, this one time cost for the life of the aircraft will drastically decreasethe cost to power the aircraft over time.

16. Conclusion

The preliminary design of the narrow-body, short to medium range hybrid transport vehicle demonstrates the feasibility of a hybrid powered aircraft fueld by both lithium ion batteries and jet fuel. Through a series of Class I estimates, including configuration design, weight sizing and sensitivities, determination of performance constraints, fuselage and cockpit design, wing design, empennage design, landing gear design, weight and balance analysis, stability and control analysis, and drag polar estimation, and Class II estimates of the V-n maneuver diagram, and weight and balance, and cost analysis, the early design calculations carefully layout the conversion of a jet aircraft to a hybrid powered aircraft.

This vehicle provides an environmentally friendly form of flight, reducing emissions and dependence on oil. As the number of general aviation aircraft increase and FAA standards call for reduced emissions, designing aircraft with less dependence on oil and fuel is becoming necessary. With battery technology developing, a hybrid aircraft is the perfect transition to greener aircraft for the near future.

Compared to the Boeing 737-100 model, the HTA has comparable weights, with the possibility of a lower takeoff weight. Additionally, with the research behind the SUGAR aircraft,

the availability of hybrid engines would make the transition of power between fuel and electricity much more simple to integrate.

In regards to future work, the battery technology will continue to develop, and, as a result the weight may decrease and the specific energy densities may increase. Additionally, more studies could be performed on the benefits of using fuel and battery power during different phases of the flight. Trade studies could show the advantages and disadvantages of each power source during the phase of flight. The direct operating cost, although preliminary, demonstrates that the batteries, as a power source, are competitive from a cost perspective.

Overall, the hybrid transport aircraft demonstrates strong potential as a preliminary design to meet FAA standards, reduce emissions, and utilize future battery technology to pave the way toward new-age transport jets.

References

Airbus Commerial Aircraft. (n.d.). Retrieved July 5, 2017, from

      http://www.aircraft.airbus.com/aircraftfamilies/passengeraircraft/a320family/a320neo/

Aircraft Technical Data and Specifications: Boeing 737-100/200. (2017). Retrieved from

      Airliners: http://www.airliners.net/aircraft-data/boeing-737-100200/91

An Encyclopedia of the History of Technology. (2002). In I. McNeil (Ed.). Routledge.

Boeing Commercial Airplanes. (2013). *737 Airplane Characteristics for Airport Planning.*

Bradley, M. K., & Droney, C. K. (2011). *Subsonic Ultra Green Aircraft Research: Phase I Final*

      Report. Huntington Beach: Boeing Research and Technology.

Bradley, M. K., & Droney, C. K. (2015). *Subsonic Ultra Green Aircraft Research: Phase II-*

      Volume II- Hybrid Electric Design Exploration. NASA. Huntington Beach: Boeing

      Research and Technology.

Bradley, M. K., & Droney, K. C. (2011). *Subsonic Ultra Green Aircraft Research: Phase I Final*

      Report. Langley Research Center. Hampton: National Aeronautics and Space

      Administration.

Bradley, M. K., Droney, C. K., & Allen, T. J. (2015). *Subsonic Ultra Green Aircraft Research:*

      Phase II Volume I Truss Braced Wing Design Exploration. NASA.

Brady, C. (1999). *Detailed Technical Data*. Retrieved from The 737 Technical Site:

      http://www.b737.org.uk/techspecsdetailed.htm

Canadair Regional Jet. (2016). *Canadair Regional Jet Airport Planning Manual.* Toronto:

      Bombardier Inc.

Crawford, B. (2009). *Flightlab Ground School.* Flight Emergency and Advanced Maneuvers

      Training Inc.

Creative Aviation Photography. (2017). Retrieved from Airplane Pictures: http://www.airplane-

pictures.net

Daggett, D. L., Hendricks, R. C., Rainer, W., & Corporan, E. (2008). *Alternate Fuels for Use in*

Commercial Aircraft. National Aeronautics and Space Administration, Glenn Research

Center, Cleveland.

Davis, S. C., Williams, S. E., & Boundy, R. G. (2016). *Transportation Energy Data Book* (35

ed.). Oak Ridge, Tennessee: Oak Ridge National Laboratory.

Farhadi, M., & Mohammed, O. (2016). Energy Storage Technologies for High-Powered

Applications. *IEEE Transaction on Industry Applications, 52*(3), 1953-1961.

Federal Aviation Administration. (2015). *Aviation Emissions, Impacts, and Mitigation: A Primer.*

Office of Environment and Energy.

Fuel Price Analysis. (2017). Retrieved from IATA:

http://www.iata.org/publications/economics/fuel-monitor/Pages/price-analysis.aspx

Hansen, D. (n.d.). *Airframe Design*. Retrieved from The Boeing Company:

http://www.boeing.com/commercial/aeromagazine/aero_05/textonly/fo01txt.html

Hepperle, M. (n.d.). Electric Flight- Potential and Limitations. *NATO OTAN*.

Jane's All the World's Aircraft. (2013). IHS Markit.

Jet Fuel Daily Price. (2018, May 14). Retrieved from index mundi:

https://www.indexmundi.com/commodities/?commodity=jet-fuel

Maddalon, D. V., Molloy, J. K., & Neubauer, Jr., M. J. (1980). *NASA Technical Memorandum*

80196: Computer Programs for Estimating Civil Aircraft Economics. Hampton: NASA

Langley Research Center.

Mason, W. H. (2006). Aerodynamic Configuration Design Options. In *Configuration Aerodynamics*.

Matsushita, T., Yabuta, K., Tsujikawa, T., Matsushima, T., Arakawa, M., & Kurita, K. (2008). Construction of Three-Dimensional Thermal Simulation Model of Lithium Ion Secondary Battery. *IEEE*, 1-6.

Moore, R. H., Shook, M., Beyersdorf, A., Corr, C., Hendon, S., Knighton, W. B., . . . Anderson, B. E. (2015). Influence of Jet Fuel Composition on Aircraft Engine Emissions: A Synthesis of Aerosol Emissions Data from the NASA APEX, AAFEX, and ACCESS Missions. *Energy & Fuels, 29*, 2591-2600.

NASA. (2014, January 24). *In Future Aircraft Designs We "Truss"*. (L. Gipson, Editor) Retrieved 2017, from https://www.nasa.gov/aero/boeing_sugar_wind_tunnel.html

Nikolai, L. M. (1984). *Fundamentals of Aircraft Design.* San Jose: METS, Inc.

Obert, E. (2009). *Aerodynamic Design of Transport Aircraft.* Delft University of Technology .

Ploetner, K. O., Schmidt, M., Baranowski, D., Isikveren, A. T., & Hornung, M. (2013). Operating Cost Estimation for Electric-Powered Transport Aircraft. *American Institute of Aeronautics and Astronautics*.

Riboldi, C., & Gualdoni, F. (2016). An integrated approach to the preliminary weight sizing of small aircraft. *Aerospace Science and Technology, 58*, 134-149.

Roskam, J. (2003). *Airplane Design Part V: Component Weight Estimation.* Lawrence: DARcorporation.

Roskam, J. (2006). *Airplane Design Part VII: Determination of Stability, Control and Performance Characteristics: FAR and Military Requirements.* Lawrence : DARcorporation.

Roskam, J. (2011). *Airplane Design Part 3: Layout Design of Cockpit, Fuselage, Wing, and Empennage: Cutaways and Inboard Profiles.* Lawrence: DARcorporation.

Roskam, J. (2011). *Airplane Design Part II: Preliminary Configuration Design and Integration of the Propulsion System.* Lawrence: DARcorporation .

Roskam, J. (2011). *Airplane Design Part III: Layout Design of Cockpit, Fuselage, Wing, and Empennage: Cutaways and Inboard Profiles.* Lawrence: DARcorporation.

Roskam, J. (2015). *Airplane Design Part VIII: Airplane Cost Estimation: Design, Development, Manufacturing, and Operating.* Lawrence: DARcorporation.

Roskam, J. (2017). *Airplane Design Part 1: Preliminary Sizing of Airplanes.* DARcorporation.

Rudolph, P. C. (1996). *High-Lift Systems on Commercial Subsonic Airliners.* Moffett Field: NASA Ames Research Center.

Sales. (2018, Feb. 10). Retrieved from The Boeing 737 Technical Site: http://www.b737.org.uk/sales.htm

Tariq, M., Maswood, A. I., Gajanayake, C. J., & Gupta, A. K. (2017). Aircraft batteries: current trend towards more electric aircraft. *The Institute of Engineering and Technology, 7*(2), 93-103.

Thauvin, J., Barraud, G., Roboam, X., Sareni, B., Budinger, M., & Leray, D. (2016). Hybrid Propulsion for Regional Aircraft: a Comparative Analysis Based on Energy Efficiency. *IEEE*.

True Blue Power. (2018). *TB46.* Retrieved from True Blue Power: https://www.truebluepowerusa.com/aviation-products/advanced-lithium-ion-batteries/tb46/

Ullman, D. (n.d.). The Electric Powered Aircraft: Technical Challenges.

Xue, N. (2014). *Design and Optimization of Lithium-Ion Batteries For Electric Vehicle Applications* .

Zayat, K. A., Dray, L., & Schafer, A. (2017). *A First Order Analysis of Direct Operating Costs of Battery Electric Aircraft.* Antwerp: Engineering and Physical Sciences Research Council.